CONFINING LAYER STUDY IN THE

WEST EDMOND OIL FIELD AREA

USING SUBSURFACE, REMOTE

SENSING, AND GEOCHEMICAL

METHODS

BY

LONNIE G. KENNEDY

Bachelor of Science

University of Oklahoma

Norman, Oklahoma

1986

Submitted to the Faculty of the
Graduate College of the
Oklahoma State University
in partial fulfillment of
the requirements for
the Degree of
MASTER OF SCIENCE
May, 1990

Thesis
1990
K35c
cop.2

CONFINING LAYER STUDY IN THE

WEST EDMOND OIL FIELD AREA

USING SUBSURFACE, REMOTE

SENSING AND GEOCHEMICAL

METHODS

Thesis Approved:

Wayne Pettyjohn
Thesis Advisor

Arthur W Hounslow

Gary F. Stewart

Norman N. Durham
Dean of the Graduate College

ii

ACKNOWLEDGMENTS

TABLE OF CONTENTS

LIST OF FIGURES

LIST OF TABLES

LIST OF PLATES

CHAPTER I

INTRODUCTION

Statement of Problem

A survey conducted by the U.S Environmental Protection Agency (EPA) in 1983 determined that there are currently 195 hazardous injection wells in operation in the United States today (Brasier 1987). In addition, almost 100,000 enhanced recovery wells are now in operation injecting water into oil-producing zones to aid recovery. Finally, it is estimated that there are some 20,000 wells used strictly for the purpose of oil-field brine disposal (Clark 1983).

Underground injection is presently the cheapest method of waste management. According to Gordon and Bloom (1978), the costs of using deep-well injection for waste disposal are:

o   28% of the cost of surface impoundment;

o   16% of the cost of using a landfill;

o   1% of the cost of incineration.

Because underground injection is currently the least expensive, and often the most practical, disposal alternative a trend now exists toward heavier reliance on deep-well injection. Unless new requirements are imposed to counteract economic incentives, the future will probably show increased dependence on deep-well injection.

EPA has determined that the average depth for injection wells is 4,000 feet. Typically, 2,800 feet of strata separate the injection zone from shallower aquifers containing water with dissolved solids concentrations of 10,000 mg/l or less. Approximately 95% of hazardous waste injection wells dispose of wastes in zones that lie below usable water resources (Brasier 1987).

The oil and gas industry introduced the use of injection wells. Beginning in the middle 1930's, injection wells were substituted for open evaporation pits. These wells were used both to enhance oil recovery and to dispose of highly corrosive, often chemical-laden brines and drilling fluids.

Injection of toxic and hazardous chemical waste from the steel and chemical industries began in the 1950's. The practice of injection came into favor following the enactment of environmental laws designed to protect surface waters from pollution (Gordon and Bloom 1987).

The object of deep-well injection is the disposal of liquid wastes into a suitably porous and permeable deep formation in such a fashion that it does not impinge upon human health or the environment. There are several engineering and geologic design criteria which must be taken into account in planning a deep injection system.

The engineering concerns of proper injection system design center on well design and operations. Many methods have been developed in order insure the mechanical integrity of an injection well, including cement bond logging and pressure testing (Whiteside and Raef 1987).

To be acceptable for injection purposes, a formation must possess the following geologic qualifications:

o   Have no value as a resource;

o   Have sufficient porosity and volume to accept the anticipated volume of liquids;

o   Be located in a seismically inactive area;

o   Be chemically compatible with the wastes to be injected;

o   Be sealed above and below by formations with sufficient strength, thickness, and low permeability to prevent migration of waste from the disposal zone.

Many of the geologic parameters of concern in injection well planning are inexact. The collection of geologic information typically depends upon rock cores, adjacent well records, adjacent open hole logs, and seismic surveys. These methods, at best, provide only a

one-dimensional snapshot of subsurface characteristics. Extrapolation and assumptions of homogeneity are generally used to infer formation qualities between data points.

A critical geologic factor in injection well emplacement is the recognition of pervasive fault structures: those faults extending from the potential injection zone up to the surface. Such features represent a significant breach in confining zone integrity, and provide a potential pathway for the migration of wastes into shallow ground water supplies.

The recognition of faulting on the land surface is often obscured by a veneer of soil or vegetation. However, with adequate data some subsurface faults can be discerned, but subsurface studies with the necessary detail are expensive, tedious, and time-consuming. Because fault identification is so troublesome, the true character of the confining unit is often unknown.

Utilizing remote sensing for fault delineation may provide an attractive supplement to other forms of investigation. Remote sensing and fracture trace analysis can be used quickly and inexpensively over large geographic regions.

Nomenclature Used

Where differences arise between surface and subsurface terminology, the subsurface titles will be used in this report. Additionally, several stratigraphically-

4

successive formations have similar lithologies and cannot easily be differentiated using bore hole geophysical logs. For this report, the following stratigraphic terminology will be used:

o   The various formations within the Hennessey Group will be referred to collectively as "Hennessey Shale";

o   The Garber and Wellington Formations will be called the "Garber-Wellington";

o   The Frisco and Bois d'Arc Formations of the Hunton Group will be called "Frisco-Bois d'Arc";

o   The Haragan and Henryhouse Formations of the Hunton Group will be called "Haragan-Henryhouse";

o   The Chimney Hill Subgroup of the Hunton Group, comprised of the Clarita, Cochrane, and Keel Formations, will be referred to as the "Chimney Hill".

Scope and Purpose

This project explores the application of remote sensing for pervasive fault identification. The object of the research was to compare lineament sets for several types of remote sensing media to recognizable subsurface fault patterns. The hypotheses was that if a significant correlation between lineament and fault sets exists, then remote sensing could be considered a viable method of pervasive fault identification.

The project site is located around the old West Edmond oil field just north of Oklahoma City, Oklahoma. Geophysical logs and completion records from about 1,400 oil wells drilled in the field provided an excellent data base for subsurface information.

Deep fault patterns were established by first analyzing the structure of the Hunton Group. The Hunton is comprised of limestone belonging to the Devonian and Silurian systems and is approximately 6,500 feet below the surface. Vertical fault continuity was determined by creating a structure map on a shallow limestone marker believed to be near the base of the Permian system at a depth of approximately 1,500 feet.

A production data map was constructed, listing important oil and gas information for each well. Data from the production map were used to make a contour map of initial twenty-four hour oil production from Hunton-productive wells. Isopach maps were made for the Hunton Group, as well as for several overlying formations, including the Woodford Shale and Mississippi Limestone. Analysis of trends in initial oil production and variations in isopach patterns were used to verify many subsurface faults.

A fracture-trace analysis for the project area was performed by identifying lineaments on Landsat, band 7 imagery and on color infrared photographs at scales of 1:120,000 and 1:60,000, respectively. Also, lineaments

6

corresponding to straight reaches of streams were identified on a topographic map, at a scale of 1:2,400.

To determine the reliability of remote sensing analysis for fault identification, the lineament fields were directly compared with the base of Permian fault pattern. In addition, the frequency distribution for the orientations of the lineament sets were statistically compared with that of subsurface fault pattern.

Finally, a method was proposed for using stream water conductivity measurements during dry-weather flow conditions to distinguish lineaments that correspond to pervasive faults. A test site was established along a portion of Deer Creek where remote sensing lineaments corresponded to a recognizable subsurface fault.

During dry-weather flow, a series of water conductivity measurements were made along the stream. Water conductivity values were graphically and statistically compared to determine if significant changes in gross water chemistry could be recognized through the suspected fault interval.

Location

The area of study consists of 160 square miles including the east half of Townships 12 to 15 North, Range 5 West and most of Townships 12 to 15 North, Range 4 West (Figure 1). The project area includes portions of Oklahoma, Logan, Kingfisher, and Canadian counties.

Physiography and Drainage

Much of the southern third of the study area is within metropolitan Oklahoma City. Urban areas are predominantly residential, with some light industry. The northern two-thirds of the project area is generally agricultural (farming and cattle ranching), though several rural housing developments dot the landscape.

Grass-covered prairies and gently-rolling hills typify the native topography. The highest elevation is 1320 feet in the south central portion of the study area. The land slopes gently toward the north and east, attaining a study-area minimum of 990 feet in the alluvial valley of Spring Creek.

The soil, developed from the underlying Hennessey Shale, is red to reddish brown. Streams, both intermittent and perennial,dissect the landscape. The streams occupy narrow, relatively flat-floored, sandy, alluvial valleys. A thin canopy of trees and brush usually parallels creeks and streams, outlining the drainage system.

The North Canadian River meanders across the southwest corner of the site. Deep Fork Creek, a major tributary to the Cimmaron River, is fed by two major streams: Spring Creek and Deer Creek. Spring Creek flows nearly due east near the northern boundary of the project. Deer
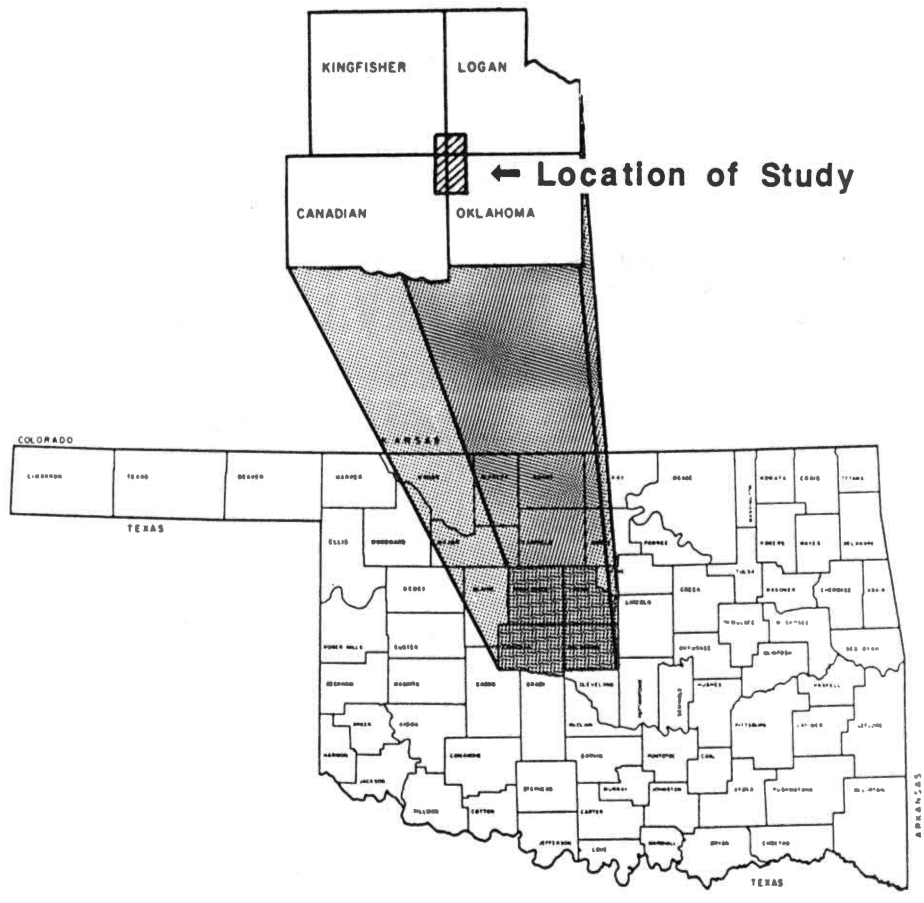
Figure 1. General Location Map.

Creek flows northeast across the center of the study area. Other local tributaries include Wolf Creek, Cottonwood Creek, Soldier Creek, Walnut Creek, Bluff Creek, and Bloody Rush Creek.

The largest streams are perennial, with ground water runoff providing baseflow even during dry years. Minor tributaries tend to be intermittent. The overall drainage pattern is dendritic, but individual stream reaches tend to be linear in form.

Lake Hefner covers 2,600 acres of portions of Sections 26 and 27, T13N-R4W. This lake provides part of the water supply for Oklahoma City and has a capacity of 75,000 acre-feet.

Climate

The Oklahoma City area is subject to wide ranges in both temperature and average precipitation. This is caused by the interaction of tropical and polar air masses. U.S. Weather Bureau climatological data indicate that the average temperature is about 60° F. The coldest month, January, averages 39° F. The warmest month, August, has an average temperature of 82° F.

The average precipitation for central Oklahoma is thirty-two inches. The greatest rainfall occurs during May, averaging 5.44 inches. December is the driest month, averaging only 1.53 inches of precipitation. During the

hot summer months, active evapotranspiration creates a
net water loss.

Petroleum History

Petroleum Production

The West Edmond Field extends over most of the of
the study area (Figure 2). The field is five miles wide
and eighteen miles long, covering fifty-five square miles
(35,200 acres). The major producing units are the upper
two formations of the Hunton Group: the Bois d'Arc and
Frisco.

Hunton Group production in the West Edmond field
represents a classic example of an erosional carbonate
wedge hydrocarbon trap. During the Pennsylvanian, the
study area was elevated above sea level and tilted up to
the east, resulting in the systematic erosion of the
Hunton Group in that direction. During the lower Pennsyl-
vanian, the region was submerged and shales were deposit-
ed over the area, providing a confining zone sufficient
for hydrocarbon entrapment.

The Bois d'Arc and Frisco produce from fracture-
enhanced matrix porosity. Production from the Bois d'Arc
and Frisco formations in the West Edmond Field is limited
on the west by a water contact and on the east by ero-
sional thinning of the pay section. Fractured production
from the lower formations of the Hunton Group, including
the Haragan, Henryhouse, and Chimney Hill, has been

11

R7W R6W R5W R4W R3W R2W

T20N
T19N
T18N
T17N
T16N
T15N
T14N
T13N
T12N
T11N
T10N

Sooner Trend Field

West Edmond Field

STUDY AREA

Oklahoma City Field
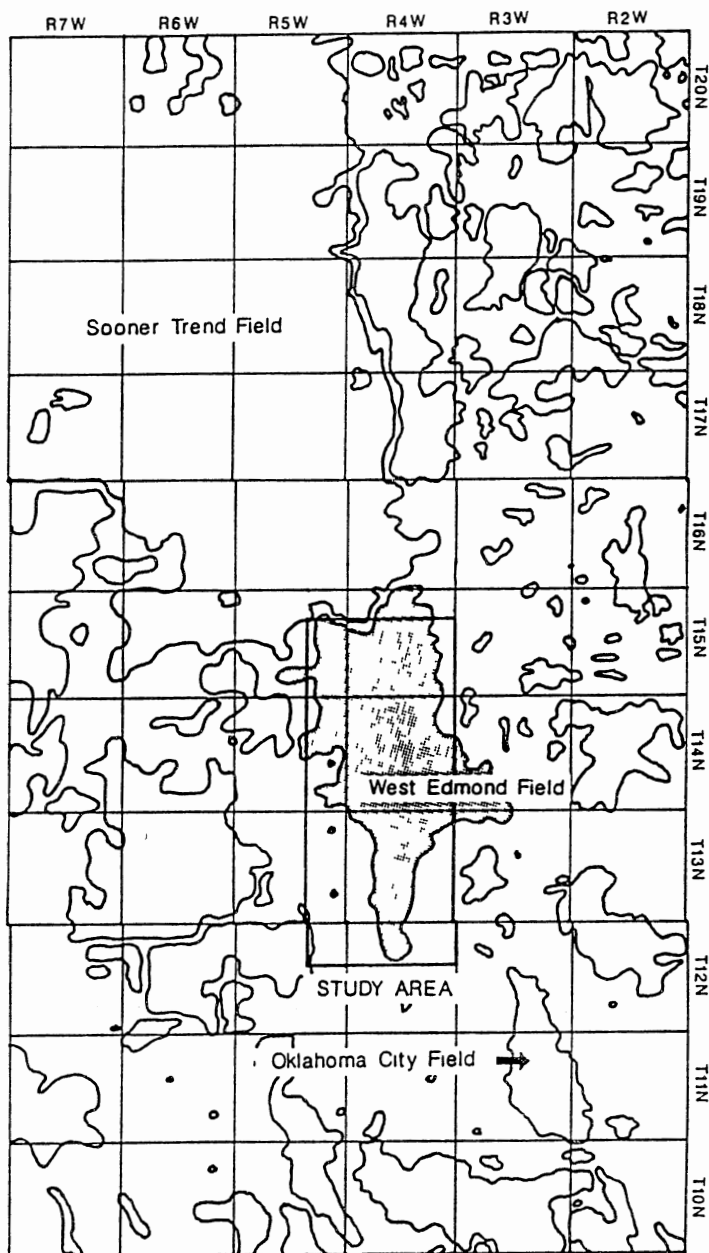
Figure 2. West Edmond Oil Field in
relation to other oil
fields in central
Oklahoma.

established beyond the eastern updip limit of the Bois d'Arc and Frisco.

Wells producing from the Hunton Group often had initial production exceeding 1,200 barrels of oil per day. Initial production values were as high as 4,800 barrels per day (Plates 1 and 2). Cumulative reserves average 115,000 barrels of oil per well.

In addition to the Hunton Group there are several other producing horizons in the West Edmond field including the Hogshooter, Layton, Checkerboard, Oswego, Prue, Skinner, and Mississippi formations, as well as the Viola and Simpson Groups. Typical well performance data are listed on Table 1.

History of the West Edmond Field

The West Edmond field was discovered in 1943 by Ace Gutowsky, an independent wildcat operator. The field was largely developed by 1945, and supplied much of the oil used in World War II (McGee 1946). Currently (1989), the field has accumulated over 160 million barrels of oil and still yields nearly 0.5 million barrels annually.

The completion practices for wells producing from the Hunton Group were generally uniform and universally applied throughout the field. Casing was set completely through the Bois d'Arc. The zone was perforated with the hole loaded with mud. After the tubing was installed and

TABLE 1
Productive Formations and Typical
Depth and Production Values
for the West Edmond Field.

Formation Name	Approx. Depth	# of Wells Producing	Typical I.P. (B.O.P.D)	Typical Cum. (B.O.)
Hogshooter Sand	5,500	60	100	60,000
Layton Sand	5,550	9	180	40,000
Cleveland Sand	5,650	42	40	41,000
Oswego Lime	6,400	33	100	<10,000
Prue Sand	6,500	38	50	30,000
Skinner Sand	6,600	3	<25	<10,000
"Bartlesville Sand"	6,450	162	70	50,000
Mississippi Lime	6,600	137	250	60,000
Misener Sand	6,800	?	?	?
Bois d'Arc-Frisco Lime	6,800	1,392	>500	115,000
Haragan, Henryhouse & Chimney Hill	6,600	>35	50	>25,000
Viola Lime	6,500	2	50	?
Simpson	6,700	31	600	>200,000

the drilling mud removed, the formation was acidized with about 1,000 gallons of 15% hydrochloric acid.

Most wells were allowed to flow at relatively high rates initially in order to clean up the reservoir. However, the State of Oklahoma restricted normal daily oil production to less than 300 barrels of oil per day per well during the 1940's.

On July 29, 1947, the Hunton limestone in the West Edmond Field was unitized by order of the Corporation Commission of Oklahoma, permitting water or gas to be injected into the Hunton to maintain reservoir pressure. Under Oklahoma pooling laws, only gross field production must be reported to the state. Therefore, public records concerning individual well or lease performance are unavailable after 1947.

CHAPTER II

REGIONAL AND SITE GEOLOGY

Geologic Setting

The study area lies on the northwest flank of the Oklahoma City Anticline. This anticline is part of the southern end of the Nemaha Ridge, a long, narrow complex of faulted anticlines extending over 300 miles from south central Oklahoma to southeastern Nebraska (Figure 3).

The project area also lies on the northeast rim of the Anadarko Basin. This sedimentary basin covers most of the southwestern quarter of the state. The basin is asymmetrical, with a northwest axial trend.

Surface Geology

The surface geology in the study area is shown on Figure 4. The Hennessey Shale crops out over nearly the entire project area (Bingman and Moore, 1975). The formation dips towards the southwest at a rate of approximately ninety feet per mile.

The Garber Sandstone is exposed in the northeast portion of the study area. Quaternary sand, silt, clay,
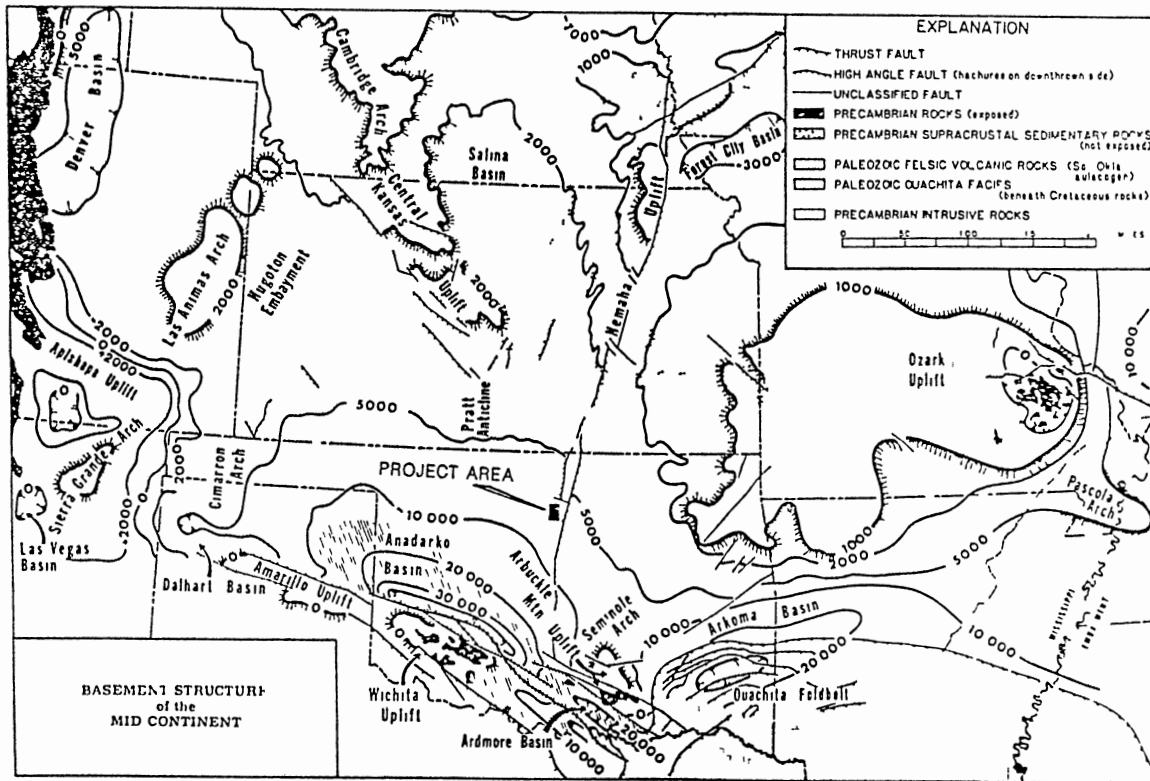
Figure 3. Regional Geologic Province Map.

Ph

Ph

Pgw

Ph

Pgw

STUDY AREA

Qal

Ph

Qal

Pe

Lake
Hefner

Qt

Pe

Pe

Qt

Pgw

Qal

Qal

Pe

Qt

Qt

Pgw

Ph
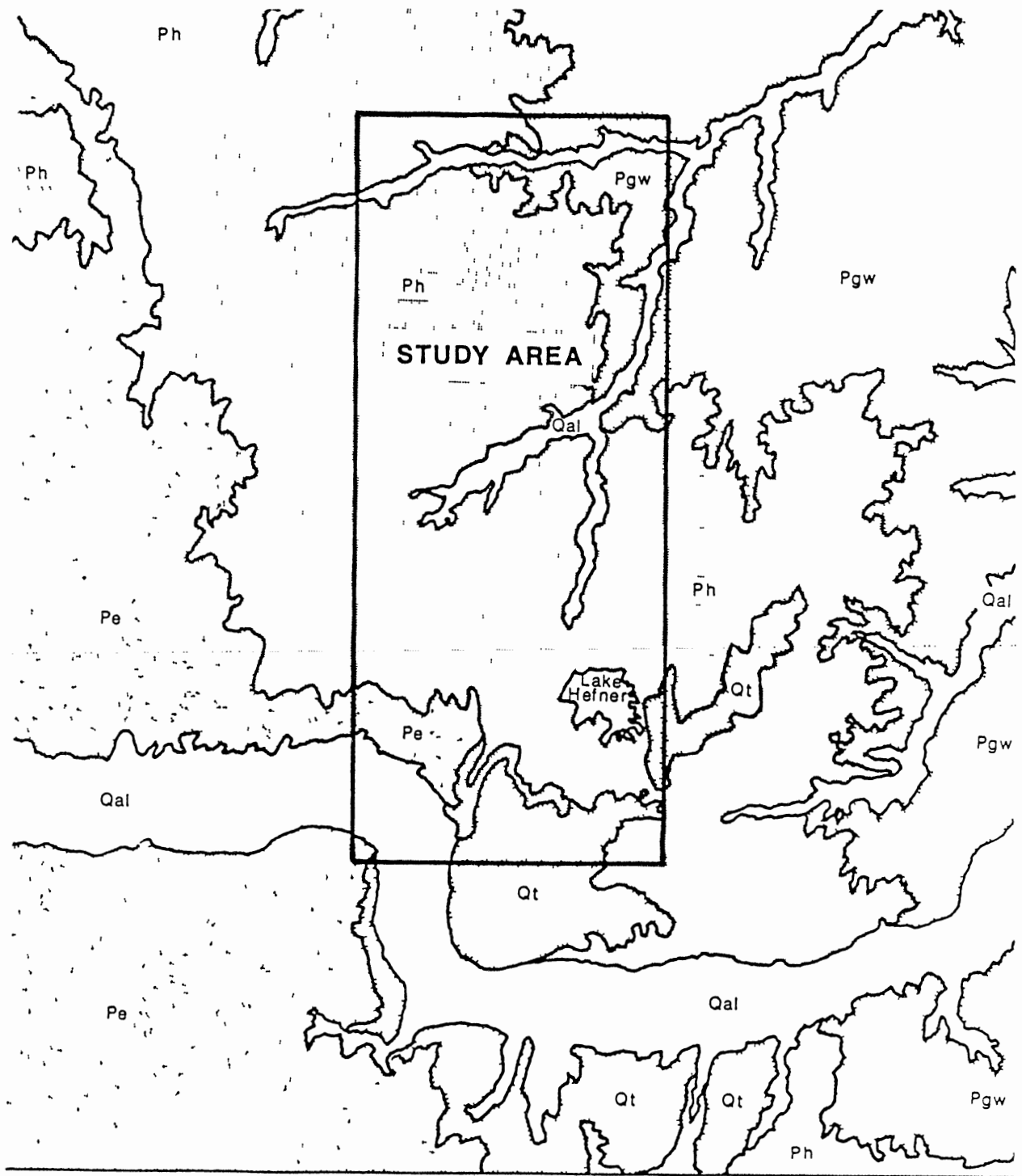
LEGEND

| Pe | El Reno Group | Pgw | Garber-Wellington | Qal | Quaternary Alluvium |
| Ph | Hennessey Group | Qt | Pleistocene Terrace Deposits | | |

Figure 4. Surface Geologic Map.

and gravel lie along the North Canadian River and all major streams. Quaternary-age dune and terrace deposits are present in the southeastern portions of the area.

Stratigraphy

The stratigraphy of the project area is well known, although there are disagreements concerning exact stratigraphic boundaries. The stratigraphic relationships and accompanying lithologic descriptions that apply to the West Edmond Field are derived from several studies, including:

- o Permian System from Christenson (1987) and Wood (1968);

- o Middle Pennsylvanian System (Des Moinesian) from Benoit (1966);

- o Much of the Silurian through Ordovician Systems from Swesnik (1948);

- o Nomenclature for the Hunton Group from Amsden (1960).

Permian System

Permian strata outcrop on the surface of the project area, the youngest of which belong to the Leonardian series. The contact between the Permian and the Pennsylvanian Systems is unconformable, produced by the Arbuckle Orogeny.

19

Hennessey Formation

The total formation thickness for the Hennessey is between 600 to 650 feet (Figure 5). Within the study area, the formation crops out and has been partially removed by erosion. The Hennessey consists dominantly of reddish-brown shale containing layers of siltstone and fine-grained sandstone (Figure 6a). Shale beds range in thickness from only a few inches to ten feet. Lenses of sand and silt also attain thicknesses up to ten feet.

Garber-Wellington

The contact between the Garber and Wellington formations is difficult to establish in the subsurface, and the two are not differentiated in this report. The collective thickness of the Garber-Wellington ranges between 800 and 1,000 feet. The unit consists of lenticular, red to maroon, fine-grained, cross-bedded sandstone that is irregularly interbedded with sandy, silty shale (Figure 6b). Sandstone beds may attain thicknesses of up to thirty feet, but five feet or less is typical.

Chase, Council Grove, and Admire Groups

Bingham (1975) referred to the Chase, Council Grove, and Admire as the "Oscar Group", and assigned the unit to the Pennsylvanian System. The nomenclature adopted here is after Lindburg (1987), where the stratigraphic section
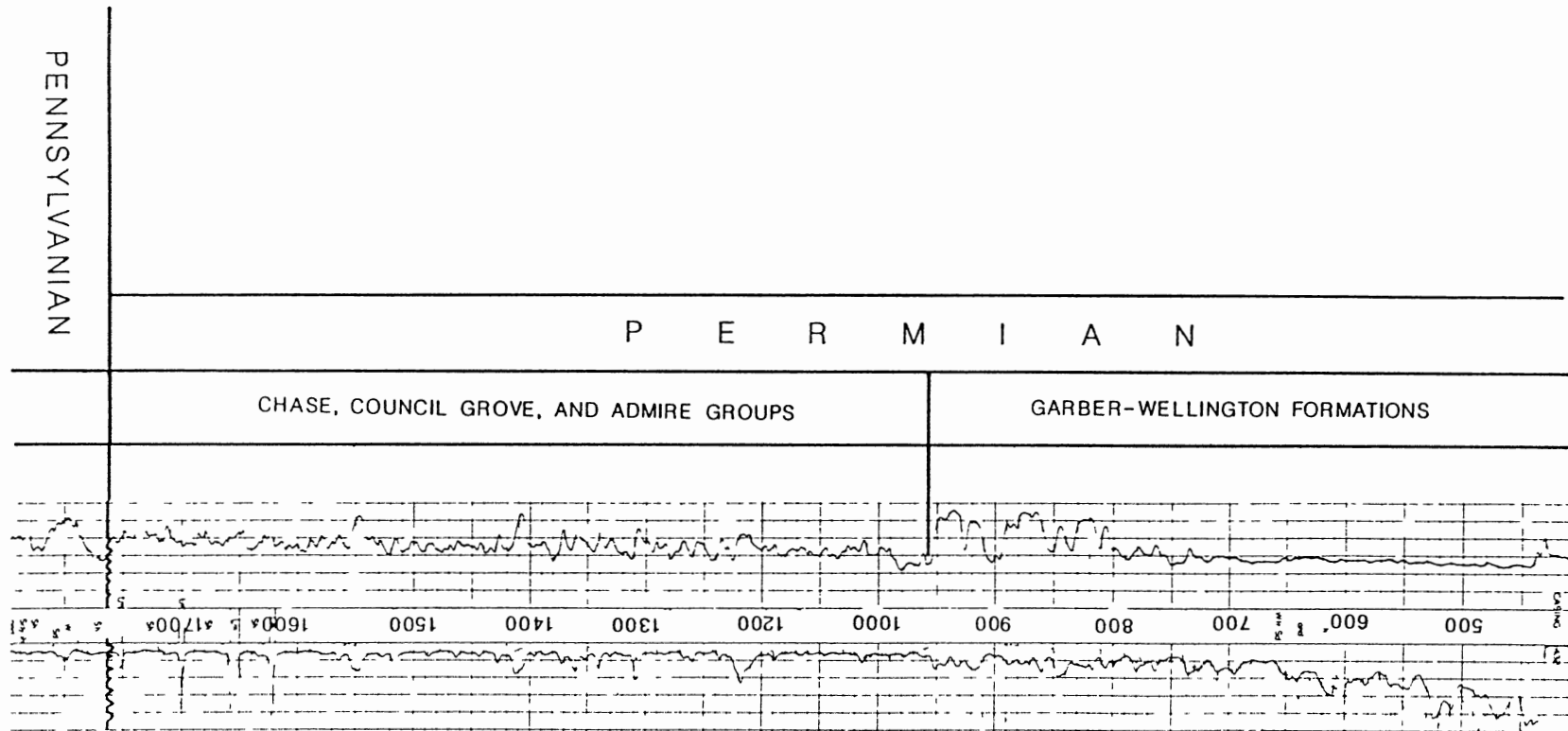
Figure 5. Electric Log Correlation of the Permian
Section in the Study Area.
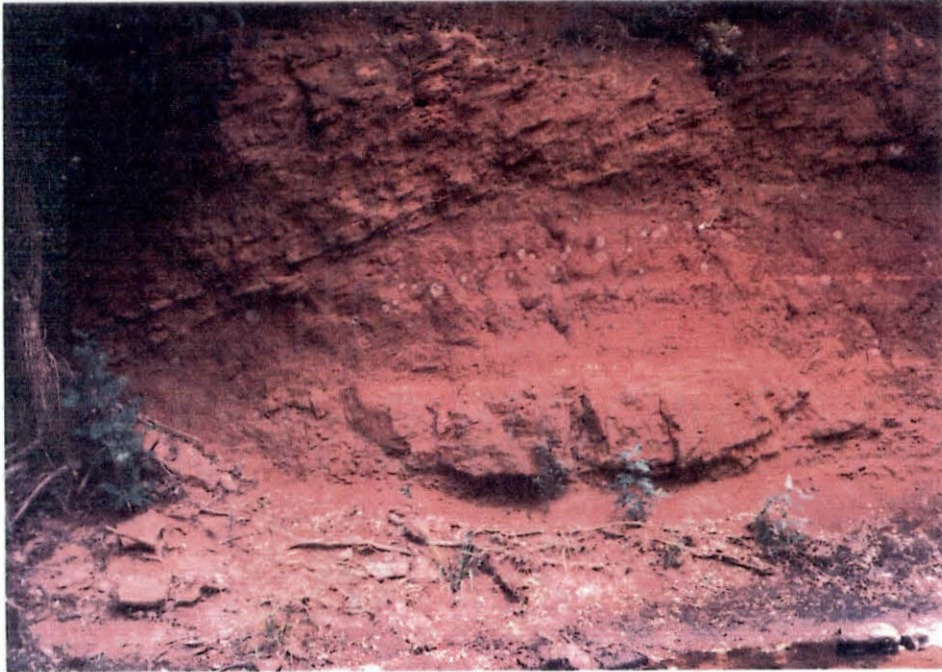
6a.

6b.

Figure 6. Photographs of a) Hennessey Shale with
Lenticular Sandstone Beds, and
b) Garber Sandstone Outcrop.

is divided into the four respective Permian System groups.

The Chase, Council Grove, and Admire groups have a combined thickness of approximately 750 feet. The different groups are lithologically similar, consisting of red to maroon, fine-grained, cross-bedded sandstone and shale. Several thin limestone beds mark the base of Permian System at the bottom of the Admire Group.

In the study area, the exact contact between Permian and Pennsylvanian strata is subject to controversy. A marker for the base of the Permian was selected by comparing subsurface geophysical logs to the documented surface stratigraphic succession. For this project, the base of the Permian is considered to be at the bottom of four thin, laterally-continuous limestone beds at a depth of approximately 1,500 feet.

Pennsylvanian System

Pennsylvanian-aged strata are approximately 5,300 feet thick in the study area. This system is punctuated on the top and bottom by unconformities resulting respectively from the Arbuckle and Upper Wichita orogenic events. The recognizable effects of the Arbuckle Unconformity are modest; however, the impact of the Upper Wichita Unconformity is more pronounced, with Pennsylvanian-aged rocks lying upon strata ranging in age from Mississippi to Ordovician.

Missourian and Virgilian Series

The top of the Pennsylvanian System represented in the project area is comprised mostly of gray shale accentuated by several sandstone units and thin limestone beds. In ascending depth, commonly identified formations include:

o   Pawhuska Limestone (3,600 feet)

o   Tonkawa Limestone (4,800 feet)

o   Avant-Dewey Limestone (5,100 feet)

o   Hogshooter Limestone (5,500 feet)

o   Layton Sand (5,550 feet)

o   Cleveland Sand (5,650 feet).

Des Moinesian Series

The stratigraphic column for the Des Moinesian Series, correlated to an electric log is shown in Figure 7.   The bottom of the Pennsylvanian section thins appreciably over the Nemaha Ridge, and formations below the Skinner, including the Bartlesville and Red Fork, are not found locally.

Oswego Lime. The Oswego is a well developed, brown, coarsely crystalline, mottled, bioclastic limestone that grades downward into a white to buff micro-crystalline limestone.   In the project area, the Oswego is approxi-

24
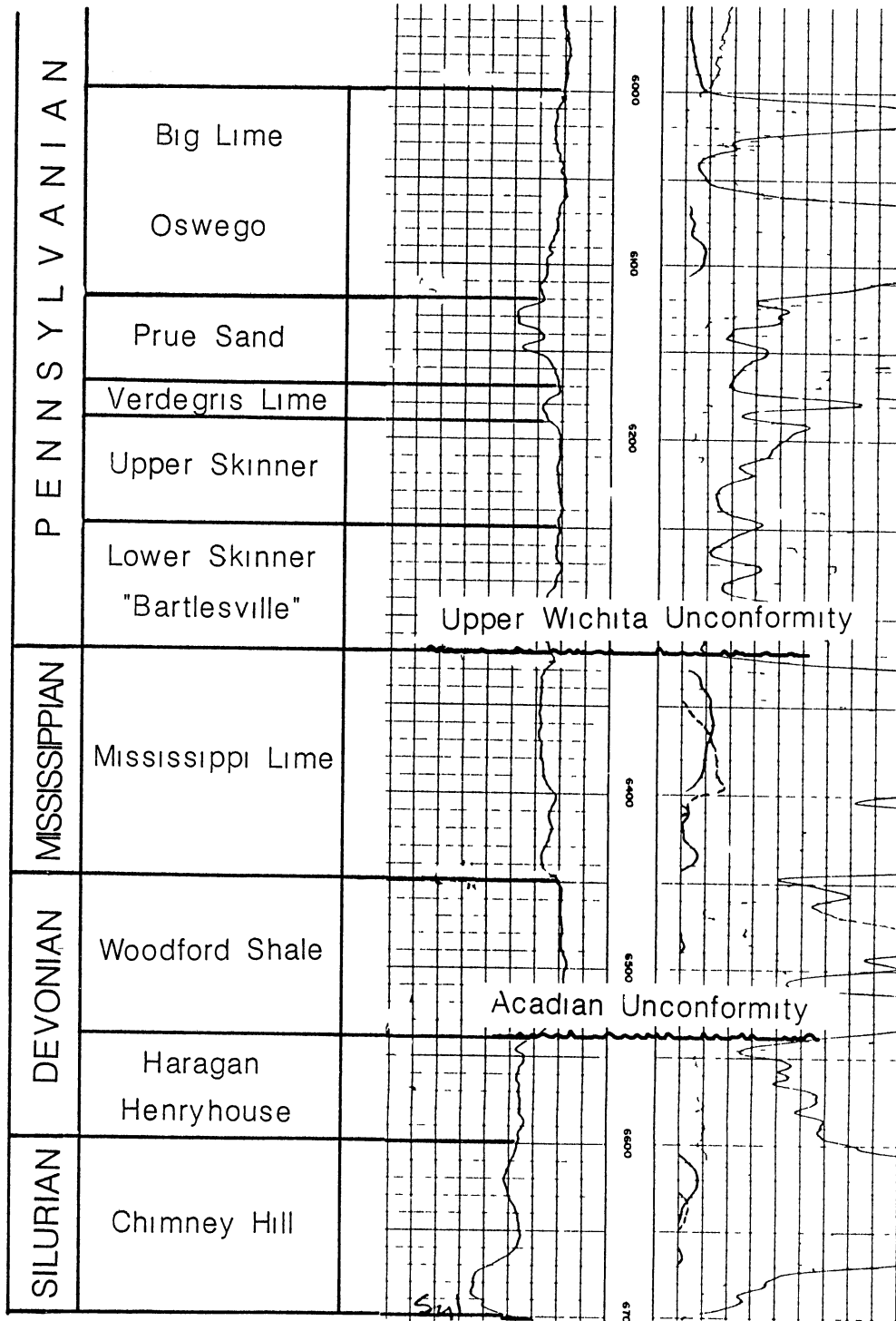
Figure 7. Electric Log Correlation of the
Pennsylvanian Section in the
Study Area.

mately 6,400 feet deep and is between fifty to one-hundred feet thick.

Prue Sand. The Prue is a lenticular sandstone that is grayish-green, fine grained, shaly, and micaceous. The formation attains a maximum thickness of seventy feet and is found at a depth of approximately 6,500 feet.

Verdigris Limestone. The Verdigris is a gray, micro-crystalline limestone. Although the formation is usually less than ten feet thick, it is laterally persistent and often is employed as a marker bed for the underlying Skinner.

Skinner Series. The Skinner consists of two lenticular sandstone units separated vertically by fifty feet of shale. These have been informally referred to as the "Upper and Lower Skinner Sands". The sandstone beds are interbedded with silt and shale. Sand from rotary cuttings is described as being gray, fine to very fine grained, shaly, and micaceous. The formation is approximately 6,600 feet below the surface. Individual sand beds are usually twenty to twenty-five feet thick.

The Lower Skinner has been commonly misidentified as the "Bartlesville" sand by local subsurface workers (Benoit 1957). The term "Bartlesville" has been universally applied throughout the West Edmond Field and will not be modified within this report. However, in acknowl-

26

edgment of the questionable classification, the term
"Bartlesville" will be enclosed in quotation marks.

Mississippian System

Strata belonging to the middle and upper Mississip-
pian System (Meramecian and Chesterian Series) are absent
in the project area. The lower Mississippian System,
Osagean Series, is represented by the Mississippi Lime-
stone (Figure 7). The Mississippi Limestone lies uncon-
formably below Pennsylvanian strata everywhere in the
project area.

The Mississippi Formation is a gray to brown,
mottled, finely crystalline to granular limestone. The
formation attains a maximum thickness of 272 feet towards
the northwest, but was completely removed across the
southeastern half of the study area during the Upper
Wichita Orogeny.

Silurian and Devonian Systems

In descending order, the Silurian System in the
project area includes the Woodford and Misener forma-
tions and the Frisco, Bois d'Arc, and Haragan formations
of the Hunton Group (Figure 8). The Henryhouse Formation
and Chimneyhill Subgroup of the Hunton Group constitute
the Silurian section.

The contact between the Woodford and the overlying
Mississippi Limestone is conformable. In the eastern

27

SYSTEM	ORDOVICIAN					SILURIAN	DEVONIAN			
GROUP	SIMPSON GROUP	VIOLA GROUP					HUNTON GROUP			
FORMATION	WILCOX SAND	DOLO-MITE	VIOLA LIME	SYLVAN		CHIMNEYHILL	HARAGAN HENRYHOUSE	BOIS d ARC FRISCO		WOODFORD

Figure 8. Electric Log Correlation of the
Silurian to Ordovician Strata
in the Study Area.

portions of the study area, where the effects of weathering during of the Upper Wichita Orogeny are more pronounced, all Silurian strata are in unconformable contact with Pennsylvanian-aged strata.

Woodford and Misener

The Woodford is a dark brown to black, carbonaceous, siliceous shale which typically contains microfossil plant spores. The formation is radioactive, producing gamma-ray responses in excess of 160 API units.

The Woodford and Hunton contact is unconformable, produced by uplift during the Acadian Orogenic event. The effects of this unconformity are subtle and restricted to the Hunton.

The Woodford is believed to be a prolific hydrocarbon source rock that has been documented to be thermally mature over most of the Anadarko Basin (Cardott 1986). A complete section of Woodford is typically forty-five to fifty-five feet thick, but the unit was completely removed by Pennsylvanian-age erosion in the eastern half of the study area.

Up to five feet of Misener Sandstone occasionally develops in the base of the Woodford. This formation is a medium to fine grained, poorly sorted sandstone with

rounded, frosted grains consisting of quartz, chert, or detrital limestone.

Frisco-Bois d'Arc

The contact between the Frisco and the underlying Bois d'Arc is unconformable. The Frisco and Bois d'Arc can not be distinguished by interpreting open hole logs alone. Except in the following discussion, no attempt will be made to differentiate the two formations.

Locally, the Frisco is a coarse-textured, rhombic, crystalline limestone with abundant fossils, consisting predominantly of light pink crinoid fragments. A bluish-white, translucent to opaque chert is common in the upper half of the formation. The maximum documented thickness within the study area is forty feet.

In the project area, the Bois d'Arc consists of four lithologic units including, in descending order:

- o   Fifty feet of buff, coarse to fine crystalline limestone with some pink crinoidal fragments;

- o   Ten feet of finely crystalline limestone with abundant rhombohedral dolomite;

- o   Fifteen feet of gray to black oolitic limestone;

- o   Twenty feet of gray, finely crystalline, very argillaceous limestone.

Haragan-Henryhouse

Based on paleontological data, Aamsden (1967) deter-
mined that the Haragan and underlying Henryhouse forma-
tions of the Hunton Group were separated by an unconform-
ity. There is no structural evidence for this unconform-
ity in the project area. The two formations are nearly
identical in lithology. A typical description of Hara-
gan-Henryhouse for the West Edmond Field area, in de-
scending order, includes:

o   Eighty feet of gray, buff, or tan, fine crys-
        talline to sucrosic, slightly dolomitic,
        argillaceous limestone;

o   Fifty to sixty feet of coarse to sucrosic
        limestone with pink to red crinoidal fragments;

o   Forty to fifty feet of gray to reddish brown,
        fine crystalline to sucrosic, slightly dolomit-
        ic, argillaceous limestone.

Chimney Hill

The Chimney Hill is comformable with both the over-
lying Henryhouse and the underlying Sylvan Shale. Indi-
vidual formations in the Chimney Hill Subgroup include
the Clarita, Cochrane, and Keel. The entire subgroup is
forty to fifty feet thick.

The Clarita is a light gray, coarsely crystalline
limestone with dark red to reddish pink crinoidal frag-
ments. The glauconitic and oolitic lithotypes, typifying
the Cochrane and Keel formations, are rare in the area.

Ordovician System

In descending order, the Ordovician System is comprised of the Sylvan Formation, and the Viola, Simpson, and Arbuckle Groups. Formations below the Simpson will not be addressed in this report.

Sylvan Shale

The Sylvan Formation lies conformably below the Hunton and above the Viola (Figure 8). The Sylvan is approximately 100 feet thick and is comprised of pale green to gray splintery shale.

Viola Group

The Viola is approximately 100 feet thick and is comprised of the Fernvale and Trenton Formations. The Fernvale is a coarsely crystalline, gray to white limestone. The Trenton is a gray, dense, microcrystalline limestone.

Simpson Group

The Simpson Group is comprised of alternating sequences of dolomitic sand, dolomite, lime, and shale. The Simpson begins with forty to fifty feet of limy dolomite, often referred to as the "Simpson Dolomite". A few feet of green shale or white to gray sandy lime usually separate the dolomite unit from the underlying

32

Wilcox Sandstone. The Wilcox is approximately ninety
feet thick and is comprised of white, well rounded,
slightly limy, dolomitic sandstone. Below the Wilcox,
the remainder of the Simpson is mostly thin-bedded dolom-
itic limestone and shale.

Geologic History

Both the Chimney Hill Subgroup and the Henryhouse
Formation were deposited as successive lithofacies of a
very shallow-water, transgressive-phase, carbonate ramp
model. Conversely, the Haragan, Bois d'Arc, and Frisco
Formations probably were deposited in a shallow-water,
regressive-phase, carbonate ramp environment (Manni, 1985
and Beardall 1979).

Compressional tectonism culminated in regional
uplift and retreat of the seas after Hunton deposition
during the Acadian orogenic event. Much physical evi-
dence concerning the magnitude of the Acadian Uplift was
destroyed by subsequent unconformity. Available informa-
tion suggests that the Acadian orogenic event was rela-
tively mild, and in no instance were pre-Hunton strata
exposed.

Some early faulting may have initiated during the
hiatus between Hunton and Woodford deposition and may
have continued through Woodford deposition. Following
the Acadian Orogeny, seas again transgressed the region.

The Misener, Woodford, and Mississippi formations were each deposited in succession.

The Upper Wichita Orogeny produced a second episode of uplift, resulting in unconformity during the Middle Pennsylvanian System. The area was tilted up to the east and strongly folded. Strata ranging from Mississippian to Cambrian in age were exposed concentrically about the Oklahoma City Anticline (Figure 9).

Faults that had originally formed during the Acadian Orogeny were reactivated during the Upper Wichita Orogeny, and many new faults were propagated. Most of the fault separation occurred during this episode. Fault slip was generally vertical, but lateral offset across some fault boundaries suggests slight strike-slip movement.

Structural quiescence typified the remainder of the Pennsylvanian Age. Southwest downwarping occurred in response to subsidence in the Anadarko Basin, and a thick sequence of principally deltaic sediments were deposited.

At the close of the Pennsylvanian Period, much of southern Oklahoma was uplifted and deformed in response to the Arbuckle Orogeny. The project area was affected only mildly by this event, but several pre-existing faults may have been reactivated.

Permian rocks were folded in a subdued pattern similar to the structure of the underlying Hunton. Many of the faults present at the Hunton level penetrated

LEGEND

Mc Chester Group
Mn Mississippi Lime
Dw Woodford Shale
Dsh Hunton Lime
Os Sylvan Shale
Ov Viola
Oss Simpson
OC Arbuckle
DSwh Woodford & Hunton
Osv Sylvan & Viola
M Springer
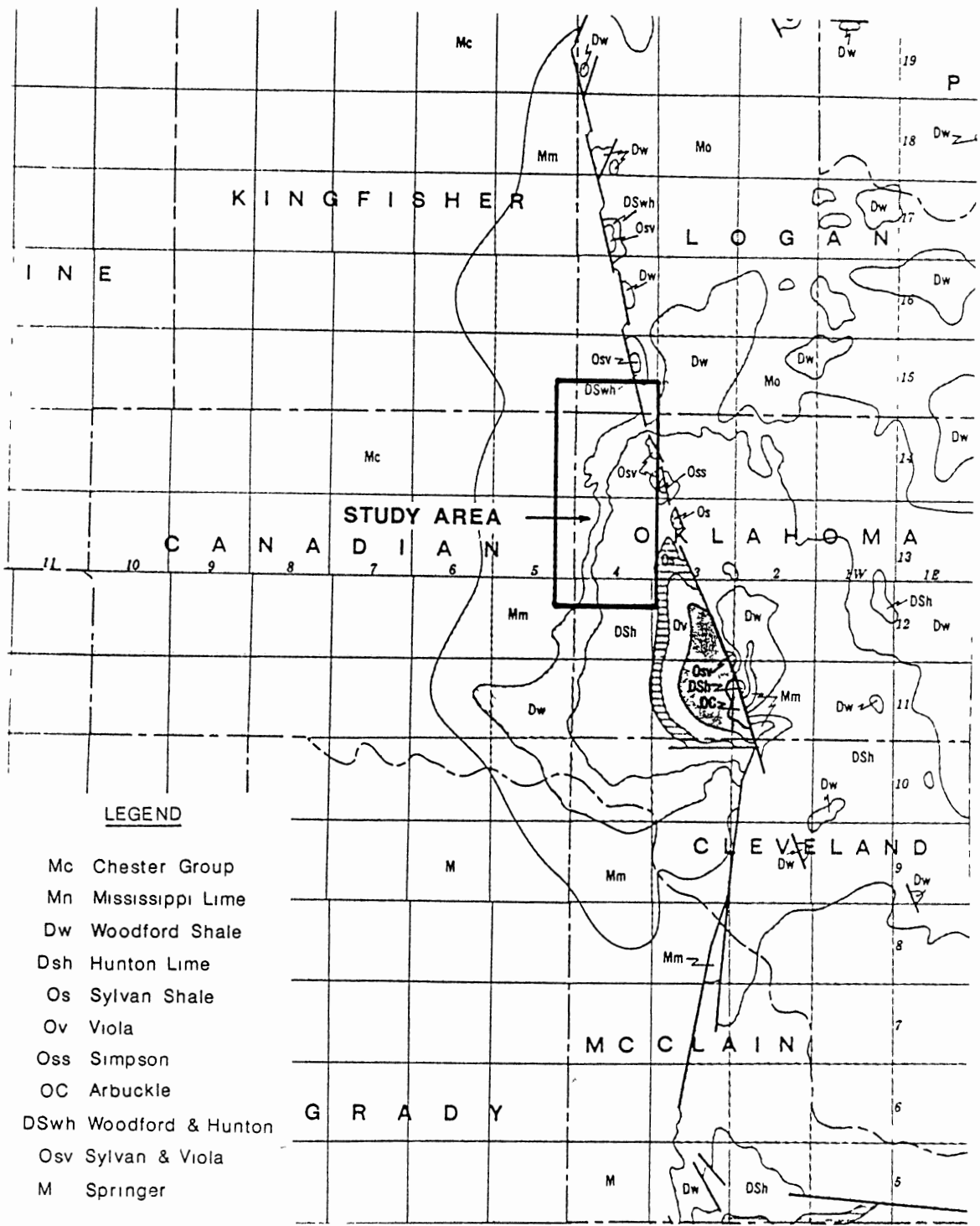
Figure 9. Pre-Pennsylvanian Subcrop Map for
Oklahoma City Anticline Area.

through Pennsylvanian and Permian strata. As a result of differential erosion and differential deposition, the degree of fault displacement at the Permian level is substantially less than corresponding fault slip in pre-Pennsylvanian strata.

At the close of the Permian, central Oklahoma was tilted down to the southwest. This down-warping probably created tensional forces that resulted in a final episode of mild fault reactivation. Also, many fracture and joint patterns expressed in Permian beds on the surface likely were produced at this time.

Hydrogeology

Terrace and Alluvium Deposits

Terrace and alluvium deposits supply ground water for agricultural and domestic purposes within the study area. These deposits are restricted to stream valleys or river terraces and are, therefore, not widely utilized. Wood (1968) reported sustained yields of 100 to 200 gpm in properly developed wells where the strata thicknesses exceeded fifty feet. Recharge is accomplished by direct rainwater infiltration. Discharge occurs principally by evaporation, transpiration, and ground water discharge into local streams.

Hennessey Shale

In the western two-thirds of the project area, the Hennessey Shale is the principal aquifer for domestic supply. Wells are completed to depths of less than ninety below the surface.

The fine-grained texture of the Hennessey gives the formation poor permeability. Water is produced either from an upper weathered zone, from cavities left by the removal of soluble materials, or from fractures (Wood, 1968). Aquifer tests performed by Dennis (1954) indicated transmissivity values ranging from 125 to 2,500 gpd/ft.

Rain water infiltration is the principal source of aquifer recharge. Water quality from the Hennessey is good, but in some areas concentrations of sulfates, calcium, and chlorides make the water hard.

Garber-Wellington

The Garber-Wellington constitutes the most important source of ground water in the Oklahoma City area. Although the aquifer is used for domestic and agricultural purposes, its primary importance is as a municipal and industrial supply. The Garber-Wellington is confined over most of the project area, but it outcrops to the east, providing an avenue for recharge.

The Garber-Wellington is composed fine sand lenses interbedded with silty shale. Storage coefficients range from .0001 to .0003. Transmissivity averages 2388 gpd/ft; however, the hydraulic conductivity averages only 17.63 gpd/ft^2 reflecting the fine grained nature of the formations. The average completed thickness is 135 feet with well yields ranging from 32 to 480 gpm (Gates 1983).

The natural water quality of the Garber-Wellington is generally excellent, but this varies with depth and location. Iron sulfates leach out of the Hennessey formation into underlying sand lenses of the Garber resulting in water high in sulfites. Chloride concentrations generally increase with depth.

Subsurface Mapping

Data Base

Subsurface maps were constructed using available data from open hole logs, scout tickets, and Oklahoma Corporation Commission completion forms 1002A. Some type of open hole log was available for most wells. Only electric log surveys were run in the first wells drilled in the West Edmond Field during the 1940's. Wells drilled in the 1950's and early 1960's often utilized electric log and micro-resistivity log combinations. After the 1960's, common geophysical logging suites included induc-

38

tion electric logs with combinations of micro resistivity, gamma ray-density, density-neutron, or sonic logs.

Production Data Map (Plate 1)

The Production Data Map shown on Plate 1 provided an important source of historical information and basic data. The information presented was extracted from scout tickets and Oklahoma Corporation Commission forms 1002A. Supplementary production map data is found in Appendix 1.

The symbol around each well indicates the deepest horizon penetrated. Additional information listed below individual wells includes:

- o   Original well operator and the year in which the well was drilled;

- o   Well name and number;

- o   Distinguishing drill stem or core tests;

- o   Producing formation and perforation intervals;

- o   Initial oil, gas, and water production rate.

Hunton Structure (Plates 2 and 3)

Plates 2 and 3 show the structure of the base of the Hunton and top of the Hunton Group, respectively. The top of the Hunton is not perfectly suited for structural analysis because that surface was gouged by erosion during Acadian and Upper Wichita Unconformities. The

impact of erosion is most severe in the eastern, structurally elevated, portions of the project area.

Although the base of the Hunton was not affected by unconformity, many of the wells in the western portion of the project were only drilled to the top of the Bois d'Arc to minimize water production. Consequently, in some areas, data is inadequate to depict accurately the base of Hunton structure.

Plate 2, constitutes the best overall representation of Hunton structure. By assuming similar folding, the structural elements from the top and bottom of the Hunton have been combined into a single map of reasonable accuracy. Where data density was inadequate for the base of the Hunton, similar contour intervals were extrapolated from the top of the Hunton.

The Hunton surface is depicted as a highly faulted, west to southwest-dipping homocline. The rate of dip for the base of the Hunton is between 150 to 250 feet per mile. Angular unconformity has reduced the rate of dip for the top of the Hunton to between 125 to 200 feet per mile.

Standard methods of fault detection in the subsurface include:

o   Repeated or missing stratigraphic sections in
     open hole logs;

o   Disjoint structural continuity across a roughly
     linear boundary.

The fault patterns presented in this report are, by necessity, interpretational; however, complementary lines of evidence were used to try to verify fault configuration, including:

o   Correlation of faulting to Hunton production lineaments;

o   Isopach analysis for the Hunton Group, and Frisco-Bois d'Arc, Woodford, and Mississippi Limestone formations.

One-hundred and fourteen faults were identified in the Hunton. Faults lie in conjugate sets with principal orientations averaging N47°E and N56°W (Figure 10).

The eastern portion of the project area is closer to the tectonic center of the Nemaha Ridge and appears to have been exposed to a higher degree of structural deformation. Folding, fault frequency, and the magnitude of fault-slip are all more intense towards the east. Eastern faults often surpassed 100 feet of apparent slip while western faults seldom exceeded fifty feet of throw.

The subsurface structural configuration of the project area has been mapped by many competent professional geologists. Benoit (1957), McGee and Jenkins (1946), Luza (1983), and Swesnic (1948) all published articles illustrating the structure the West Edmond
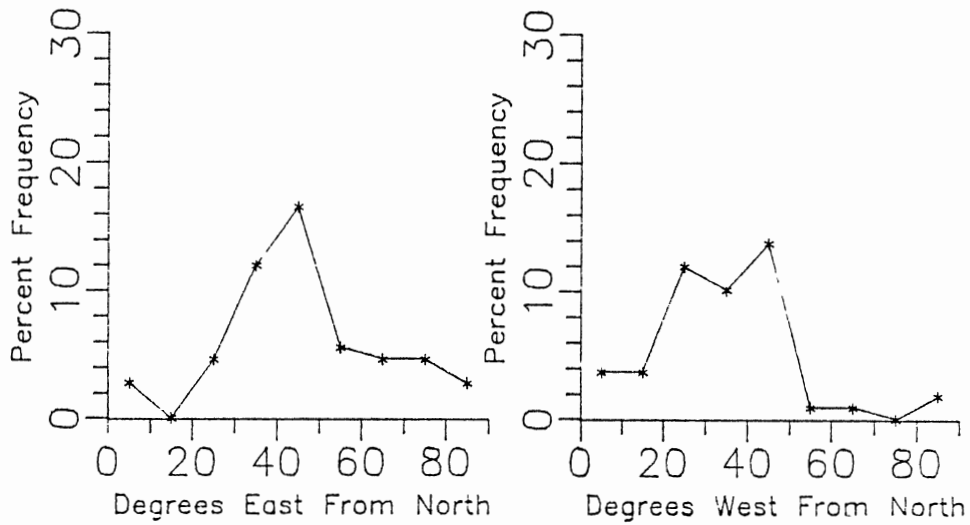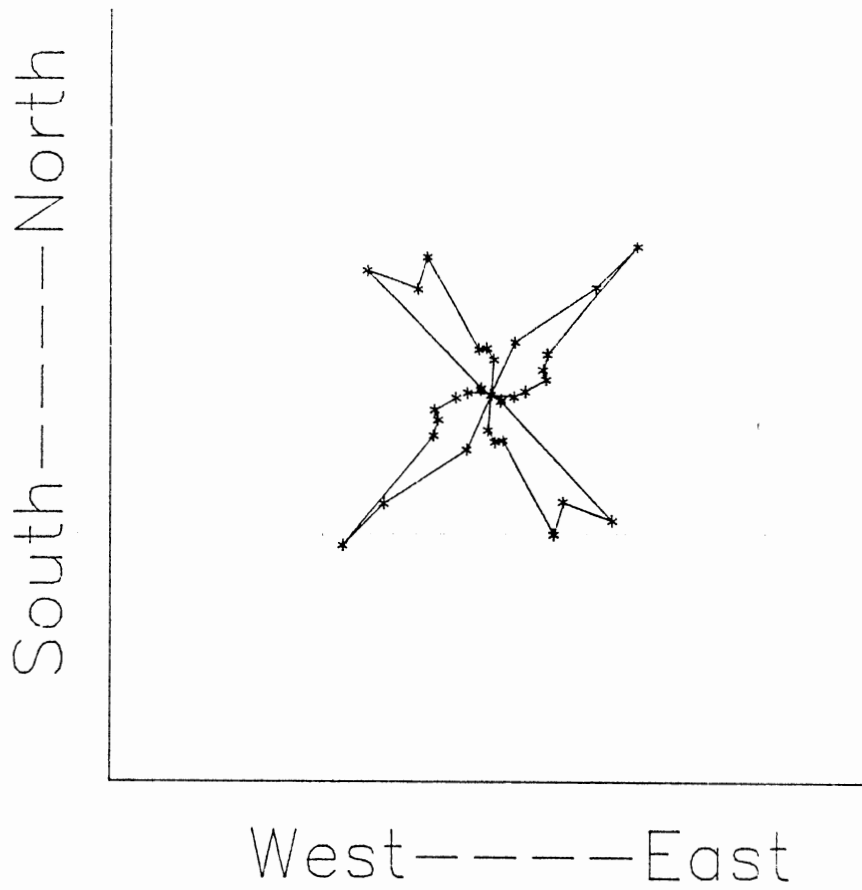
Figure 10. Rose Diagram and Frequency Distribution for Hunton Level Faults.

Field. Only eight of the most prominent faults in the project were identified by these authors.

Fault recognition in the project area is difficult because:

o   Fault planes are nearly vertical resulting in rare well bore intersections;

o   Fault displacement is nominal and easily over-looked.

Past investigations may have failed to observe many of the faults in the project area because:

o   Detailed fault identification was not the focus of previous investigations;

o   The large map contour intervals used provided insufficient detail to identify subtle fault-ing.

Hunton Production Trend Map (Plate 4)

Twenty-four-hour initial oil production for wells completed in the Hunton Group in the West Edmond Field was contoured to create Plate 4. Initial oil production was reported in several different formats. The data shown on Plate 4 have been classified according to type using the letters A through D as follows:

o   Class A: Cumulative production for a complete twenty-four-hour time period;

o   Class B: Hour by hour production rates;

43

o   Class C: Production rates for increments of several hours (ex. 200 b.o./4 hours, 150 b.o./6 hours etc.);

o   Class D: Single production values for time periods less than twenty-four hours.

A computer program was written that estimated twenty-four-hour oil production when data were reported hourly. The program converted production data versus time into log functions. Through a series of time-step iterations, a best-fit straight line was determined using the least squares method. Projected oil production values were added to the reported values.

If the data were reported as a series of time-step increments, then values were plotted on a graph. Twenty-four-hour initial production was estimated through extrapolation.

If a single production value was reported for an initial test period of less than twenty-four-hours, the average hourly production value was multiplied by twenty-four to estimate daily production. Because oil production declines with respect to time, this method results in values that tend to be higher than the actual daily production rate. To minimize error, data for less than eighteen hours were discarded.

Estimated production values are obviously subject to error. Precise accuracy, however, is not required because the production trend map was contoured on a broad 500

44

barrel per day interval. Class boundaries as assumed to be large enough so that individual data were correctly classified within the limits of the contour interval.

Linear patterns of high or low production trends extend throughout the West Edmond Field. Solid straight lines were drawn through the axis of lineations of high production. Dashed lines were drawn through the axis of zones of low initial well production. Linear trends in initial oil production are oriented in two principal directions, averaging N48°E and N36°W with standard deviations of 15.32 and 9.82, respectively (Figure 11).

The observed variations in initial production do not appear to be caused by differences in completion techniques, because operators used fairly uniform completion practices throughout the West Edmond Field. Also, the production patterns do not appear to be caused by variations in the thickness of the pay section because:

o   As shown on Table 2 and Figure 12, there is poor correlation between average well production with respect to total thickness of the Bois d'Arc-Frisco;

o   Areas of relatively thick Bois d'Arc-Frisco isopach values express little linearity, and there is no tendency for such areas to correspond with high production trends.

There is strong correlation between the Hunton fault system and the production lineament pattern. Eighty-six percent of all of the production lineaments corre-
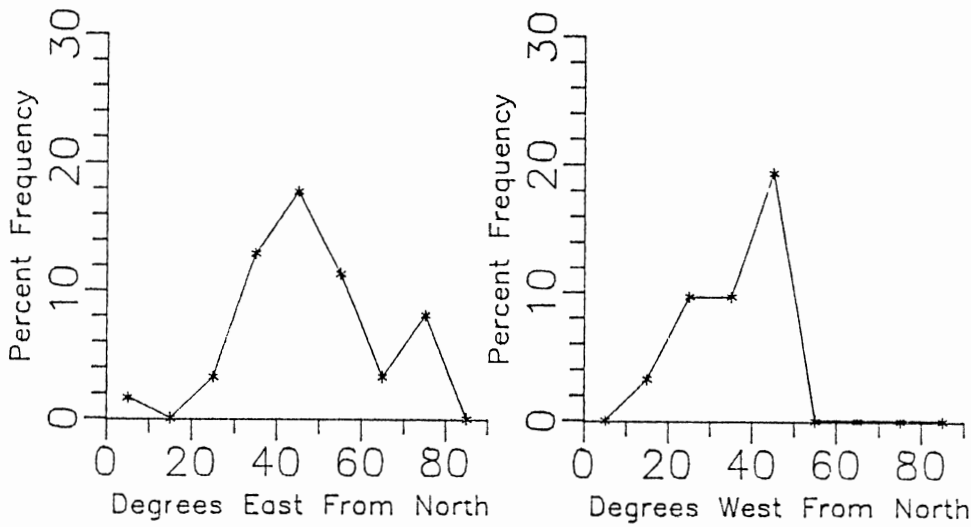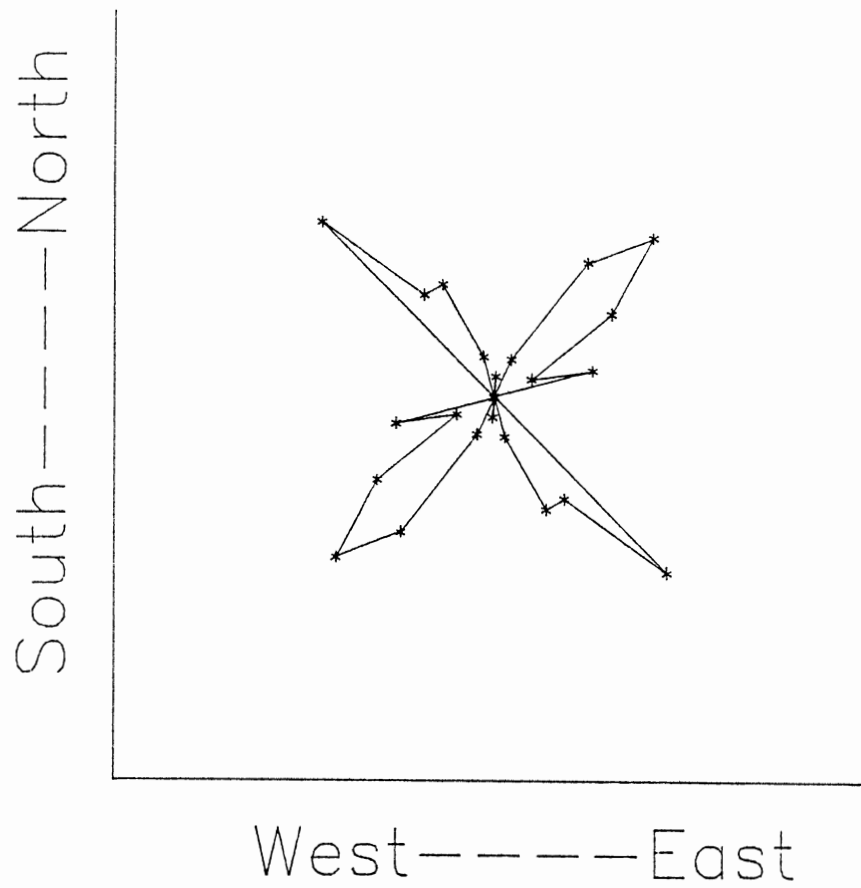
Figure 11. Rose Diagram and Frequency Distribution
for Hunton Production Lineaments.

TABLE 2

BOIS D'ARC-FRISCO THICKNESS VERSUS INITIAL OIL PRODUCTION IN BARRELS PER DAY

Upper Class Boundary Bois d'Arc-Frisco Thickness	Initial Oil Production Barrels/Day
20	539
30	582
40	933
50	760
60	1159
70	1061
80	913
90	535
100	830
110	523
120	820
130	853

Bois d'Arc–Frisco Thicknes

Versus Initial Production
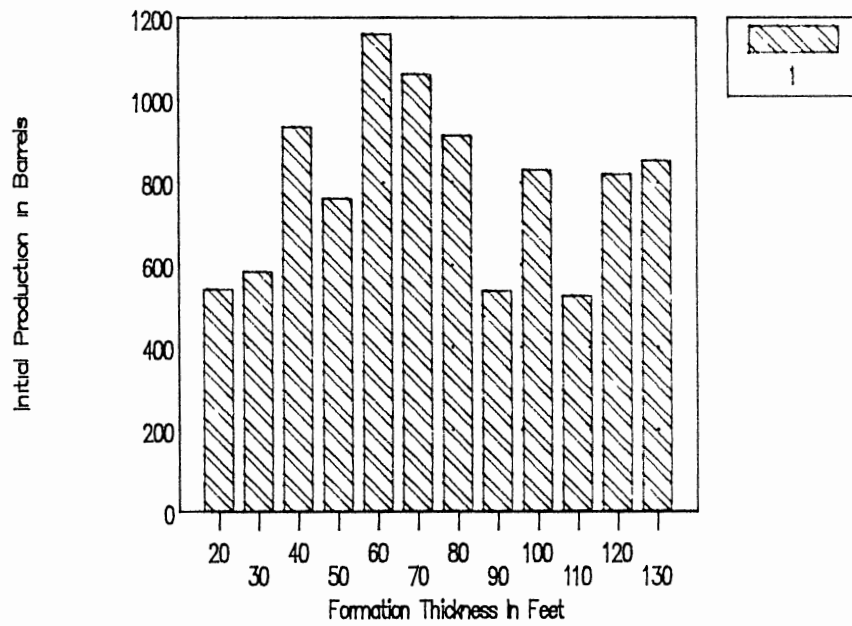
Figure 12. Histogram of Average Hunton Production
Versus Bois d'Arc Thickness.

sponded with faults identified in the Hunton. Figure 13 and Table 3 show an inverse relationship between initial well performance and distance from a fault.

High initial oil production in the vicinity of a fault is believed to result from fracture-enhanced permeability, that augments the productive capacity of the reservoir. The effect of natural fracturing on oil production is well documented. Wilkinson (1977), documented fracture-controlled production in the Spraberry Siltstone of the Spraberry Field in the Permian Basin of Texas (Figure 14). Well lithified, low-porosity limestones, such as the Hunton, tend to be brittle and especially susceptible fracture-enhanced porosity.

Many trends of low oil production simply represent areas of nominal fracturing between two parallel fault zones of high production. However, in some instances, trends of low initial oil production coincide with normal fault zones where significant portions of the hydrocarbon pay section have been fault removed.

Isopach Map Analysis

Isopach maps have been constructed for the Hunton Group and the Frisco-Bois d' Arc, Woodford, and Mississippi Formations. The analysis of these maps can be used to aid fault recognition and verification.

In the project area, much of the pre-Pennsylvanian surface was subjected to subaerial weathering during the

TABLE 3

INITIAL HUNTON PRODUCITON VERSUS
PERPINDICULAR DISTANCE TO
NEAREST FAULT

Average I.P. Per Class	Class Interval
1547	200
1486	400
1131	600
738	800
848	1000
578	1200
397	1400
277	1600
253	1800
220	2000
189	>2000

Figure 13. Histogram of Average Hunton Production
Versus Perpendicular Distance From
Nearest Fault.
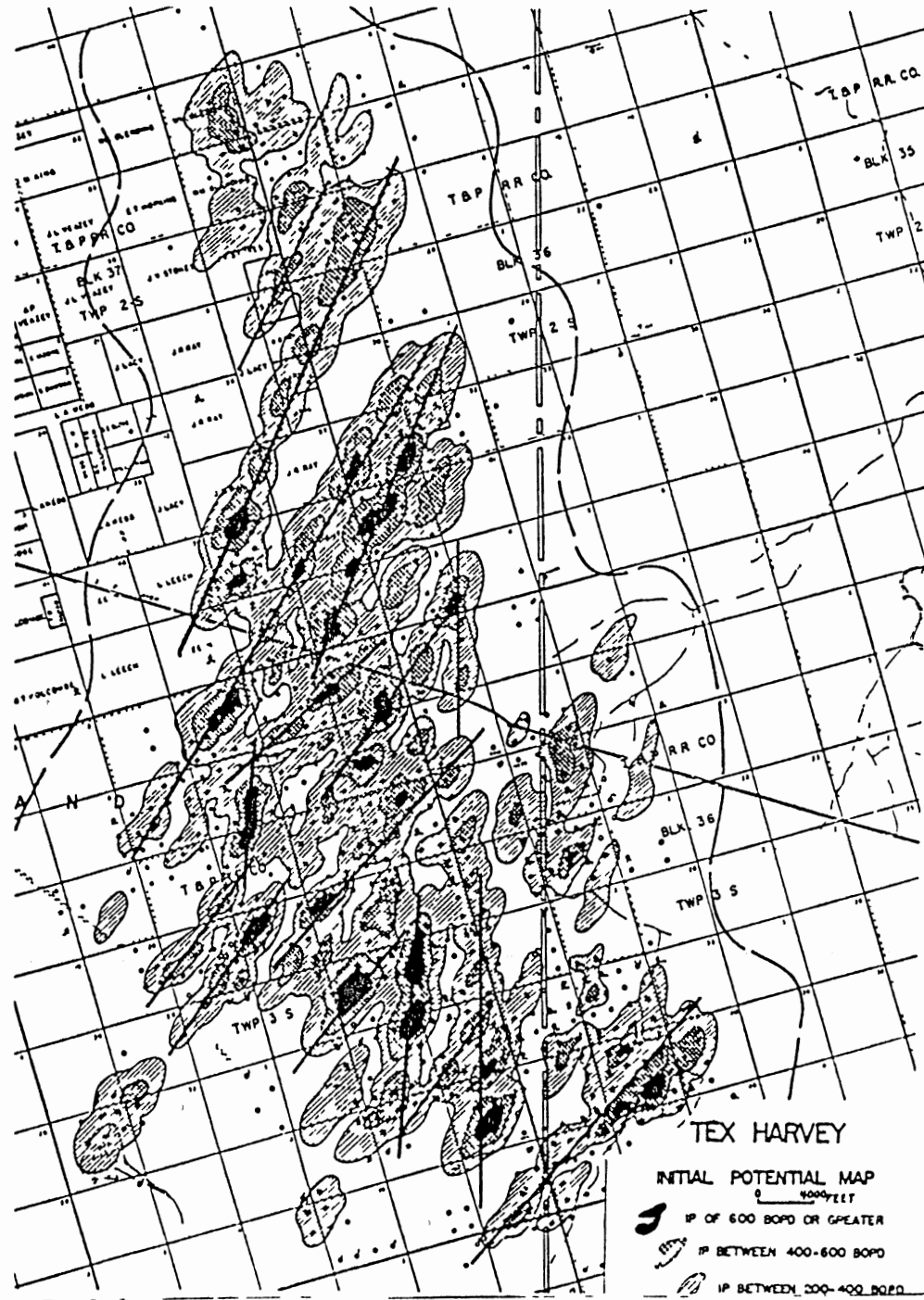
Figure 14.   Contour of Initial Well Production
Showing Fracture Control in the
Sprayberry Field, Texas.

Upper Wichita Orogeny, resulting in the development of a drainage network. The vestige of ancient stream channels are sometimes preserved in the geologic record as an incised stratigraphic section. Under these conditions, an isopach map can be considered a paleo-topographic map. Ancient drainage systems can, in some instances, be delineated by tracing networks of curvilinear thin isopach values.

Stream channels develop not randomly, but in response to many controlling factors. An important physical agent that typically governs channel development is geologic structure. Stream channels often develop along fault or fracture zones because fracture-weakened rock is susceptible to enhanced weathering and erosion.

Isopach map patterns were compared with the Hunton fault system. Paleo-channels corresponding to an identified fault were denoted by dashed lines. Isopach features suggesting actual fault separation were delineated with solid lines.

Hunton Isopach Maps (Plates 5 & 6)

Isopach maps for the total Hunton Group and the Bois d'Arc-Frisco are shown on Plates 5 and 6, respectively. Some changes in Hunton thickness may be depositional in origin; however, erosion from the Acadian and Upper Wichita unconformities accounts for most of the isopach variance. Where the Woodford exists, the Hunton was only

weathered during Acadian disturbance. Where the Woodford is absent, the Hunton was also subjected to weathering during the Upper Wichita event.

The Hunton Group attains a maximum thickness of 429 feet in the southwestern portion of the study area, but thins gradually towards the east. The Hunton is completely absent in Sections 12, 13, and 36 of T14N-R4W and Section 14, T15N-R4W. The Bois d'Arc-Frisco attains a maximum inferred thickness of 130 feet in the southwestern portion of the study area.

Many Hunton faults corresponded with isopach thins on the Bois d'Arc isopach. In addition, much of the Bois d'Arc subcrop margin coincides with the subsurface fault pattern. Fault control of the subcrop limit may have been caused by the differential weathering and removal of up-dip, highly fractured, limestone along fault zones.

Woodford Isopach (Plate 7)

Where the Woodford is capped by the Mississippi Limestone, the formation was not subjected to erosion during the Upper Wichita Orogeny. Where the Woodford was not weathered, isopach variability is mild, and thickness ranges from fifty to sixty feet. Across a one- to two-mile wide arc, through the center of the project area, the Woodford was subaerially exposed and the isopach pattern becomes erratic.

The erosional pattern on the Woodford surface coincides well with many Hunton faults. The updip pinch-out of the Woodford lies on a northeast diagonal across T14N-R4W, then south. As in the case of the Hunton, the location of the updip erosional limit of the Woodford appears to coincide with several faults.

Mississippi Limestone Isopach (Plate 8)

The Mississippi Limestone was subjected to weathering during Upper Wichita Orogeny everywhere in the study area. The formation attains a maximum thickness of 275 feet in the northwestern portions of the study area, and gradually thins towards the east-southeast at a rate of approximately fifty feet per mile.

Excellent correlation exists between isopach patterns of the Mississippi and the Hunton fault system. The influence of fault structure on the location of the updip limit of the Mississippi is conspicuous. The position of nearly all the updip zero isopach margin parallels a series of Hunton faults.

Base of Permian Structure Map (Plate 9)

It was recognized that many of the faults that are present at the Hunton level do not extent vertically to the surface. By examining the structure of a shallow horizon, insight could be gained as to which faults were, in fact, pervasive.

A structure map was prepared on a marker bed thought to represent the base of the Permian System. The marker bed consisted of four thin, laterally-persistent limestone beds at a depth of approximately 1,500 feet below the surface.

The methods used to identify faults at the base of the Permian were generally the same as the methods used for fault delineation in the Hunton. Faulting at the base of Permian level is more difficult to verify than the faulting within the Hunton for several reasons, including:

o   The lack of laterally contiguous marker beds;

o   Small vertical fault slip;

o   Nearly vertical fault planes;

The fault pattern established for the Hunton was used to highlight probable áreas where faulting might be expected within the Permian. Based on the structural configuration of the Permian, a judgment was made as to the probable presence of a pervasive fault.

The pattern of folding for the base of Permian is similar to that of the Hunton, but much milder. Uplifted areas in the Hunton are structurally positive in the Permian section, but with much less absolute relief. The regional dip of the base of Permian is oriented towards the southwest at a rate of fifty to sixty feet per mile.

The amount of vertical displacement at the Permian level is generally much less than the amount of vertical displacement for any given through-going fault at the Hunton level (Figure 15). Increasing fault displacement with depth is apparently produced by:

o   Differential erosion and peneplaination of pre-Pennsylvanian aged formations during the Upper Wichita unconformity;

o   Differential deposition across fault boundaries, coupled with periodic fault reactivation and quiescence.

In many instances, the intersection of the fault plane at the base of Permian is slightly east of the fault plane intersection at the Hunton surface. This indicates near-vertical fault planes with a slight westerly inclination.

Out of 114 faults identified in the Hunton, seventy-two (63%) are interpreted to penetrate the base of the Permian. Average base of Permian fault orientations are N48^{o}E and N35^{o}W (Figure 16).

Legend markings within figure:

Surface

±20 ft throw

Lower Wichita
Unconformity

±100 ft throw
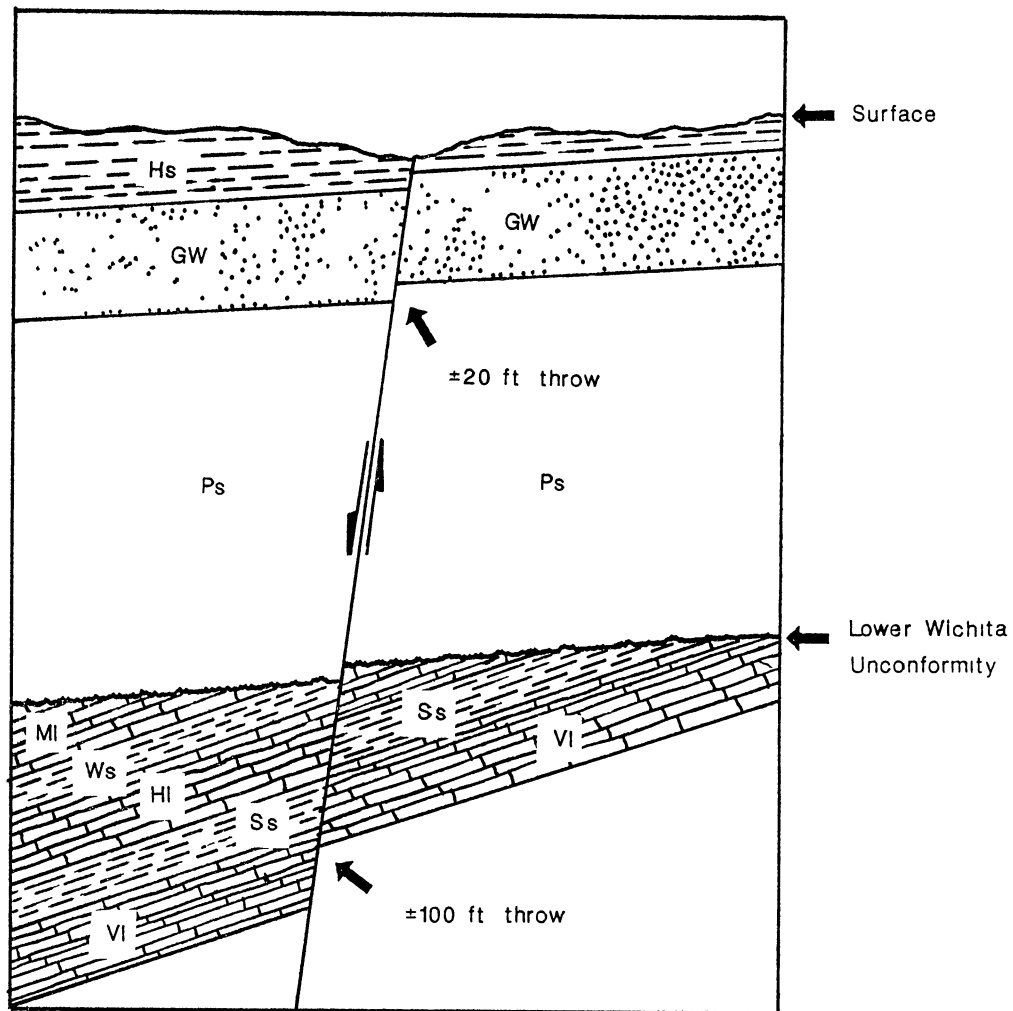
LEGEND

Hs Hennessey shale   Hl Hunton lime
GW Garber/Wellington   Ws Woodford shale
PS Pennsylvanian Shale   Ss Sylvan shale
Ml Mississippi lime   Vl Viola lime

Figure 15.   Schematic Cross-Section Showing Increasing
Fault Displacement With Depth.
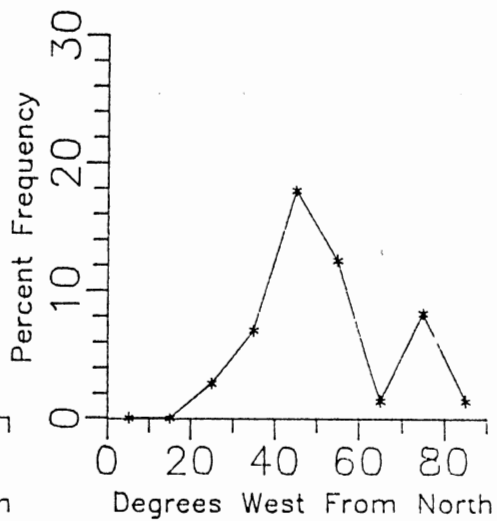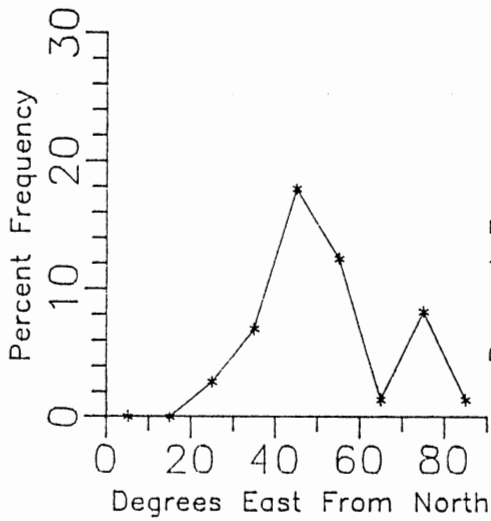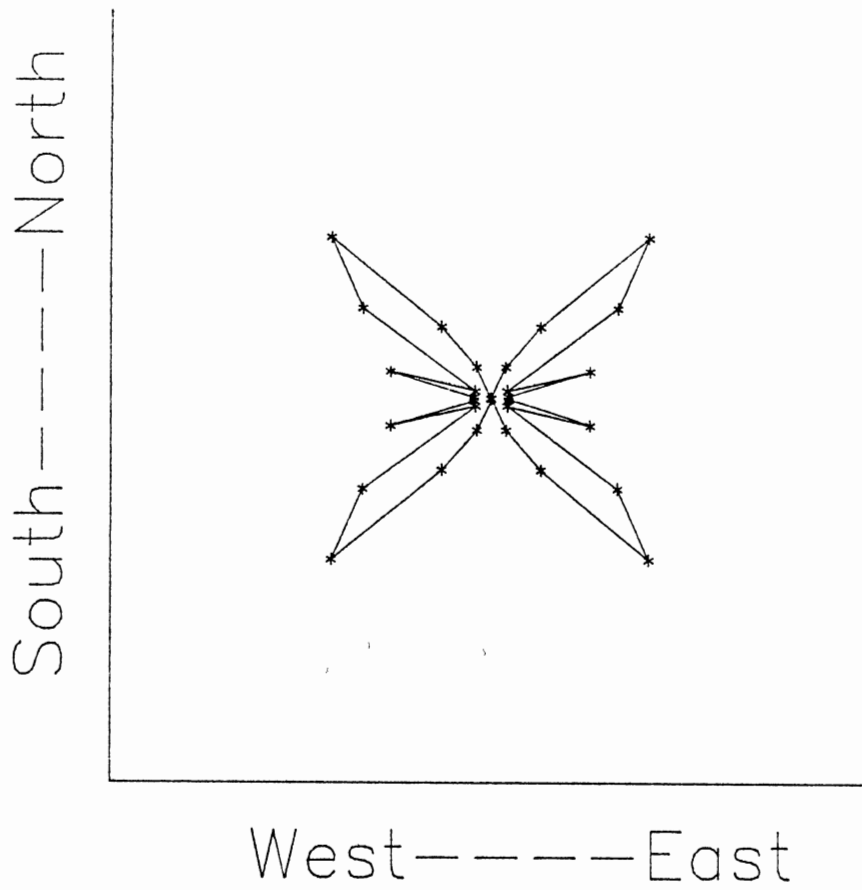
Figure 16. Rose Diagram and Frequency Distribution
for Base of Permian Level Faults.

CHAPTER III

REMOTE SENSING

Introduction to Lineament Analysis

A lineament is a mappable simple or composite linear feature of a surface, whose parts are aligned in a straight or slightly curving relationship, which differs distinctly from the patterns of adjacent features and presumably reflects a subsurface phenomenon (O'Leary, and others, 1976).

Surface features making up a lineament may be geomorphic (caused by relief) or tonal (caused by contrast differences). Geomorphic features may be land-forms, the linear boundaries between different types of terrain, or breaks within a uniform terrain. Straight stream valleys and aligned valley segments are typical geomorphic expressions of lineaments.

A tonal lineament may be either a straight boundary between areas of contrasting tone or a stripe against a background of contrasting tone. Differences in vegetation, moisture content, and soil or rock composition account for most tonal contrasts (Sabins 1978).

60

Even if the fault plane can not be directly ob-
served, certain secondary affects of faulting often can
be detected using remote sensing. Stream orientation can
be determined by the underlying structural fabric.
Fracturing also can alter soil moisture content, which
can affect vegetation type and vigor.

For this project, lineaments were analyzed using
both Landsat imagery and high-altitude, near-infrared
photographs. Lineations were identified and marked. Care
was exercised to exclude anthropomorphic features such as
roads or man-made channels.

Landsat Lineament Analysis (Plate 10)

Band 7 panchromatic Landsat imagery was used to
identify visually lineaments in the project area. Band 7
imagery is low infrared, capable of detecting radiation
wavelengths between 0.8 and 1.1 micrometers.

Zall and Russell (1981) determined that band 7
imagery was the best spectral band for fracture and fault
delineation. This infrared band is especially sensitive
to both water and vegetation. On panchromatic imagery,
water is generally black or dark gray, and vegetation is
light gray to white.

The original Landsat imagery, at a scale of
1:1,000,000 was too large to allow meaningful lineament
interpretation over the project area. Therefore, the
imagery was photo-enlarged to a scale of 1:120,000. Any

61

additional enlargement would have resulted in unaccept-
able loss of resolution.

The spatial resolution of Landsat imagery is deter-
mined by several factors, including a seventy-nine meter
square ground resolution cell, atmospheric conditions,
playback, and reproduction of the imagery. In general,
the spatial resolution ranges from 200 to 250 meters;
however, smaller features can be detected on many
images. Narrow objects, such as highways and canals, can
be detected where the contrast is optimum.

One-hundred thirty-three lineaments were identified
on the Landsat imagery shown on Plate 10. Both northeast
and northwest conjugate sets were found. Average linea-
ment orientations were N43^{o}E and N41^{o}W (Figure 17).
Lineament orientation data is shown in Appendix 1.

Lineaments corresponding to faults are shown as
thick lines on Plate 10. Lineaments not related to fault-
ing are shown as thin lines. Of the seventy-two faults
identified on the base of the Permian structure map,
thirty-nine (54%) were identified using Landsat imagery.
Although there were 133 Landsat lineaments found, only
forty-five (34%) coincided with base of known faults.

Nearly all of the Landsat lineaments corresponded to
stream channels, with the balance comprised of tonal
variations. The ratio of northeast to northwest linea-
ments is 2:1. The regional drainage direction is towards
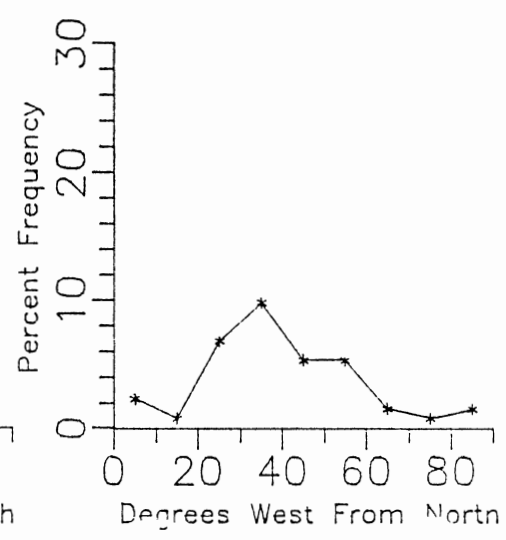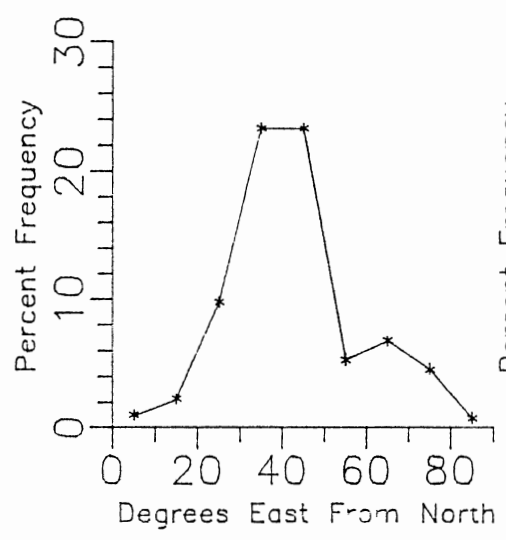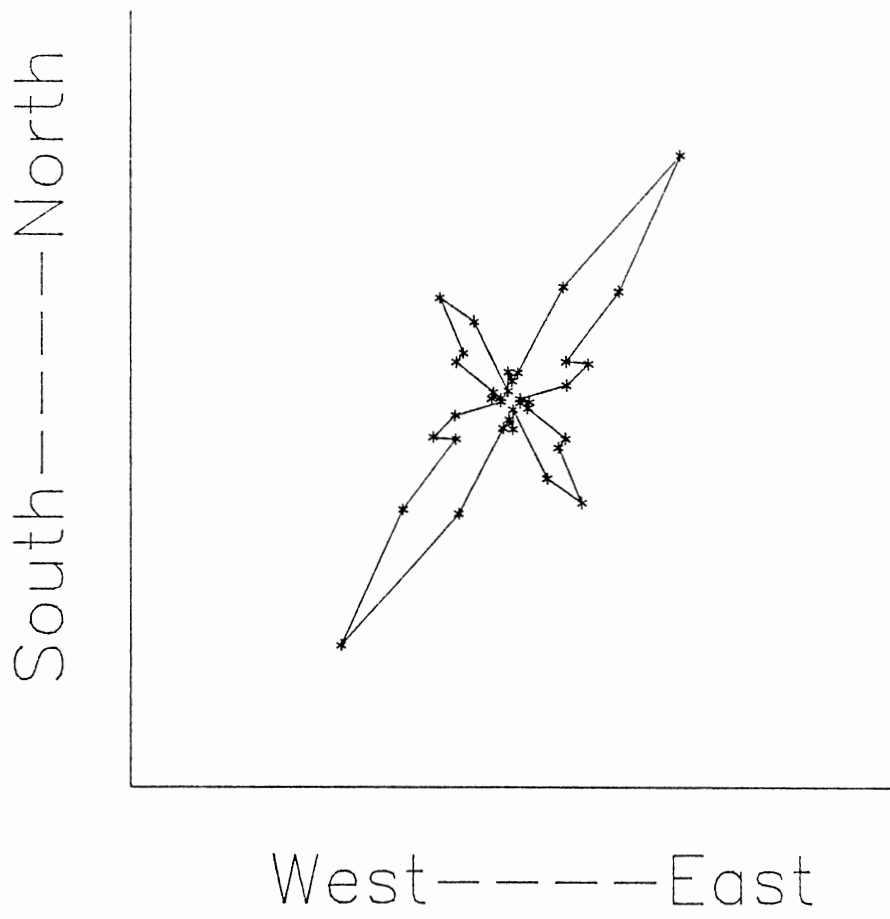
Figure 17. Rose Diagram and Frequency Distribution
for Landsat Lineaments.

the northeast, and the largest streams are oriented in that direction. Because of limitations in image resolution, the larger drainage features are expressed better on the imagery, resulting in the preferential representation of northeast oriented streams.

The frequency distributions for Landsat lineaments and base of Hunton fault orientations were statistically compared to test the hypothesis that no statistical difference exists between the two populations. This hypothesis was evaluated using the standard F and Student's T tests (Table 4). Although only 34% of Landsat lineaments were found to correlate to subsurface faults, lineament and fault orientations are essentially the same.

High Altitude Infrared Lineament
Analysis (Plate 11)

The infrared images used in this research were photographed as part of the Airborne Instrumentation Research Project (AIRP). The AIRP program was originally sponsored by the National Aeronautics and Space Administration (NASA) to provide data in support of satellite programs, such as Landsat or Skylab. Imagery was made available by the Center for Applied Remote Sensing (CARS), located on the Oklahoma State University campus.

The term "high altitude" refers to the normal cruising altitude of the aircraft commonly used in obtaining

64

TABLE 4

RESULTS OF STATISTICAL ANALYSIS USING
STANDARD F AND STUDENT'S T TESTS

Source	F Calculated	F.01	F.05	Ho.
N.E. Landsat	1.25	1.61	1.96	Pass
N.W. Landsat	1.03	1.48	1.76	Pass
N.E. Infrared	1.01	1.44	1.68	Pass
N.W. Infrared	1.13	1.48	2.06	Pass
N.E. Drainage	1.42	1.45	1.69	Pass
N.W. Drainage	1.11	1.46	1.75	Pass

Source	T Calculated	T.05	Ho:
N.E. Landsat	1.27	2.01	Pass
N.W. Landsat	1.31	1.99	Pass
N.E. Infrared	2.01	2.03	Pass
N.W. Infrared	2.06	1.98	Fail
N.E. Drainage	1.76	2.00	Pass
N.W. Drainage	0.97	2.00	Pass

this type of photography, the RB-57F, U-2, and the Lear Jet. Typical operating altitudes range from 40,000 to 70,000 feet.

Like conventional color reversal film, color infrared film has three emulsion layers sensitive to blue, green, and red. The red, or magenta-forming, layer is primarily sensitive to photographic infrared energy of wavelengths from 0.7 to 0.9 micrometers, the reflected infrared spectral band. The cyan-forming layer is sensitive to red light, and the yellow-forming layer is sensitive to green light. All three film layers are sensitive to blue light, but this spectral band is largely eliminated by placing a yellow (minus blue) filter over the camera lens.

In effect, color infrared film generates a color shift towards the red end of the spectral band. Infrared (not visible to humans) is displayed as red, normally red objects appear green, and green objects appear blue. Objects that are naturally blue appear to be black.

The most striking difference between color infrared photographs and normal-color film is the red color of healthy vegetation in the infrared photograph. Blue and green light are absorbed by the leaf structure in the process of photosynthesis. Up to twenty percent of the incident green light is reflected, causing the familiar green color of leaves. However, spectral reflectance increases abruptly in the photographic infrared region.

Though much more infrared radiation is reflected, vegetation appears to be green because human eyes can not detect infrared emissions.

Sensitivity to photographic infrared emissions facilitates identification of vegetation type and vigor. Infrared is especially useful in geologic studies because vegetation patterns can indicate the nature of the underlying rock and soil units.

Because infrared radiation is adsorbed by clear water, rivers and streams appear to be dark blue or black on infrared color photographs. This dark color contrasts well with the red signature of adjacent vegetation. The ability to enhance the difference between vegetation and water is particularly valuable for mapping drainage patterns. Damp ground may be recognized on color infrared photographs by its relatively darker signature caused by infrared adsorption.

The nominal resolution for infrared photographs taken at an altitude of 65,000 feet is reported to be as small as 0.3 meters (Richason 1978). This high resolution, coupled with the relatively large scale of 1:60,000, permits detailed geologic analysis.

The photography was available as a strip of overlapping scenes along north-south flight lines. Several frames were required to provide coverage over the entire study area. Lineament analysis was performed using 1:60,000 scale photographs. To allow comparison with

other maps, the original lineament map was enlarged to a scale of 1:2,400.

Three-hundred seventy lineaments were identified on color infrared photographs (See Plate 11). Average lineament orientations were N41°E and N41°W (Figure 18). Basic lineament orientation data is shown on Appendix 1.

Lineaments corresponding to subsurface faults are shown as solid lines on Plate 11. Lineaments not related to faults are dashed. Of seventy-two faults, forty-two (58%) were correctly identified by color infrared lineaments. Of the total field of 370 infrared lineaments, only forty-five (12%) corresponded to subsurface faults.

The high contrast ratio and excellent spatial resolution of color infrared facilitates detailed lineament analysis resulting in the identification of numerous lineaments. A great number of color infrared lineaments correspond to smaller drainage features not visible on lower resolution Landsat images.

The abundance of color infrared lineaments increases the possibility that lineaments and faults may correlate by random chance alone. As the number of non-significant lineaments increases, it decreases greatly the chance that an interpreter, with no foreknowledge of subsurface structure, can discern which lineaments truly correspond to fault structure.

There is a tendency for faults to be represented on color infrared imagery as a series of discontinuous
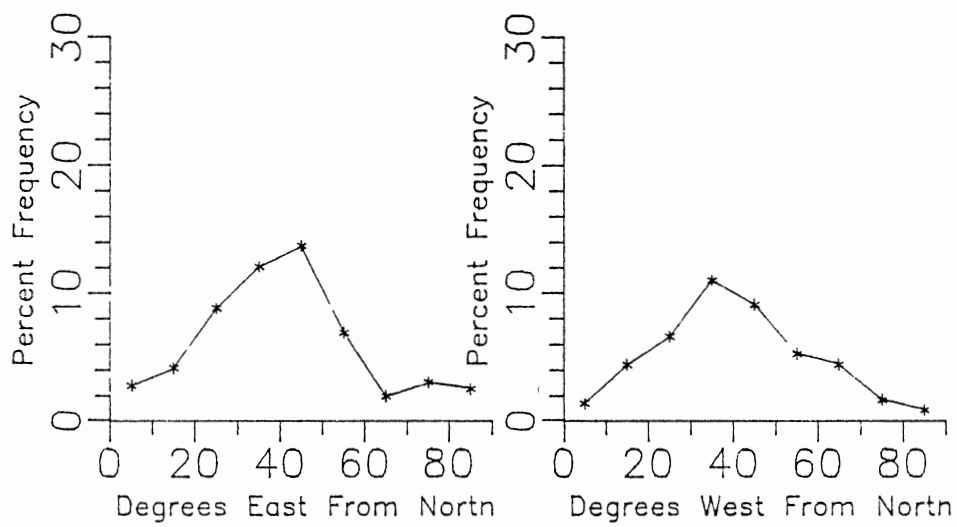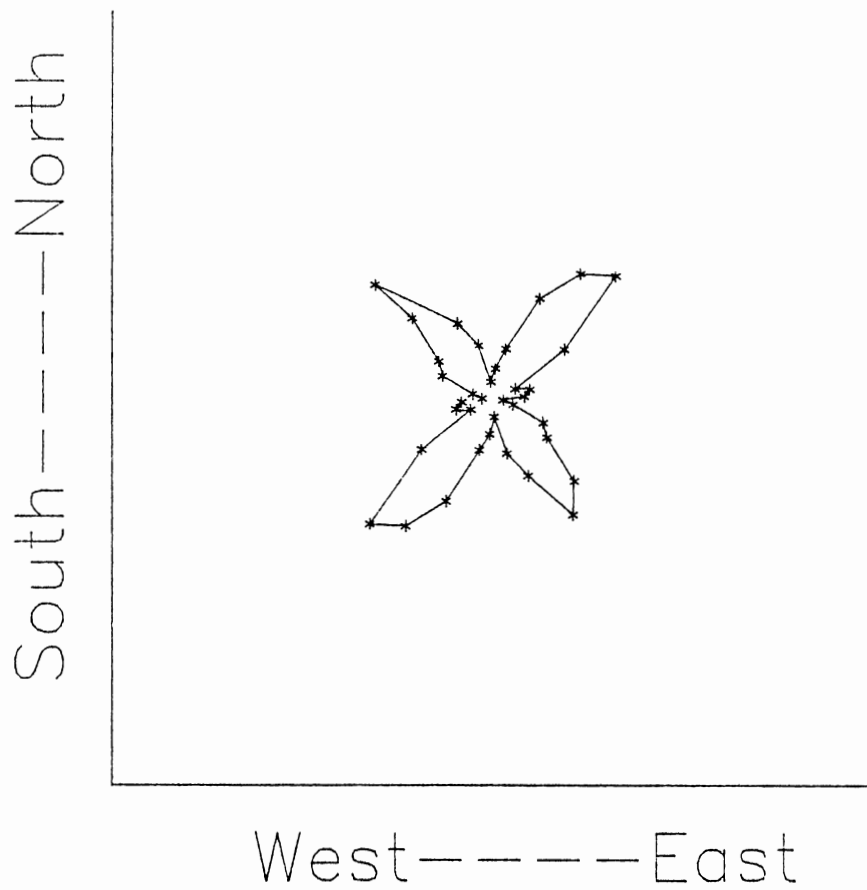
Figure 18. Rose Diagram and Frequency Distribution
for Color Infrared Photograph.

lineaments, making interpretation difficult. On Landsat imagery, a single lineament commonly represents a single fault.

A statistical evaluation was made to test the hypothesis that there was no difference between color infrared lineament and Hunton fault orientations. The standard F test and Student's T analysis were used. Results are shown on Table 4.

Statistical tests infer that there is no difference between color infrared lineament orientation and the underlying orientation of faults in the Hunton, with one exception. Both northwest and northeast data sets passed the F test. The northwest data set passed the Student's T test but the northeast data set failed. Further, the G-1 test for normal distribution failed for the northwest data set and parametric analysis may not be applicable for that group.

Topographic Fault Trace Map (Plate 12)

A comparison was made between fault features interpreted on the base of Permian structure map, Plate 9, and the surface physiography expressed on a U.S.G.S. 7-1/2 minute topographic map. The result is a projection of some subsurface faults to the surface (Plate 12).

Each subsurface fault was visually examined to determine if there was topographic expression coincident with the fault's location and orientation. A small amount

of lateral shift was permitted. This allowed for horizontal drift created by an inclined fault plane passing through the stratigraphic section which separates the base of Permian from the surface.

Of seventy-two base of Permian faults, portions of forty-five faults (63%) had discernible surface expression. Such fault expression commonly correlates with straight channel segments along the largest streams. Across T14N-R4W, fault systems parallel much of Deer Creek, Walnut Creek, Bluff Creek and Bloody Rush Creek. In T15N-R5W, many tributaries of Cottonwood Creek are associated with subsurface faults.

Drainage Lineament Map (Plate 13)

The overall stream pattern in the West Edmond Field is dendritic; however, individual stream channels are comprised of numerous linear elements. Straight channel patterns may infer underlying structural control. Fractures, faults, or joints have been shown to control drainage development (Dolan 1978, Morasawa 1985, Judson and Andrews 1955).

Plate 13 was created to determine if a relationship between stream channel orientations and subsurface faults exists in the project area. The map was made by initially highlighting the natural drainage pattern. Straight lines were subsequently drawn through the center of all straight, second-order or higher stream segments.

71

The classification method used to determine stream order was based on Harden (1945). First-order streams are defined as "unbranched fingertips" of streams in the headwaters of a drainage basin. Two first-order streams may join to form a second-order; two second-order streams will combine to form a third-order; and so on.

The decision to measure linear stream channels of only second order rank or higher was based on two premises:

o   As a function of practicality, many first-order streams were simply too short to interpret linearity visually;

o   Research by Woodruff and Parizek (1956) shows that first-order channels are not sensitive to rock structure, and tend to develop in response to surface slope.

As drainage networks develop, higher-order streams become sensitized to underlying structures. A stream will tend to enlarge in accordance with weaknesses of the underlying rock. Or, alternatively, those channels that can take advantage of structural weaknesses grow at the expense of those which do not.

A total of 360 streams were measured: 203 northeast- and 157 northwest-trending channels. Average orientations were N42°E and N39°W with standard deviations of 16.52° and 15.34° respectively (Figure 19). Basic stream orientation data is shown in Appendix 1.
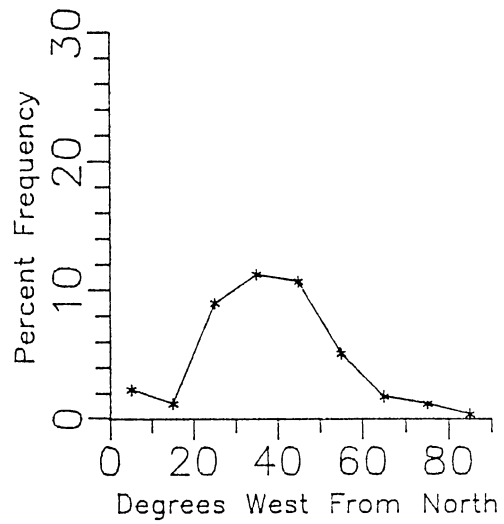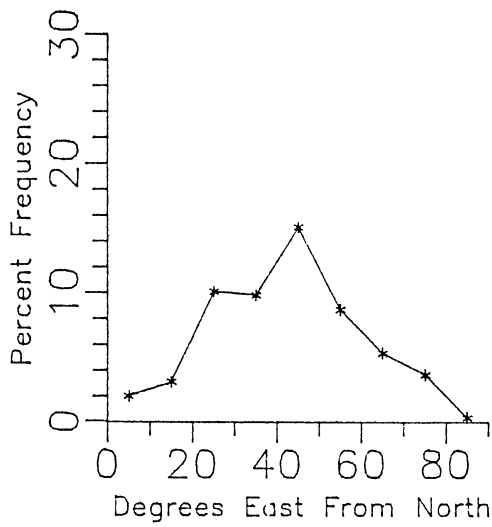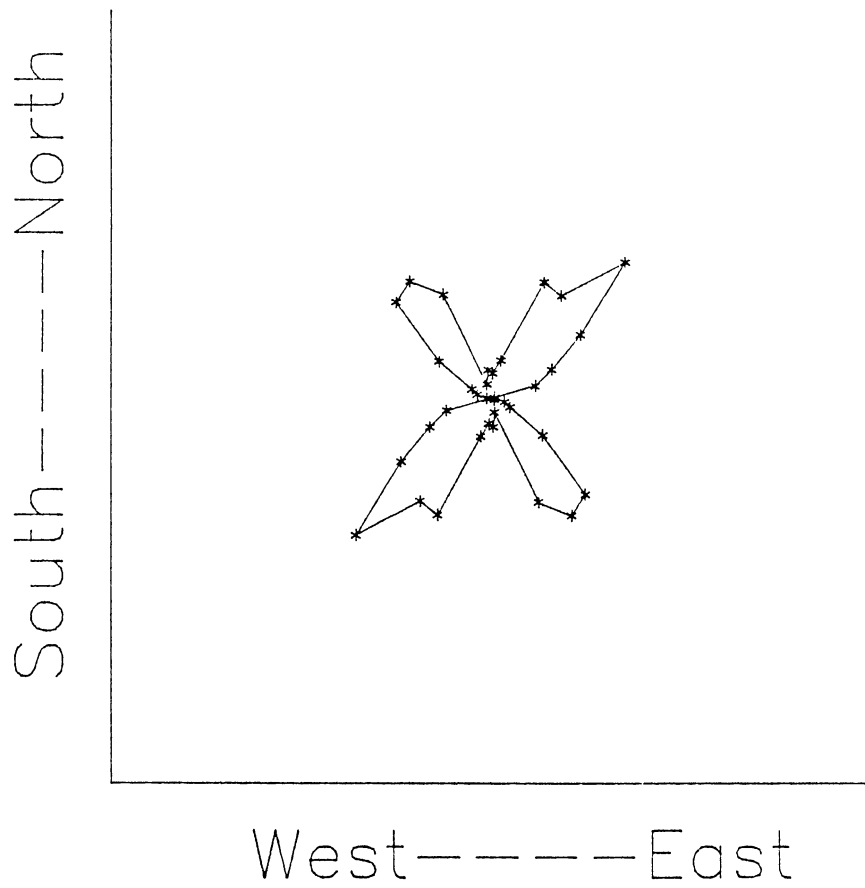
Figure 19.   Rose Diagram and Frequency Distribution
for Drainage Lineaments.

There is no statistical difference between stream and Hunton fault orientations when respective data sets were compared using the standard F analysis for variance and the Student's T test for means (Table 4). It is assumed that stream channels in the project area have adjusted to underlying structural components such as faulting or fracturing.

Plate 13 shows that many of the highest-order streams in the study correlate with surface projections of several prominent subsurface faults. It is likely that the highest-order streams in the study area occupy their current positions as a function of differential erosion of fractured bedrock associated with faulting.

Although a relationship appears to exist between some high-order stream channels and faults no direct association exists between discrete faults and low-order streams. However, because low-order stream orientations conform to the overall fault orientation, it is suggested that smaller-order streams developed in response to some structural control, presumably shallow joints or fractures.

Surface bedrock exposures often display enhanced weathering along joints and fractures (Figure 20). Over prolonged periods of time, differential erosion along fracture planes could ultimately dictate stream development.

Figure 20. Photograph Showing Enhanced Weathering Along Fractures in the Garber Sandstone.

CHAPTER IV

DRY-WEATHER FLOW STREAM CONDUCTIVITY PROFILE

Purpose of Method

Though certain lineaments correlate with specific subsurface faults, many more lineaments can be interpreted on remote sensing images than can be accounted for by subsurface faulting. Using remote sensing alone, it is impossible to specify which lineaments correspond to pervasive fault structure.

Discerning which lineaments correspond to fractured or faulted strata requires additional data. This supplemental information could be obtained by additional surface or subsurface geologic investigations.

There is an abundance of quality subsurface data in the West Edmond Field area; however, such information is atypical for most of the United States. Subsurface geologic or geophysical studies of sufficient detail to delineate subsurface faults are time-consuming, expensive, and subject to human interpretation and error. Moreover, surface verification of faulting is often hampered by vegetative or soil cover. An alternative method of fault verification is the use of stream water

conductivity surveys made during dry-weather flow.

In the project area, remote sensing lineaments often coincide with surface drainage features including many perennial streams. During dry-weather flow conditions, variations stream water conductivity may reflect local alterations in ground water chemistry induced by adjacent faulting. Variations in water chemistry could be detected by taking a series of closely-spaced conductivity measurements along a stream reach.

Conceptual Model

The stream conductivity profile method of fault verification is based on elementary hydrogeologic and geochemical principles. During dry-weather flow, the ground water contribution constitutes total stream discharge. Under dry-weather flow conditions, the water, at any given point along a stream, is comprised of a cumulative mixture of released ground water from up-stream. In essence, stream water represents an aggregate cross-section of ground water chemistry along the flow path. If a fault significantly alters local ground water conditions, then gross changes water chemistry might be detected by monitoring conductivity along the stream channel.

Water conductivity is a rough indicator of dissolved solids content. Increasing mineral concentrations increase the conductance of water as a linear function.

Conductivity can be measured easily in the field by using a portable conductivity meter.

Following a rainfall, a fraction of the total precipitation will penetrate the upper soil layers and become a source of ground water recharge. Ground water will migrate in the direction of lower head, generally discharging in local streams.

Ground water moving through the subsurface environment will interact with the host rock matrix to dissolve, transport, and/or deposit mineral constituents. Given sufficient time, systematic variations in the water chemistry occur along the flow path resulting in a type of chemical evolution. Because rainwater entering an aquifer is typically very low in dissolved mineral content the ground water ion concentration nearly always increases along the flow path by dissolution of mineral salts from the rock matrix.

The most important factors controlling the chemical composition of ground water include:

o   Temperature

o   Pressure

o   Surface contact area between rock and water

o   Time in contact with sediment

o   Amount and distribution of soluble minerals

o   Antecedent water quality.

Although no aquifer exhibits perfectly homogeneous conditions, temperature, pressure, and antecedent water quality should remain relatively constant. Factors that may control ground water chemistry and that may be affected by faulting include the surface area between rock and water, time in contact with the rock matrix, and the amount and distribution of soluble minerals. Faulting may affect local ground water chemistry by:

o   Juxtaposing rocks of variable lithology, thereby altering the distribution of soluble minerals;

o   Increasing ground water velocity, thereby diminishing time in contact with the rock matrix;

o   Creating preferential flow pathways through the aquifer via fractures diminishing surface area contact;

o   Providing an avenue for overpressured, mineralized water from deep aquifers to migrate into shallow aquifer systems.

Field Test and Results

Dry-weather flow conductivity analysis for fault verification was tested along a 3.75-mile section of Deer Creek. The test site spanned the northeast corner of Section 2, T13N-R5W, to the northwest corner of Section 31, T14N-R4W (Figure 21). Through the central portion of this interval, lineaments, found on both Landsat and color infrared imagery, corresponded to a fault identified in the subsurface.

79

Figure 21. Topographic Map Showing Water Conductivity Values Along Stream Traverse.
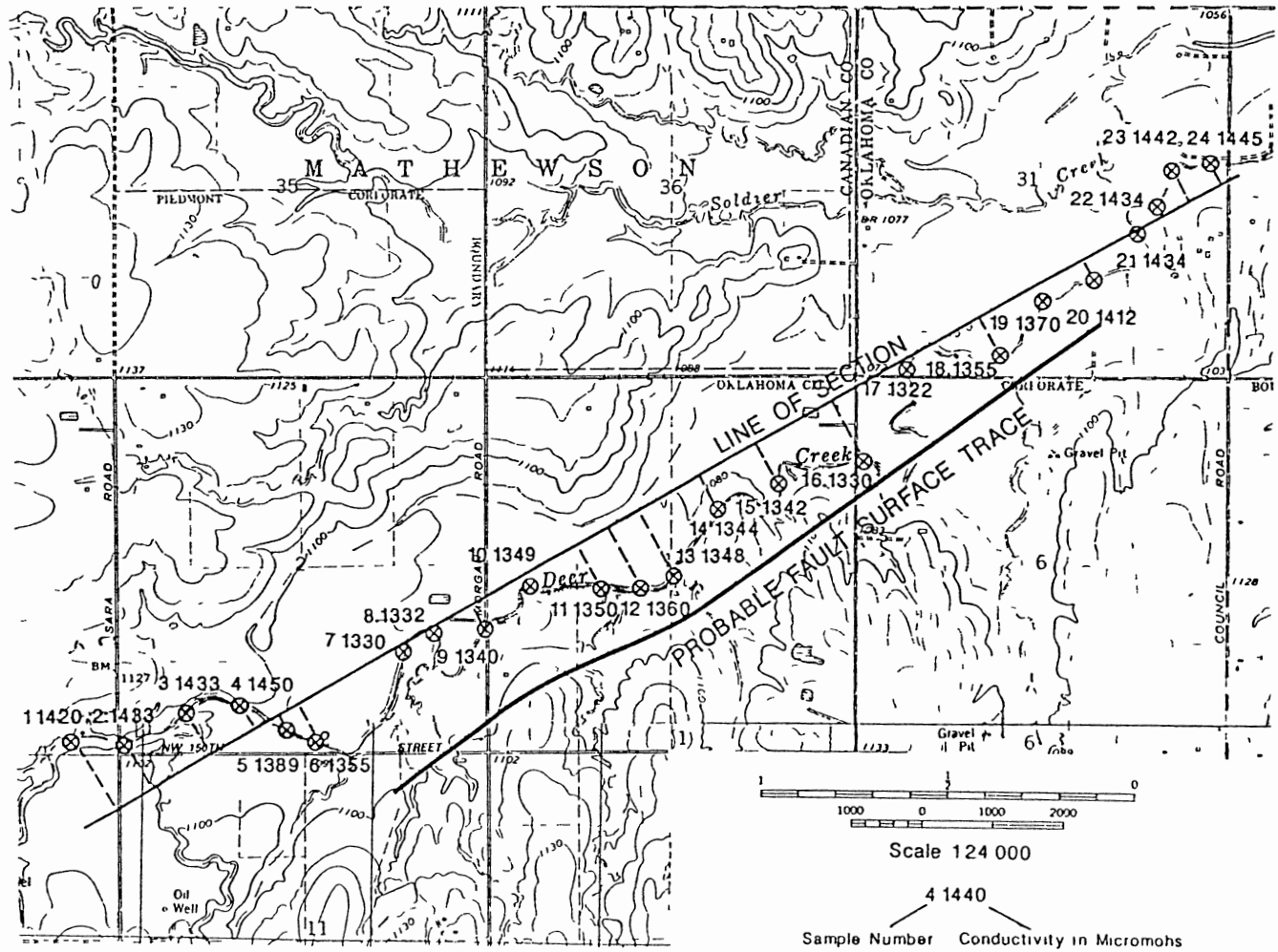
Dry-weather flow stream conditions were established using the following equation from Graham (1985):

$$N=A^{0.2}$$

Where:

        N=number of days after a peak when surface run-off ceases.

        A=basin area in square miles.

The drainage area upstream from the sampling traverse was measured and found to be 37.9 square miles. Applied to the equation above,

$$N=37.9^{0.2}$$
$$N=2.06 \text{ days}$$

Water was sampled during an arid summer on August 14, 1988, following several weeks without rain. Dry-weather flow conditions were assured.

Twenty-four water conductivity readings were made at various intervals, averaging about 900 feet apart. Sampling locations were selected based upon their ability to be recognized in the field on a topographic reference map.

The results of the stream conductivity measurements are shown on Table 5 and presented graphically on Figure

22.   Stations one through four are located upstream from the inferred fault zone. The water conductivity of station one was 1420 micromhos. Downstream, conductivity increased steadily to 1450 micromhos at station four.

Stations five through twenty parallel the suspected fault trace. Through this interval stream conductivity gradually diminished from 1389 micromhos at station five to 1330 micromhos at station seven. Water conductivity did not rise above 1360 micromhos until station eighteen.

Stations eighteen through twenty-two are downstream from the fault zone. From a low of 1320 micromhos at station seventeen, the water conductivity steadily increased to a maximum of 1445 micromhos at station twenty-two.

Most of the bedrock along the traverse was covered with vegetation, soil, or alluvium, but some outcrops were visible. Bedrock exposures were characteristic of the Hennessey Formation, consisting predominantly of maroon shale with thin lenses of shaly sandstone and siltstone.

The Hennessey is exposed upstream from the fault zone, between sample stations 1 and 2, in a steep twenty to twenty-five feet high cut bank (Figure 23). The outcrop consists of red to maroon shale, with thin lenses of fine grained sandstone and siltstone. At this point there are only a few fine fractures and joints.

TABLE 5

STREAM CONDUCTIVITY DATA BY STATION

Station Number	Conductivity Micromhos/cm
1	1420
2	1433
3	1433
4	1450
5	1389
6	1355
7	1330
8	1332
9	1340
10	1349
11	1350
12	1360
13	1348
14	1344
15	1342
16	1330
17	1322
18	1355
19	1370
20	1412
21	1434
22	1434
23	1442
24	1445
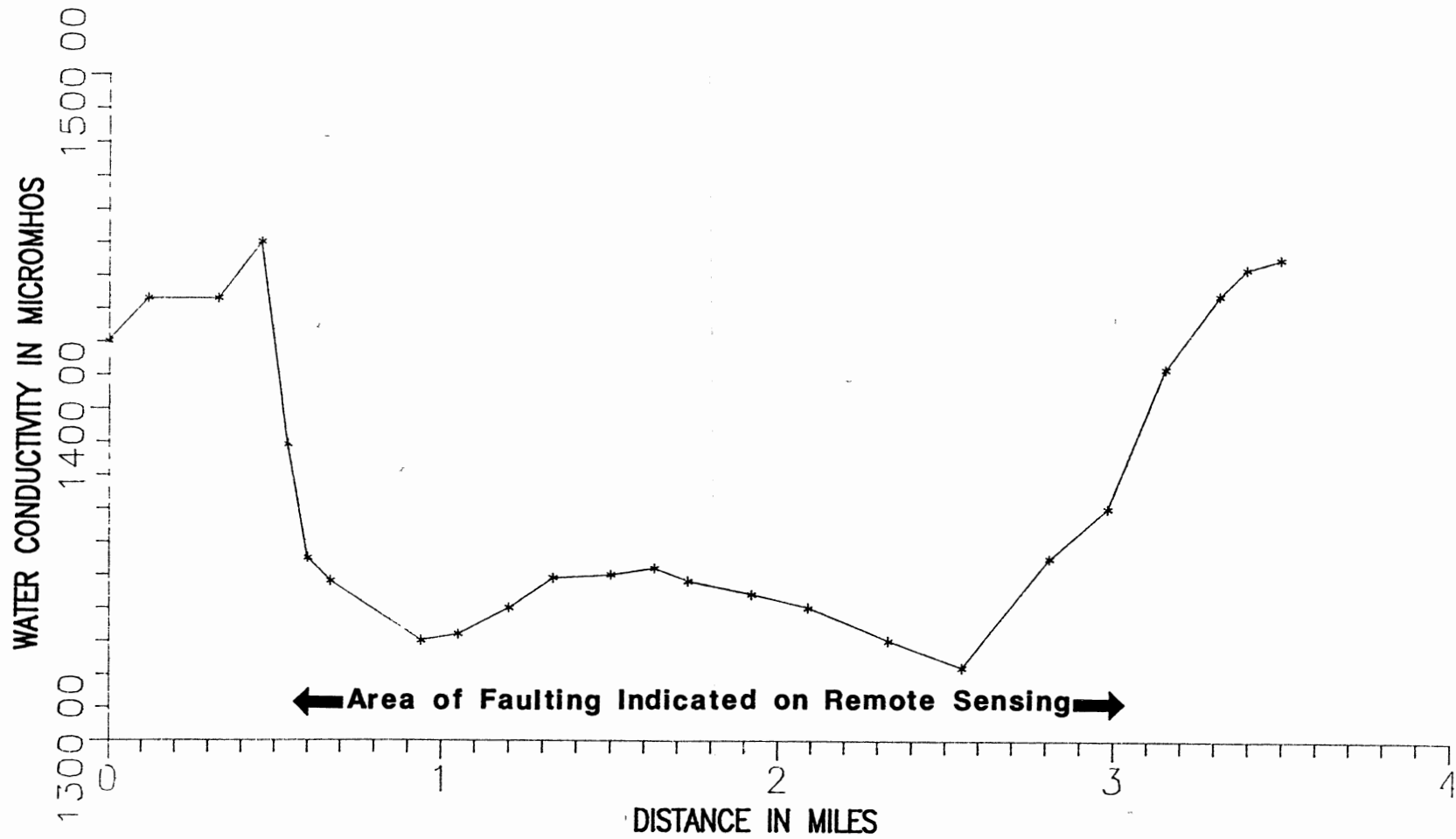
Figure 22. Graph of Stream Conductivity Values
Versus Distance Along Traverse.
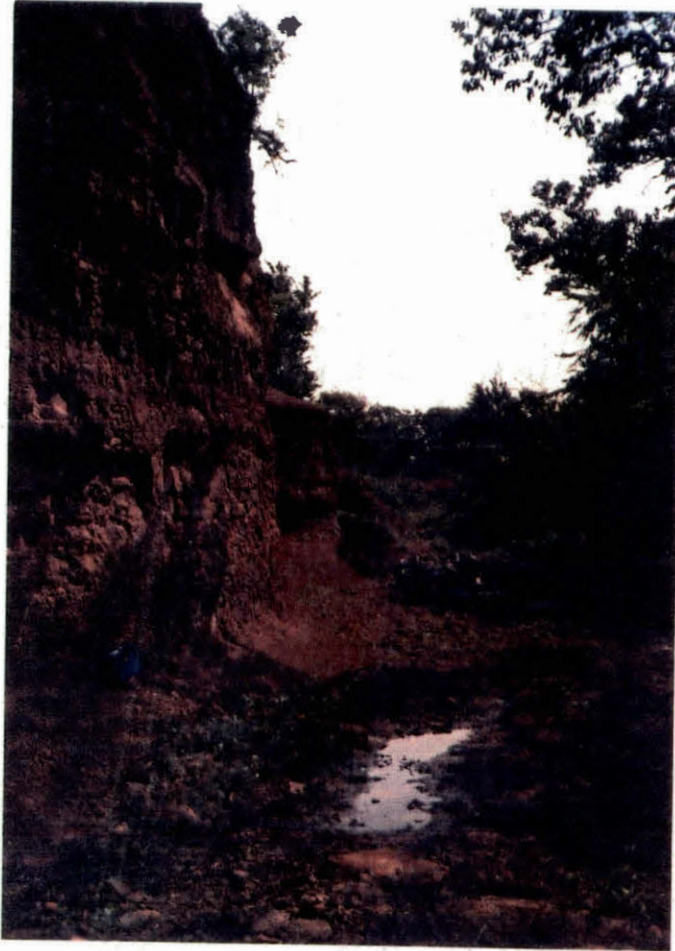
Figure 23.   Photograph of Unfractured Hennessey
             Shale With Sand Lenses Up Stream
             From Fault Zone.

In the suspected fault interval, between sample stations eleven and twelve, a reddish brown massively-bedded sandstone lense is present in the shale outcrop exposed on the south side of the stream (Figure 24). The sandstone lens was ten feet thick and extended approximately fifty feet laterally. The sandstone exposure has several prominent joints paralleling the stream. There is a large disattached slump block that was created when the stream undercut the sandstone along a prominent fracture.

Near the end of the suspected fault zone, between sample stations seventeen and eighteen, there is a section of shale containing lenses of thin-bedded silstones (Figure 25). This outcrop displayed substantial fracturing.

Near station seven, several small pools of water were observed. These pools were isolated from the main stream by several feet. Water from these pools had conductivity of 819 micromhos, considerably lower than the adjacent stream value of 1355 micromhos. These pools are believed to be small seeps or springs. Water found in these seeps may represent closely the true local ground water conductivity before it is mixed with higher conductivity stream water.

Water conductivity data through the fault interval was compared with conductivity readings taken above and below the fault zone using the Student's T test. The

Figure 24.   Photograph of Fractured Sandstone
             Outcrop with Slump Block in Fault
             Zone.

Figure 25.   Photograph of Fractured Hennessey
Siltstone in Fault Zone.

results, shown on Table 6, indicate that there is a statistical difference between the two groups.

Stream conductivity data verifies the presence of a fault, initially recognized on remote sensing and subsurface geology, between stations five and nineteen. The faulted interval is demarcated geochemically by a distinct zone of low-conductivity stream water. Further confirmation is provided by fresh water seeps and fractured bedrock through the fault interval.

Explanation of Field Observations

It is probable that faulting has reduced stream water conductivity by:

o   Increasing ground water velocity and reducing water residence time;

o   Providing a fracture conduit system shortening travel length and decreasing water contact with the formation matrix;

o   Increasing ground water discharge volume, thus diluting background stream water conductivity.

If consistent variations in ground water composition can be detected along a ground water flow path a Kinematic model can be employed to describe the reaction pathway. A Kinematic system is typified by chemical reactions which are relatively slow, irreversible, and heterogeneous (Langmuir and Mahoney, 1984). Applying this model to the ground water system, the dissolved concentration of

89

TABLE 6

BASE FLOW STREAM CONDUCTIVITY DATA
STATISTICAL ANALYSIS

Non-Fault Conductivity	Fault Conductivity
1,420.00	1,330.00
1,433.00	1,332.00
1,433.00	1,340.00
1,450.00	1,349.00
1,434.00	1,350.00
1,434.00	1,360.00
1,442.00	1,348.00
1,445.00	1,344.00
	1,342.00
	1,330.00
	1,322.00

Average	1,436.38	Average	1,340.64
Variance	74.23	Variance	113.50
Deviation	8.62	Deviation	10.65
T calc.=	8.57	T(.05)=	2.11

T calc >T(.05   Ho   Fail, Populations statistically different.

reaction product B with respect to reactant A can be
expressed as:

$$C_B/C_A = 1/K_{AB} + t/(0.693 * T_R)$$

where

C_A=Concentration of reactant
C_B=Concentration of product
K_{AB}=Rate constant of AB
t=Half-life of reaction
T_R=Residence time of water

When $T_R >> t$, the equation reduces to the equilibrium
expression. Therefore, provided the system is not at
equilibrium, the ground water mineral concentration will
increase as a function of residence time in the aquifer.
This equation can be applied to Darcy's Law for flow
through a porous medium in the following fashion:

$$V = K * I$$
$$V = T_R/D$$
$$T_R = D/(K * I)$$

where:

V=Velocity through a porous medium

K=Hydraulic conductivity

D=Flow path distance

I=Hydraulic gradient

By substitution,

$$C_B/C_A = K_{AB} + (.693/(t*I))*D/K$$

The expression above infers that the mineral concentration along a ground water flow path increases directly with the length of the flow path and inversely to the hydraulic conductivity. Fault-induced fracturing should increase the hydraulic conductivity of the aquifer, resulting in decreased total dissolved solids content.

Fracturing within an aquifer undoubtedly controls, to some degree, the length of the ground water flow path and formation contact area (Figure 26). Fluid, which, is otherwise restricted to a tortuous pathway through the interstices of the formation matrix, is at liberty to flow rapidly through a conduit system of naturally occurring fractures. Water moving through a fracture conduit should have minimal contact with the formation and exhibit less mineralization.

The quantity of ground water discharge to a stream can be expressed terms of Darcy's Law as

$$Q = K*I*A$$
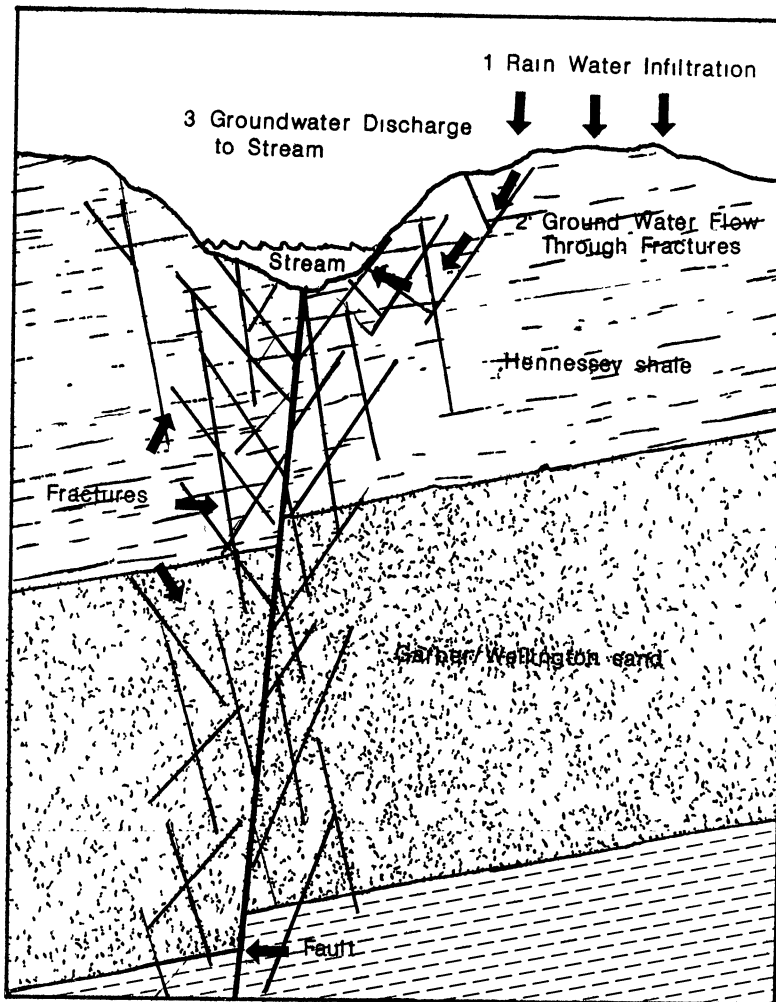
Figure 26. Schematic Ground Water Flow Through Fractured Aquifer System.

where

Q=Ground water discharge

A=Aquifer cross-sectional area of flow

The equation above indicates that an increase in hydraulic conductivity, as would be present in a fractured aquifer zone, should result in higher ground-water-to-stream discharge. The fresh water seeps observed along the stream traverse may attest enhanced ground water discharge generated by fault induced fracturing.

Using remote sensing, fractured areas have been identified and correlated with higher water well yields (Zall & Russell, 1979; Davis and DeWiest, 1976; Berard and Woodruff, 1974). Lattman and Parized (1964) found that wells located near the intersections of fracture sets exhibited increased yields ten to one-hundred times greater than wells drilled between the fractures. It is logical to assume that a similar relationship exists with respect to stream discharge and fracturing.

Enhanced ground water discharge does not affect ground water chemical composition. The introduction of larger volumes of ground water in a faulted interval serves to augment observed conductivity variance by substantially diluting background stream water.

Method Limitations

Stream conductivity analysis may not be applicable in every instance. Several factors can adversely affect stream conductivity values and render the interpretation useless, including:

o   Tributary confluence

o   Changes in soil or bedrock lithology

o   Variations in matrix permeability

o   Ground water contamination.

It is obvious that variations in reservoir lithology and hydraulic characteristics occur without the influence of faulting. Care should be exercised to interpret variations in stream conductivity in light of local geologic conditions.

Stream conductivity analysis is restricted by other inherent drawbacks. In order to be useful for fault interpretation, a perennial stream must parallel a lineament interpreted on remote sensing. In addition, dry-weather flow must be established prior to sampling, which restricts field sampling to seasonal dry periods.

Despite certain limitations, stream conductivity analysis can be used to verify faulting as part of an integrated remote sensing program. This method can provide an additional source of information concerning

confining bed competency during the preliminary stage of
an investigation with minimal costs.

CHAPTER V

SUMMARY AND CONCLUSIONS

Summary of Findings

A summary of project results is shown on Table 8. Structure maps of the top and bottom of the Hunton Group show the area to be a highly faulted, westerly dipping homocline. One-hundred and fourteen faults were detected in the Hunton. Faulting occurs in conjugate sets with principal orientations averaging N47°E and N36°W. Many Hunton faults could be verified by supporting evidence from isopach and production lineament map analysis.

Oil production from the Hunton Formation in the West Edmond Field appears to be largely fault or fracture controlled. The contour map of twenty-four-hour initial production for oil wells producing from the Hunton shows distinct linear trends of either high or low initial production rates. These linear production trends correlate exceedingly well to many base-of-Hunton faults.

In most instances, initial well performance improves in the vicinity of a fault. Elevated well yields along a fault zone is attributed to fracture-enhanced permeability which augments reservoir capacity. Less commonly, some

TABLE 7

SUMMARY OF RESULTS

Item Name	Orientation	Total Frequency	% Faults Identified	% Lineaments Correlating to Faults
Production Lineaments	N48E N36W	62	86%	N/A
Hunton Faults	N47E N36W	114	N/A	N/A
Base of Permian	N48E N35W	72	N/A	N/A
Landsat Lineaments	N43E N41W	133	54%	34%
CIR Lineaments	N41E N41W	370	58%	12%
Topographic Stream	N42E N39W	360	50%	12%

decreases in production were noted along a fault when much of the pay section was removed by normal-slip movement.

Analysis of isopach maps of the Hunton Group and the Bois d'Arc, Woodford, and Mississippi Limestone Formations also provided supplementary evidence for Hunton fault verification. These strata were subjected to subaerial exposure during the Upper Wichita Orogeny. The resulting erosional surface that developed was controlled, at least in part, by geologic structure. Since fracture-weakened rock is more susceptible to weathering, preferential erosion of rock results along a fault zone. Isopach maps reflected the presence of a fault when:

o   Thin isopach zones, representing paleo-channels, parallel Hunton faults;

o   Pre-Pennsylvanian strata subcrop limits parallel Hunton faults.

It was recognized that some of the faults at the Hunton level did not extend to the surface. To delineate vertical fault continuity, the fault configuration for the base of the Permian was compared with that of the Hunton. Of 114 Hunton faults, seventy-two (63%) were interpreted to be pervasive, passing through the Pennsylvanian section to the base of the Permian.

Many of the fault planes are either nearly vertical or dip slightly to the west. Vertical fault displacement

in pre-Pennsylvanian strata is generally high compared to the fault slip in the Pennsylvanian and Permian sediments. Though fault displacement was pronounced in the pre-Pennsylvanian section, the land surface was largely denuded during the upper Wichita Orogeny. Tectonic activity during the remaining Pennsylvanian and Permian was modest, with subdued fault slip.

Using Landsat Band 7 imagery at a scale of 1:120,000, a total of 133 lineaments were identified. Average orientations were N43^{O}E and N41^{O}W. Thirty-nine of seventy-two Permian-level faults (54%) correlated to Landsat lineaments. Of the total field of 133 lineaments, forty-five (34%) coincided with subsurface faults.

Using high-altitude infrared photography at a scale of 1:60,000, a total of 370 lineaments were identified. Average orientations were N41^{O}E and N41^{O}W. Out of seventy-two faults identified on the base of Permian surface, forty-two (58%), corresponded to one or more lineaments. However, only forty-five lineaments out 370 total lineaments identified actually coincided with known faults. This infers that only 12% of color infrared lineaments was caused by pervasive fault structure, while 88% were the product of some other phenomenon.

Using USGS topographic maps at a scale of 1:2,400, the orientations of 360 second-order or higher streams were measured. Channel directions average N42^{O}E and N39^{O}W.

Landsat, color infrared, and stream lineament sets were all compared statistically with Hunton fault orientation using standard F test and Students T analysis. Results indicate that there is no statistical difference in the orientations of the lineament and fault sets.

It was observed that the highest-order streams in the project coincided with many major subsurface faults. As shown on Plate 14, the stream courses of Spring Creek, Deer Creek, Walnut Creek, and Bluff Creek correspond with dominant subsurface fault patterns.

Stream orientations are statistically identical to subsurface fault directions even though most of the measured stream channels did not correlate with a known subsurface fault. It is concluded that:

o   Drainage development within the study area is highly responsive to an impressed structural fabric;

o   Minor tributaries may be controlled by jointing or fracturing.

There also appears to be a relationship between major pervasive fault structure and high-order stream channels. It is proposed that major drainage features have evolved in response to the existence of pervasive fault structure. Enhanced weathering along zones of fracturing, typically associated with faulting, has resulted in the eventual development of high-order stream channels.

Most lineaments found using either Landsat imagery or color infrared photographs were associated with stream channels. Because of the high spatial resolution of color infrared, nearly all of the drainage features can be detected. The great majority of color infrared lineaments were attributed to small streams and tributaries. Low-order stream channels are oriented along minor fractures or joints. Therefore, most color infrared lineaments tend to reflect jointing or fracturing.

Landsat resolution, however, is poor and only major earth features can be detected. Low-order stream channels are beyond the resolution of the imagery and are mostly filtered out. Consequently, most Landsat lineaments tend to correspond to prominent drainage features which appear to be controlled pervasive faults.

Many more lineaments were identified that subsurface faults. At best, using Landsat imagery, only one of three lineaments could be attributed to subsurface faulting. Lineament mapping can be an useful for identifying fault zones on the surface. However, in the absence of additional data, it is impossible to determine which lineaments correspond to pervasive fault structures and which do not. Dry-weather-flow stream conductivity surveys could identify lineaments that are associated with true pervasive faults.

Water conductivity from Deer Creek was measured at twenty-two sites along a 3.75 mile traverse during dry-

102

weather flow conditions. Lineaments were detected on both Landsat and color infrared that corresponded to an identified subsurface fault zone extending through the central portion of the stream traverse.

Upstream from the suspected fault zone, each consecutive sampling station increased in conductivity downstream direction from 1420 to 1450 micromhos. Entering the suspected fault zone, water conductivity dropped consistently from 1389 to 1330 micromhos. Conductivity remained below 1350 micromhos through the fault interval. Leaving the fault zone, water conductivity steadily increased from 1320 to 1445 micromhos at each consecutive sample point downstream.

Although most of the bedrock along the stream profile was covered with either alluvium, soil, or vegetation, some bedrock outcrops were found. Upstream from the fault interval, the Hennessey consisted of mostly unfractured shale and silt. Along the fault trace, shale and thin sandstone beds were highly fractured. Also along the faulted interval, a fresh-water seep was found that had a conductivity of only 819 micromhos.

The water conductivity values above and below the fault interval were tested against water conductivity values from the fault interval using the Student's T test. Stream conductivity values were found to be normally distributed. At a 0.05 level of significance, it

was determined that a statistical difference exists between the respective populations.

The reduction in water conductivity through the fault interval can be explained by normal hydrogeologic processes. Rain water infiltrating the aquifer has a very low mineral content. Ground water ion concentrations increase with prolonged contact with the rock matrix. In a state of dynamic equilibrium, the mineral content of ground water generally increases as a function of the time in contact with the rock matrix. Conversely, ground water mineral concentrations will remain low if water passes quickly through the aquifer.

A highly-fractured aquifer system can retard ion dissolution into ground water by:

o Increasing aquifer permeability, thereby facilitating higher ground water velocity which reduces contact time with the rock matrix;

o Permitting water to flow through fracture conduits, supplanting interstitial flow.

In addition, fracturing within the aquifer probably increases ground-water-to-stream discharge, further reducing overall stream conductivity by dilution during dry weather flow.

Through the test interval, faulting was observed to result in reduced stream water conductivity along the Deer Creek traverse. In other cases, stream conductivity values may increase in response to fault/fracture proxim-

ity. In overpressured conditions, mineralized water from deep aquifers could seep up into fresher surface aquifers along zones of structural weakness.

CONCLUSIONS

About 55% of the base-of-Permian faults were identifiable using Landsat and infrared lineament analysis. However, only 133 total lineaments were detected on Landsat, versus 370 found on color infrared. As a result, only 12% of the color infrared lineaments corresponded to subsurface faults, compared to 34% of the Landsat lineaments.

Most lineaments identified using Landsat imagery and color infrared photographs were associated with linear stream channels. Low-order streams appear to develop along fractures or joints; however, many of the high-order streams have developed along pervasive faults.

Color infrared photographs have high spatial resolution which allows detection of many small surface drainage features. Most color infrared lineaments were attributed to small streams and tributaries believed to be oriented along minor fractures or joints.

Landsat image resolution is much poorer than color infrared photography, and only major surface features can be detected. As a result, Landsat lineaments tend to correspond to prominent drainage features which appear to be controlled by known subsurface faults. Landsat imagery

essentially filters out the multitude of small stream channels which do not appear to be associated with faulting, effectively emphasizing fault-controlled drainage features.

Many more lineaments can be recognized than identifiable faults. In some instances, a conductivity profile of stream water measured during dry-weather flow conditions may be used to discern lineaments that correspond to fault structure. A fault could alter ground water chemistry locally, resulting in water conductivity variations. Under dry-weather flow conditions, all stream flow is discharged from ground water; therefore, variations in water conductivity could manifest a nearby fault.

REFERENCES CITED

Amsden, T.W., and Roland T.L., 1967, Geologic maps and
    stratigraphic cross-sections of Silurian strata and
    Lower Devonian formations in Oklahoma: Oklahoma
    Geological Survey, GM-14.

Benoit, E. L., 1957, The Desmoinesian Series, Edmond
    area, central Oklahoma: Shale Shaker Digest, v. 16,
    pp. 338- 350.

Betard, P., 1976, Etudies Hydrologiques, Bagre-Sud:
    Ministere du Plan du Developpement Rural de L'envi-
    ronemnt et du Tourisme, autorite des Amenagements
    des Vallees des Volta, pp. 26.

Beardall, G.B. Jr., 1983, Depositional environment,
    diagenesis and dolomitization of the Henryhouse
    formation, in the western Anadarko Basin and north-
    ern shelf, Oklahoma: Unpublished Master of Science
    Thesis, Ok. State University pp. 127.

Bingham, R. H., and R. L. More, 1983, Reconnaissance of
    the water resources of the Oklahoma City quadrangle,
    central Oklahoma: Oklahoma Geological Survey, Map
    HA-4.

Brasier, Francoise, 1987, Injection of Hazardous Wastes:
    EPA overview: in International Symposium on Subsur-
    face Injection of Liquid Wastes, New Orleans,
    Louisiana, National Water Well Assoc., pp. 1-2.

Burchfield, M. R., 1985, Map of Oklahoma oil and gas
    fields, Oklahoma Geological Survey, Map GM-28.

Carr, .E., and Marcher, M.V., 1977, A preliminary ap-
    praisal of   the Garber-Wellington aquifer,
    southern Logan and northern   Oklahoma counties,
    Oklahoma: U.S. Geol. Survey Open-file Report 77-
    278, p. 23.

Cardott, B. J. and M. W. Lambert, 1987, "Thermal matura-
    tion by vitrinite reflectance of the Woodford shale,
    Anadarko basin, Oklahoma: Amer. Assoc. Petroleum
    geologists Bull., v. 69 no. 11, pp. 1982-1998.

Carr, J.E. and J. S. Havens, 1976, Records of wells and water quality for the Garber-Wellington aquifer, northern Oklahoma and southern Logan counties, Oklahoma: U.S. Geol. Survey Open-file Report 76-619, pp. 32.

Christenson, S. C. and D. L. Parkhurst, 1987, Ground-qater quality assessment of the central Oklahoma aquifer, Oklahoma: Project Description: U.S. Geol. Survey Open- file Report 87-235, pp. 30.

Clark, L.H., 1983, Briefing and policy review: Underground injection of hazardous waste, draft, U.S. Environmental Protection Agency, Washington D.C., p. 2.

Dennis, P. E., 1954, Geology and ground water hydrology of the Lake Hefner area: in Water-loss investigations, Lake Hefner studies, technical report: U.S. Geol. Survey Prof. Paper 269, p. 10-16.

Dolan, R., and A. Howard, 1978, Structural control of the rapids and pools of the Colorado River in the Grand Canyon: Science, V. 202, pp. 629-631.

Gates, M. M., J. Marsh, and J. S. Fryberger, 1983, Technical considerations for the development plan of the Garber- Wellington aquifer: v. 1, Report to Assoc. of Central Okla. Governments, pp. 180.

Gordon, W. and J. Bloom, 1987, Deeper problems: Limits to underground injection as a hazardous waste disposal method: in International symposium on subsurface injection of liquid wastes, New Orleans, Louisiana, National Water Well Assoc., pp. 3-50.

Graham, L. L., R. Heath, L. Hinkle, O. T. Love, J. F. McNabb, R. Miltner, W. Pettyhohn, 1985, Protection of public water supplies from ground-water contamination: U.S. Environmental Protection Agency, Seminar Pub., EPA/625/4-85/016, pp. 182.

Ham, W. E. 1969, Regional geology of the Arbuckle Mountains, Oklahoma: Okla. Geological Survey, Guide book 17, pp. 52.

Judson, S. and D. F. Ritter, 1955, Pattern and form of some valleys in the driftless area, Wisconsin: Joun. Geol., Vol. 63, pp. 328-36.

Kreitler, C. W., 1985, Hydrogeology of sedimentary basins as it relates to deep-well injection of chemical wastes: in Proceedings of the international symposium subsurface injection of liquid wastes, New Orleans, Louisiana, National Water Well Assoc. pp. 398-416.

Langmuir, D., and J. Mahoney, (1984), Chemical equilibrium and kinetics of geochemical processes in ground water studies: in Proceeding of the first Canadian/American conference on hydrogeology: Practical applications of ground water geochemistry, National Water Well Assoc., Worthington, Oh. pp. 323.

Lattman, L. H. and R. R. Parizek, 1964, Relationship between fracture traces and the occurrince of groundwater in carbonate rocks: Jour. of Hydrology, Vol. 2, pp. 73-91.

Lindberg, F.A., editor, 1987, Correlation of stratigraphic units of North America (COSUNA) project, Texas-Oklahoma tectonic region: American Assoc. of Petroleum Geologists: Tulsa, Ok., Charts.

Luza, K. V., and J. E. Lawson, Jr., 1979, Seismicity and tectonic relationships of the Nemaha Uplift in Oklahoma part III: U.S. Nuclear Regulatory Commission, NUREG/CR- 1500, pp. 70.

Luza, K. V., and J. E. Lawson, Jr. 1981, Seismicity and tectonic relationships of the Nemaha Uplift in Oklahoma part IV. U.S. Nuclear Regulatory Commission, NUREG/CR- 2439, pp. 52.

Luza, K. V., and J. E. Lawson, Jr. 1983. Siesmicity and tectonic relationships of the Nemaha Uplift in Oklahoma part V: U.S. Nuclear Regulatory Commission, NUREG/CR- 3109, p. 115

Manni, F. M., 1982, Depositional environment, diagenesis, and unconformity identification of the Chimneyhill subgroup, in the western Anadarko basin and northern shelf of Oklahoma: Unpublished Masters of Science Thesis, Oklahoma State University, pp. 133.

Melton, F. A., 1955, Photo-geology in flatland regions of low dip: Shale Shaker Digest, V. II, p. 31-43.

McGee, D. A. and H. D. Jenkins, 1946, West Edmond oil field, central Oklahoma: Amer. Assoc. Petroleum Geologists, v. 30, No. 11, pp. 1797-1829.

Morisawa, M. 1985, Rivers: Form and process: Logman Pub., London and N.Y., pp. 222.

O'Leary, D. W., J. D. Freidman, and H. A. Pohn, 1976, Lineaments, linear, lineation: Some proposed new standards for old terms: Geological Society of America, Bull. 87, p. 1463-1469.

Richason, B. F., Jr., 1978, Introduction to remote sensing of the environment: Kendall/Hunt Pub. Co., Dubuque, Iowa, 2ed ed., pp. 496.

Sabins, F. F., Jr., 1978, Remote sensing: Principles and interpretation: W.H. Freeman and Company, pp. 426.

Sokal, R.R. and F.J. Rohlf, 1981, BIOM: A package of statistical programs to accompany the text biometry: in Biometry: The principles and practice of statistics in biological research, 2ed ed., W.H. Freeman, N.Y., pp. 859.

Swesnic, R. M., 1948, Geology of West Edmond oil field, Oklahoma, Logan, Canadian, and King Fisher counties, Oklahoma: in J. V. Howell (ed.), Structure of typical American oil fields, American Assoc. of Petroleum Geologists Symposium, Tulsa, Ok., v. 3, p. 359-398.

Sullivan, K. L., 1985, Organic facies variation of the Woodford shale in western Oklahoma: Oklahoma City Geological Society, Shale Shaker Digest, v. 35, no.4, p. 76-89

Toth, J., 1984, The role of regional gravity flow in the chemical and thermal evolution of ground water: in Proceedings of the first Canadian/American conference on hydrogeology: Practical applications of ground water geochemistry, National Water Well Association, Worthington, Oh., p. 3-39.

Warner, D. L., S. N. Davis, and T. Syed, 1986, Evaluation of confining layers for containment of injected wastewater: in Proceedings of international symposium subsurface injection of liquid wastes, New Orleans, Louisiana, National Water Well Assoc., pp. 417-446.

Whiteside, R. F., and S. F. Raef, 1978, Michanical integrity of class 1 injection wells: in International symposium on subsurface injection of liquid wastes, New Orleans, Louisiana, National Water Well Assoc., pp. 57-76.

Wilkinson, W. M., 1977, Fracturing in Spraberry reser-
voir,   west Texas: in J. Kostrue and J. Reven-
scroft (eds.), Fracture-Controlled Production,
American Assoc. of Petroleum Geologists Reprint, no.
21, pp. 40-55.

Wood, P. R. and L. C. Burton, 1968, Ground-water re-
sources of Cleveland and Oklahoma counties: Ok.
Geological Survey, Circular 71, pp. 181.

Woodruff, J., and Parizek, E. J., 1956, Influence of
underlying rock structures on stream courses and
valley profiles in the Georgia piedmont: Assoc.
Amer. Geogr. Annals, v. 46, pp. 129-137.

Woodruff, J. D., J. H. Talley, and J.C. Miller, 1974,
Selection of sites for high yielding wells in the
Delaware piedmont: in Abstract with programs, north-
eastern section Geological Society of America,
Baltimore, Maryland, vol. 6, no. 1, pp. 87-88.

Zall, L. and O. Russell, 1979, Ground water exploration
programs in Africa: in M. Deutsch, D.R. Wiesnet and
A. Rango (eds.), Satellite hydrology: Proceedings of
5th Annual William T. Pecora Memorial Symposium on
Remote Sensing, Minneapolis, Mn., American Water
Resources Assoc., pp. 416-425.

APPENDIXES

APPENDIX I

MEASURED FAULT, LINEAMENT

AND STREAM ORIENTATIONS

WITH STATISTICAL

ANALYSIS

BAST4T
ID =Base of Hunton NE Fault Trends

        BASIC STATISTICS
    N =   58   0 CLASSES TRANSFORMATION CODE =   0
    ALPHA =   .050 T(ALPHA) =   2.000

	STATISTIC	STAND.ERROR	CONFIDENCE LIMITS (95.00 PER CENT)	
MEAN	46.70690000	2.446154000	41.81459000	51.59921000
MEDIAN	45.00000000	3.065765000	38.86847000	51.13153000
VAR.	347.0529341			
S	18.62935678			
V	39.88567000	4.251812000	31.38204000	48 38929000
G1	.07300612	.31371990	-.54200890	.68802110
G2	-.04385199	.61813580	-1.25564200	1 16793800
DMAX	.12750310			

--end--

BASTAT
ID =Base of Hunton NW Fault Trends

BASIC STATISTICS
N =   56   0 CLASSES TRANSFORMATION CODE =   0
ALPHA' =   .050 T(ALPHA) =   2.010

	STATISTIC	STAND.ERROR	CONFIDENCE LIMITS (95 00 PER CENT)	
MEAN	36.25000000	2.155520000	31.91740000	40.58260000
MEDIAN	38.00000000	2.701513000	32.56996000	43.43004000
VAR.	260.1909091			
S	16 13043425			
V	44 49775000	4.967905000	34.51226000	54 48324000
G1	.58259560	.31900000	-.04277030	1 20796200
G2	1 67495400	.62825590	44332470	2 90658400
DMAX	.14388710			

--end--

```
Base of Hunton
Lineament Data
Degrees East of North
```

n of Data	N.E. Data	N.W. Data
1	2.00	5.00
2	8.00	8.00
3	9.00	8.00
4	23.00	8.00
5	25.00	13.00
6	25.00	15.00
7	25.00	16.00
8	28.00	18.00
9	30.00	22.00
10	31.00	23.00
11	33.00	24.00
12	33.00	25.00
13	33.00	25.00
14	34.00	25.00
15	34.00	26.00
16	35.00	26.00
17	36.00	26.00
18	36.00	27.00
19	38.00	28.00
20	38.00	29.00
21	38.00	30.00
22	41.00	34.00
23	41.00	35.00
24	44.00	36.00
25	44.00	36.00
26	45.00	36.00
27	45.00	37.00
28	45.00	38.00
29	45.00	38.00
30	45.00	38.00
31	46.00	38.00
32	46.00	40 00
33	47.00	41.00
34	47.00	41.00
35	48.00	42.00
36	48.00	43.00
37	48.00	44.00
38	48.00	44.00
39	52.00	44.00
40	54.00	44.00
41	55.00	45.00
42	56.00	46.00
43	58.00	46.00
44	59.00	46.00

Base of Hunton
Lineament Data
Degrees East of North

n of Data	N.E. Data		N.W. Data
45	60.00		46.00
46	61.00		47.00
47	62.00		48.00
48	63.00		48.00
49	67.00		48.00
50	68.00		48.00
51	72.00		48.00
52	74.00		50.00
53	75.00		52 00
54	77.00		66.00
55	80.00		85.00
56	82.00		85.00
57	82.00		
58	85.00		
N =	58.00	N =	56.00
Average=	46.71	Average=	36.25
Variance=	335.19	Variance=	250.98
Deviation=	18.31	Deviation	15.84

BASTAT
ID =Northeast Topographic Lineaments

```
          BASIC STATISTICS
    N =  203        0 CLASSES  TRANSFORMATION CODE =   0
    ALPHA =    .050  T(ALPHA) =   1 960
```

	STATISTIC	STAND ERROR	CONFIDENCE LIMITS (95.00 PER CENT)	
MEAN	41.94089000	1.159491000	39 66829000	44 21349000
MEDIAN	43.00000000	1.453190000	40.15174000	45 84826000
VAR	272.9172804			
S	16 52020824			
V	39.38927000	2.237694000	35.00339000	43 77515000
G1	.01226531	17066820	-.32231180	34684240
G2	-.38257960	.33972440	-1 04857400	.28341440
DMAX	.04713297			

--end--

```
BASTAT
ID =Northwest Topographic Drainage

        BASIC STATISTICS
   N =  157         0 CLASSES  TRANSFORMATION CODE =    0
   ALPHA =    .050  T(ALPHA) =   1.960


              STATISTIC         STAND.ERROR         CONFIDENCE LIMITS
                                                   (95.00 PER CENT)


MEAN        38.59236000       1.223409000        36.19448000       40.99024000

MEDIAN      38.00000000       1.533299000        34.99474000       41.00526000

VAR.        234.9866079

S           15.32927291

V           39.72101000       2.571043000        34.68176000       44 76025000

G1            .01099640         .19365710         -.36864800         .39064070

G2            .43855260         .38497840         -.31615700        1.19326200

DMAX          .05673562

--end--
```

Topographic Drainage
Lineament Data

n of Data	N.E. Data	N.W. Data
1	24	45
2	22	38
3	28	40
4	28	52
5	22	26
6	26	34
7	21	29
8	27	22
9	47	3
10	44	2
11	10	48
12	23	30
13	54	45
14	53	36
15	43	4
16	55	9
17	23	35
18	34	3
19	45	64
20	44	41
21	4	26
22	36	82
23	37	46
24	24	55
25	24	52
26	23	43
27	25	46
28	23	29
29	21	33
30	16	19
31	33	4
32	22	23
33	43	36
34	32	27
35	35	29
36	36	49
37	26	33
38	28	46
39	32	32
40	26	28
41	12	27
42	20	52
43	28	43
44	46	60

Topographic Drainage
Lineament Data

n of Data	N.E. Data	N.W. Data
45	70	39
46	74	13
47	66	39
48	46	62
49	47	36
50	52	46
51	61	48
52	52	48
53	54	41
54	46	35
55	48	34
56	65	52
57	63	39
58	64	30
59	85	50
60	75	49
61	72	42
62	46	22
63	41	30
64	41	56
65	41	51
66	52	29
67	44	35
68	56	45
69	38	72
70	48	49
71	52	45
72	43	46
73	72	35
74	45	15
75	55	38
76	51	72
77	28	54
78	55	70
79	71	48
80	65	40
81	32	31
82	36	34
83	48	38
84	44	37
85	28	26
86	30	60
87	49	3

Topographic Drainage
Lineament Data

n of Data	N.E. Data	N.W. Data
88	8	46
89	59	44
90	46	48
91	58	28
92	38	32
93	47	75
94	28	55
95	38	28
96	28	30
97	42	32
98	40	66
99	31	22
100	33	74
101	58	41
102	5	39
103	54	44
104	46	36
105	30	39
106	44	44
107	44	58
108	36	47
109	20	32
110	54	58
111	29	47
112	33	45
113	45	39
114	58	38
115	9	35
116	45	49
117	30	43
118	65	32
119	52	56
120	36	51
121	77	45
122	65	68
123	28	36
124	66	39
125	67	37
126	40	13
127	56	29
128	45	28
129	39	36
130	44	24

Topographic Drainage
Lineament Data

n of Data	N.E. Data	N.W. Data
131	66	2
132	55	29
133	49	25
134	56	24
135	23	20
136	9	24
137	57	33
138	55	44
139	41	54
140	49	30
141	68	62
142	50	57
143	78	25
144	57	35
145	46	24
146	36	23
147	58	58
148	63	58
149	37	48
150	33	22
151	62	36
152	29	29
153	14	36
154	18	46
155	55	38
156	54	34
157	18	25
158	39	
159	58	
160	17	
161	14	
162	40	
163	20	
164	13	
165	32	
166	49	
167	32	
168	25	
169	24	
170	39	
171	77	
172	38	
173	46	

Topographic Drainage
Lineament Data

n of Data	N.E. Data	N.W. Data
174	63	
175	42	
176	23	
177	41	
178	40	
179	63	
180	45	
181	48	
182	33	
183	42	
184	54	
185	46	
186	46	
187	30	
188	64	
189	48	
190	3	
191	33	
192	46	
193	66	
194	46	
195	58	
196	42	
197	30	
198	41	
199	46	
200	23	
201	44	
202	49	
203	68	

	N =	203	N =	157
	Average=	41.94	Average=	38.59
	Variance=	272.92	Variance=	234.99
	Deviation=	16.52	Deviation	15.33

BASTAT
ID =Northeast Landsat Data

      BASIC STATISTICS
  N =   88   0 CLASSES TRANSFORMATION CODE =   0
  ALPHA =   .050 T(ALPHA) =   2.000

	STATISTIC	STAND.ERROR	CONFIDENCE LIMITS (95.00 PER CENT)	
MEAN	43.63636000	1.797056000	40.04225000	47.23048000
MEDIAN	40.00000000	2.252250000	35.49550000	44.50450000
VAR.	284.1880878			
S	16.85787910			
V	38.63264000	3.318321000	31.99600000	45.26928000
G1	.44250440	.25680980	-.06094433	.94595310
G2	-.05221066	.50832950	-1.04873700	.94431600
DMAX	.11948260			

--end--

```
BASTAT
ID =Northwest Landsat Data

        BASIC STATISTICS
   N =   45        0 CLASSES  TRANSFORMATION CODE =    0
   ALPHA =    .050  T(ALPHA) =    2.010
```

	STATISTIC	STAND.ERROR	CONFIDENCE LIMITS -(95.00 PER CENT)	
MEAN	40.64444000	2.694018000	35.22947000	46 05942000
MEDIAN	38.00000000	3.376413000	31.21341000	44 78659000
VAR.	326.5979798			
S	18.07202202			
V	44.46370000	5 536487000	33 33536000	55 59203000
G1	.56553570	.35373210	-.12791890	1 25899000
G2	.60757680	.69454450	- 75400480	1.96915800
DMAX	.09366226			

```
--end--
```

Landsat Lineament
Data Listing

n of Data	N.E. Data	N.W. Data
1	3.00	7.00
2	10.00	8.00
3	15.00	8.00
4	18.00	20.00
5	20.00	22.00
6	22.00	24.00
7	24.00	24.00
8	24.00	24.00
9	24.00	25.00
10	25.00	28.00
11	25.00	30.00
12	26.00	30.00
13	28.00	30.00
14	30.00	32.00
15	30.00	32.00
16	30.00	32.00
17	30.00	33.00
18	30.00	34.00
19	32.00	35.00
20	32.00	36.00
21	33.00	37.00
22	34.00	38.00
23	34.00	38.00
24	35.00	39.00
25	35.00	40.00
26	35.00	40.00
27	35.00	42.00
28	36.00	44.00
29	36.00	45.00
30	36.00	45.00
31	36.00	45.00
32	36.00	48.00
33	36.00	50.00
34	37.00	52.00
35	37.00	52.00
36	38.00	53.00
37	38.00	54.00
38	38.00	55.00
39	38.00	58.00
40	38.00	60.00
41	38.00	65.00
42	38.00	68.00
43	40.00	74.00
44	40.00	85.00

n of Data	N.E. Data	N.W. Data
45	40.00	88.00
46	40.00	
47	40.00	
48	41.00	
49	42.00	
50	43.00	
51	43.00	
52	44.00	
53	44.00	
54	44.00	
55	45.00	
56	45.00	
57	45.00	
58	46.00	
59	48.00	
60	48.00	
61	48.00	
62	48.00	
63	48.00	
64	50.00	
65	52.00	
66	52.00	
67	54.00	
68	58.00	
69	58.00	
70	60.00	
71	60.00	
72	62.00	
73	62.00	
74	62.00	
75	63.00	
76	63.00	
77	65.00	
78	67.00	
79	70.00	
80	70.00	
81	72.00	
82	73.00	
83	74.00	
84	74.00	
85	75.00	
86	80.00	
87	82.00	

Landsat Lineament
Data Listing

n of Data	N.E. Data		N.W. Data
88	85.00		
	N = 88.00	N =	45.00
	Average= 43.64	Average=	40.64
	Variance= 284.19	Variance=	326.60
	Deviation= 16.86	Deviation=	18.07

```
BASTAT
ID =Northwest Infrared Lineament

        BASIC STATISTICS
   N =  167         0 CLASSES  TRANSFORMATION CODE =   0
   ALPHA =     .050  T(ALPHA) =   1.960
```

	STATISTIC	STAND.ERROR	CONFIDENCE LIMITS (95.00 PER CENT)	
MEAN	41.46707000	1.325737000	38.86863000	44.06551000
MEDIAN	40.00000000	1.661546000	36.74337000	43.25663000
VAR.	293.5154751			
S	17.13229334			
V	41.31542000	2.618285000	36.18358000	46 44726000
G1	.26489180	.18787410	-.10341560	.63319920
G2	.02064745	.37361070	-.71177720	.75307210
DMAX	.05208051			

```
--end--
```

```
BASTAT
ID =Northeast Infrared Lineaments

        BASIC STATISTICS
    N =  203         0 CLASSES  TRANSFORMATION CODE =   0
    ALPHA =    050  T(ALPHA) =   1.960
```

	STATISTIC	STAND.ERROR	CONFIDENCE LIMITS (95.00 PER CENT)	
MEAN	41.10838000	1.315343000	38.53030000	43.68645000
MEDIAN	41.00000000	1.648520000	37.76890000	44.23110000
VAR.	351.2159196			
S	18.74075558			
V	45.58865000	2.691993000	40.31235000	50 86496000
G1	.40995490	.17066820	.07537779	.74453190
G2	-.06643032	.33972440	-.73242430	59956370
DMAX	.07334542			

```
--end--
```

```
Infrared Lineament
Data Listing
```

n of Data	N.E. Data	N.W. Data
1	5.00	51.00
2	5.00	35.00
3	7.00	32.00
4	8.00	29.00
5	8.00	51.00
6	8.00	20.00
7	8.00	53.00
8	8.00	30.00
9	9.00	48.00
10	10.00	12.00
11	12.00	64.00
12	12.00	35.00
13	12.00	44.00
14	12.00	32.00
15	14.00	34.00
16	15.00	28.00
17	16.00	86.00
18	17.00	65.00
19	17.00	76.00
20	18.00	30.00
21	18.00	38.00
22	18.00	54.00
23	18.00	40.00
24	18.00	30.00
25	18.00	45.00
26	21.00	45.00
27	21.00	38.00
28	21.00	34.00
29	22.00	38.00
30	22.00	39.00
31	22.00	43.00
32	22.00	46.00
33	22.00	47.00
34	22.00	38.00
35	23.00	43.00
36	23.00	38.00
37	23.00	37.00
38	23.00	30.00
39	23.00	5.00
40	24.00	12.00
41	24.00	44.00
42	24.00	45.00
43	24.00	23.00
44	25.00	46.00

Infrared Lineament
Data Listing

n of Data	N.E. Data	N.W. Data
45	26.00	47.00
46	26.00	53.00
47	28.00	45.00
48	28.00	53.00
49	28.00	29.00
50	28.00	44.00
51	28.00	52.00
52	28.00	48.00
53	28.00	40.00
54	30.00	30.00
55	30.00	56.00
56	30.00	38.00
57	30.00	11.00
58	31.00	42.00
59	31.00	5.00
60	31.00	41.00
61	31.00	65.00
62	33.00	31.00
63	33.00	34.00
64	33.00	46.00
65	33.00	20.00
66	33.00	46.00
67	33.00	34.00
68	33.00	48.00
69	33.00	68.00
70	34.00	65.00
71	34.00	48.00
72	34.00	46.00
73	34.00	42.00
74	34.00	35.00
75	34.00	45.00
76	34.00	56.00
77	35.00	61.00
78	35.00	50.00
79	35.00	28.00
80	35.00	45.00
81	35.00	30.00
82	35.00	51.00
83	35.00	50.00
84	36.00	40.00
85	36.00	18.00
86	36.00	22.00
87	36.00	20.00

Infrared Lineament
Data Listing

n of Data	N.E. Data	N.W. Data
88	36.00	20.00
89	38.00	83.00
90	38.00	24.00
91	38.00	56.00
92	38.00	26.00
93	38.00	9.00
94	38.00	9.00
95	38.00	30.00
96	38.00	54.00
97	39.00	42.00
98	39.00	84.00
99	40.00	32.00
100	40.00	80.00
101	40.00	56.00
102	41.00	56.00
103	41.00	23.00
104	42.00	20.00
105	42.00	58.00
106	42.00	65.00
107	42.00	50.00
108	42.00	41.00
109	42.00	62.00
110	43.00	51.00
111	43.00	52.00
112	43.00	18.00
113	43.00	45.00
114	44.00	30.00
115	44.00	80.00
116	44.00	18.00
117	44.00	50.00
118	44.00	34.00
119	44.00	63.00
120	45.00	68.00
121	45.00	40.00
122	45.00	24.00
123	45.00	36.00
124	45.00	36.00
125	45.00	26.00
126	45.00	50.00
127	46.00	26.00
128	46.00	30.00
129	46.00	64.00
130	46.00	41.00

Infrared Lineament
Data Listing

n of Data	N.E. Data	N.W. Data
131	46.00	18.00
132	46.00	11.00
133	47.00	36.00
134	47.00	38.00
135	47.00	14.00
136	48.00	35.00
137	48.00	40.00
138	48.00	5.00
139	48.00	33.00
140	48.00	29.00
141	48.00	73.00
142	48.00	50.00
143	48.00	77.00
144	48.00	70.00
145	48.00	37.00
146	49.00	54.00
147	50.00	36.00
148	50.00	36.00
149	50.00	22.00
150	51.00	62.00
151	51.00	40.00
152	51.00	28.00
153	51.00	54.00
154	52.00	20.00
155	52.00	80.00
156	52.00	48.00
157	52.00	55.00
158	52.00	36.00
159	53.00	12.00
160	53.00	44.00
161	54.00	69.00
162	54.00	33.00
163	54.00	68.00
164	54.00	48.00
165	54.00	40.00
166	54.00	46.00
167	54.00	35.00
168	54.00	
169	55.00	
170	55.00	
171	56.00	
172	57.00	
173	58.00	

Infrared Lineament
Data Listing

n of Data	N.E. Data	N.W. Data
174	58.00	
175	60.00	
176	60.00	
177	62.00	
178	63.00	
179	66.00	
180	66.00	
181	67.00	
182	68.00	
183	70.00	
184	71.00	
185	71.00	
186	71.00	
187	72.00	
188	73.00	
189	73.00	
190	75.00	
191	77.00	
192	80.00	
193	80.00	
194	80.00	
195	81.00	
196	81.00	
197	82.00	
198	83.00	
199	83.00	
200	83.00	
201	87.00	
202	87.00	
203	88.00	

N =	203	N =	167	
Average=	41.11	Average=	41.47	
Variance=	349.49	Variance=	291.76	
Deviation=	18.69	Deviation=	17.08	

Base of Permian
Fault Orientation Data

n of Data	N.E. Data	N.W. Data
1	68	45
2	38	30
3	82	45
4	84	36
5	55	37
6	36	36
7	42	4
8	45	26
9	36	15
10	45	36
11	54	30
12	46	36
13	48	26
14	25	36
15	46	48
16	57	46
17	41	44
18	54	16
19	40	22
20	48	44
21	48	22
22	54	50
23	40	31
24	35	33
25	42	24
26	72	37
27	56	38
28	40	48
29	58	26
30	26	40
31	34	46
32	35	36
33	77	26
34	26	44
35	66	38
36	39	
37	59	

	N =	37	N =	35
	Average=	48.57	Average=	34.20
	Variance=	219.19	Variance=	113.54
	Deviation=	14.81	Deviation	10.66

Initial Oil Production
Lineament Data

n of Data	N.E. Data	N.W. Data
1	54	46
2	53	34
3	38	43
4	55	15
5	4	46
6	43	15
7	48	30
8	57	44
9	45	37
10	46	23
11	57	43
12	45	36
13	45	47
14	50	43
15	52	38
16	38	29
17	30	42
18	26	38
19	50	45
20	61	43
21	34	38
22	44	45
23	74	44
24	36	24
25	54	26
26	7.7	23
27	66	
28	38	
29	45	
30	42	
31	40	
32	39	
33	38	
34	77	
35	74	
36	73	

N =	36	N =	26
Average=	46.95	Average=	34.39
Variance=	233.27	Variance=	95.43
Deviation=	15.27	Deviation	9.77

APPENDIX II

SUPPLIMENTAL PRODUCTION

MAP DATA

Map Reference Number   Well Information

#1 PHILLIPS PETROLEUM #2 KNUTH CWWO; PB 6759 PERF M 6700-50
S 50/-/8, F 176/-/17

#2   HEARTLAND EXP 75 JAMESON #1 DST BTV 6522-45/1 HR GTS 2
MIN F 25 MCF 5/15 ISIP 1984/30 MIN PERF M 6620-96 F 11/-/22
+ 198 MCF

#3   PHILLIPS 44 HAT #1 PERF H 6802-42 ACID W/1000 GA F 2941-
124 F4301-124 TP #150

#4   ROYALTY PET 77 LENHART #1 PERF H 6892-872, 6830-40,
6946-54, 6962-72 FRC PERF M 6564-70, 6574-90, 6602-12 FRC F
20/-/24 + 190 MCF

#5   ANDERSON PRITCHARD 45 BUELL #1 PERF H 6578-94 ACID
W/10M GA F 60/-/24 CWPB 6453 PERF H 6375-87 & 6270-80, 6235-
80 6206-15 6660-70 ACID W/2M GA SQZ PERF H 5490-5535 P 30/-
/24

#6 HEARTLAND 84 BLEHM #1-3 PERF HS 5586-604 F 17/0/24 + 250
MCF

#7   HEARTLAND 84 SEYLLER 1-3 PERF HS 5573-582 P 15/15/24
+ 50

#8   CARTER 45 BLEHM #4 PERF H 6601-37 F 440/-/6 CWWO 1982
HEARLAND PERF M 6475-45 P 24/10/24 + 175 PERF CL 5722-96 S
21/6/24 + 25 MCF P CK 5694-5700 S 2/5/24 + 25

#9   CARTER 45 BLEHM #3 PERF H 6645-80 HR 1:103, 2:87,
3:70, F:70, F 42516 CWWO 1984 HEARTLAND PERF M 6516-6579 P
E/1/24 + 40 MCF

#10   CITIES 44 SEYLLER #2 PERF H 6549-662 ACID W/1000 GA F
761/-/20 CWWO 1983 HEARTLAND PERF HS 6652-60 P 14/2/24 + TR
GAS F 1171/-/24

#11   PHILLIPS 45 KOSAR #2 PERF H 6663-728 F 998/-/22 CWWO
1983 HEARTLAND PERF PR 6343-58 F 10 MCG PB PERF HS 5582-607
F 17/3/24 + 35 MCF

#12   CONTINENTAL OIL 44 SEYLLER #1 PERF H 6565-6618 F
386/-/12 + 2 MMCF CWWO 1977 CONTINENTAL OIL PERF HS 5333-610
SWB NSO D&A

#13   CONTINENTAL OIL 45 MCAULIFF #3 PERF H 6675-6706 Г
254/-/24 + 2.24 MMCF CWWO SOHIO 1980 PERF PR 6366070 F 90
MCF

#14   CONTINENTAL OIL 45 LENHART #2 PERF H 6754-96 F 277/0/3 CWWO CONT. OIL 1966 PERF M 6650-80 F 40/350/24 CWWO 1967 CONT. OIL PERF PR 6434-38 PERF BTV 6558-62 P 6/11/24 + 225 MCG

#15   SOHIO 44 MURPHY #4 PERF 6790-864 F 226/0/4 CWWO 1984 HEARTLAND PERF M 6689-720 ACID W/4000 GA 17.5% PERF 6467-480 ACID Q/15% 1600 GA NTR

#16 STANOLIND 44 KELLY B-3 PERF H 6990-7000 ACID Q/1000 F 61/-/4 F 161/6.72/24 F 346/-/24 CWPP 1959 PAN AMERICAN PERF PR 6546-52 GTS 10 MIN F 1.62 MMCF ACID W/500 GA F 13/-24 + 6.9 MMCF

#17   PHILLIPS 44 EDMOND #1 PERF H F 419/-/24 673/-/24 CWPB PHILLIPS 1958 PERF PR 6528-53 F 73/-/6 + 2.55 MMCF/6 HRS

#18   GULF 44 CHRISTNER #4 PERF H 6870-72 F 65,54,49,46 CWWO GULF 1955 PERF BTV 6635-64 F 51/-/24 + 732 MCF

#19   SOHIO 44 WILLIAMS B-4 PERF H 6968-7014 F 110-126-124-130 EST 30278/-/24 CWPB SOHIO 1951 PERF BTV 6740-64 F 20/-/24 + 2.3 MMCF

#20   OR&R 54 ELOISE #1 TD BTV D&A NTR

#22   CHAMPLIN PER 81 O'BRIEN #1 PERF BTV 6629-37 F 150 MCF

#23   PEPPERS REFG CO 53 LONG 4A PERF BTV 6684-30 F 28/-/24 + 4.22 MMCF

#25   SOHIO 44 CASEY #2 PERF H 6704-30 F 320/-/24

#26   SOHIO 85 CASEY #5 DST BTV 6547-75 R 90' GCM PERF BTV 6541-566 DRY D&A

#27   SOHIO 44 HARRIS #3 PERF H 6675-6728 F 469/-/24 CWWO SOHIO 79 PERF PR 6338-52 F 250 MCF

#28   CALVERT 76 MCKINNIS #1 PERF PR 76336-48 F 5.6/2.4/24 + 411 MCF

#29   PHILLIPS 44 JORGENSEN #1 PERF H 6541-6625 F 101/-/6

#30   JR HOP GILMORE 1-15B PERF BTV 6360-72 P 27/-/14 + 50 MCF

#31   PHILLIPS 63 GILMORE A1 PERF HS & CH 5558-5726 P 27/1/24 PERF PR 6292-324 F 340 MCF + P 7/1/27

#32   STEGER 79 GILMORE 1A PERF TONK 3143-55 PROD GAS AMT UNKN

#33   CWPP DUNCAN DRLG 59 PERF BTV 6641-51 F 103 MCF

#34   PEPPERS 44 WINTERS #1 PERF H 6954 OH F 200/-/24 CWWO
CHAMPLIN 83 PERF BTV 6693-704 710-26 F 24/4056/24 + 41 MCF

#35   OK WELL SERVICE 64 WALLER #3 CWWO PERF PR 6568-78 F
23/-/24 GOR 3900/1

#37   CWPB SOHIO 1958 WARD #4 PERF BTV AT 6616 F 109/-/24 +
220 MCF

#38   CWWO SOHIO 1959 PERF PR 6519 6664-67 6656-60 IN BTV F
83/-/24 PR F 8.25 MMCFG

#39   CONTINENTAL 55 CASA #5 CWWO PERF BTV 5766-84 F 11/-
/24 CWWO 1981 AMOCO CH 5912-19 P 12/5/12 + 9 MCF

#40   CWWO GULF 80 PERF BTV 6636-52 P 24/8/24

#41   CWWO GULF 82 PERF DSW 6434-48 P 2/10/24

#42   CWPB SOHIO 59 PERF BTV 6648-58 F104/-/24

#43   HEARTLAND 92 FWWP PERF BTV 6575-6380 PERF PR 6562-
6480 ACID 2000 GA MCA FRC W/13.64M# SD & 20M GA FOAM KCL   PR
4 150 MCF BTV F 1/4/-/24

#44   MADDEN & HOGAN 53 DAVIS 1A PERF BTV 6402-18 PERF PR
6265-6303 BTV F 150 BOPH PR F 17 MMCF W/1.25 MMCF FROM BTV

#45   PHILLIPS 54 SCHINN #5 PERF BTV 6510-35 F 175/-/24 +
500 MCF

#46   PEPPERS 54 BEBBER 1A PERF BTV 6349 OH F 1.99 MMCF
PERF PR 6266-92 F 4.49 MMCF + 43/-24

#47   PEPPERS 53 LOWERY 1A PERF PR 6248-80 FRC F 51/-/24 +
11 MMCF

#48   PEPPERS 45 LOWERY #1 PERF H 6590-6630 6660-90 F 38,
30/-/2 GOR 912

#49   PEPPERS 44 LYONS #2 PERF H 6620-50 6700-45 F 800/-/10

#50   PEPPERS LYONS #1A PERF PR 6412-28 PERF BTV 6292-6318
F 2.75 MMCF

#51   CALVERT 54 REMUND #3 PERF 2 WX 6627-37 F 644/-/24P
DOLO 6504-36 F 120/133/24

#52   CWWO WAS PERF IN BTV F 102/-/24 PAN AM 58 PERF HS
5488-90 546769 P 21/7/24

#563   STANOLIND 40 PATTON B2 PERF BTV 6374-6404 F 42/-/24
CWWO PAN AM 69 PERF HG 5508-19 P 13/10/24

#55   RUSSELL 44 PALEY #1 PERF H 6590-520 F 70/-/24

#55   SIMMONS 53 PAULEY A2 PERF PR 6307-17 P 33/-/6 GOR
43000

#56   TRIGG DRLG 54 KIRSHNER #1 PERF BTV 6403 OH F 300/-/24

#57   TRIGG DRLG 54 KIRSHNER #2 PERF BTV 6400 ON F 59/-/24
+ 120 MCF

#58   TRIGG DRLG 54 KIRSHNER #2B PERF BTV 6430 OH F 50/-/24
+ 100 MCF

#59   TRIGG DRLG 54 PATTON #1 PERF PR & PERF BTV 6455-75
6340-55 F 14 MMCF + 10/-/24 PERF PR & F 14/-/24 150 MCF FROM
BTV

#60   STANOLIND 45 KIRCHNER PERF BTV 6433 OH F 138/-/24

#61   CWWO AMOCO 82 PERF BTV PR NTR D&A

#62   DUNCAN 54 DILLON #1A PERF PR 6428-50 F 10/-/24+30
MMCF PERF BTV 6575-85 F 90/-/24

#63   HEARTLAND 74 MCDOWELL 1B CWWO PERF BTV 6583-93 6593-
6608 F 12/0/24 + 148 MMCF

#64   CWPB PEPPERS 46 PERF BTV 6669 F 410/-/24

#65   FOX & FOX ARNOLD #1 CWPB PERF H 6830-58 F 150/-/24

#66   SKELLY 49 SPIVEY #5 CWWO PERF OSW 6520-50 P 5/524

#67   SOHIO 46 HARPER #6 PERF BTV 6745-66 S 266/-/24

#68   STANOLIND YOUNG #3 PERF BTV 6702-27 F 10/-/24 FRC F
25/-/18

#69   CHAMPLIN 55 YOUNG #1 PERF BTV 6688-713 P 35/-/24

#70   PHILLIPS 57 FLYNN #3 CWWO PERF BTV 6600-14 F 3100 MCF

#71   CWWO CORNELL 67 MCKEE C2 PERF CK 5684-92 WSB DRY P CH
5515-30 F 19/-/24

#72   CWWO CORNELL 70 HOLMES B1 PERF CR 5682-88 F 25/-/24

#73   H&R 70 MCKEE #1 PERF HG 5488-98 F 53/2/24

#74   DENVER PRODN 48 SHERMAN #1 PERF H 6572-6650 F 80/-/24 OWWO THOMAS ENG 68 PERF HG 5520-5568 CH 5694-5704 OSW 6281-6228 F 126/40/24

#75   OWWO GULF 51 PERF BTV 6808-12 REC WTR D&A

#76   CHAMPLIN 85 PERF PR 6518-532 PERF KC 5922-929 NTR D&A

#77   OWWO UNION OF TEXAS 66 PERF PR 6536-40 FRC W/SW GEL S LOAD & F 500 MCF PERF OSW 6484-92 ACID 500 GA 15% & FL W/15000 GAL OIL FC W/12M GAL KCL F 14/86/17.5

#78   OWWO SOHIO 76 PERF PR 6591-601 PERF OSW 6535-55 ACID & F 1/1/24 D&A

#79   THOMAS ENG 84 LEIGH #1 PERF OSW 6420-30 PERF CK 5870-80 CH F 48/54/24 + 288 MCF

#80   CALVERT 77 MEEKER #1 PERF SK 6550-54 NSO PERF CK 6014-18 FRC NSO PERF CK 5806-14 ACID W/13M GA F 47/19/24

#81   CAMEO 76 SITILINGTON 1-10 PERF CK 5799-5806 PERF LY 5400-06 F 44/32/24+50 MCF

#82   PHILLIPS 87 BLUFF B2 OWWO PERF HG 5830-848 P 61/2/24

#83   PHILLIPS 55 BLUFF 2C OWWO PERF BTV 6776-90 DID NOT REC LOAD D&A

#84   PHILLIPS 55 OWWO PERF CK 5930-88 P 75/5/24

#85   OWWO CHAMPLIN 55 PERF CK 5957-67 P 114/-/24

#86   CHAMPLIN 64 ANDERSON #1 PERF CK 5925-34 SB NSO PERF CK 5660-70 LY SWB NSO D&A CHAMPLIN 55 PERF BTV 6716-728 FRC S 40/-/24

#87   GULF STREETER-FLYNN B1 PERF OSW 6652-6666 R SSO D&A

#88   TIDEWATER 52 MOTTER #3 PERF BTV INTERVAL UNKN D&A

#89   TIDEWATER 52 MOTTER #3 PERF ETV 6874-81 R MCW D&A

#90   GULF 53 STREETER #2 PERF BTV 5883-89 NSO D&A

#91   GULF 53 STREETER #2 PERF BTV 6670-90 NSO D&A

#92   PHILLIPS 55 STINCHCOMB #1 PERF CH 6104-14 NSO PERS OSW 6675-105 NSO ACID OSW & CK P 22/2/24 + 78 MCF

#93   PAN AM 66 PERF OSW 6786-848 F 264/-24 OWWO AMOCO 82 PERF CH 6236-239 NTR D&A

#94   PAN AM 57 YMCA #1 PERF OSW 6673-789 S 1/-/3 FRC S 5/5/3.5 D&A

#94   CWWO GULF 69 TCM-TCM #2 PERF OSW 6834-55 5.25 BO/0/1 D&A

#95   C&S RESOURCES 78 STORIM #1A DST BTV 6557-566 GTS 3 MIN F 461 MCF PERF H 6922-934 PERF BTV 6564-572 P 16/3.5/24 + GAS

#96   C&S RESOURCES 78 STORIM B1 PERF M 6780-857 PERF BTV 6567-574 F 1 MMCF + P 8/8/24

#97   ATLANTIC 44 TRINDLE #6 PERF H 6975-7000 F 782/-/12

#98   ATLANTIC 62 TRINDLE #9 TWIN PERF BTV 6574-96 F 2.98 MMCF

#99   ANDERSON-PRITCHARD 50 COLLETT #4 PERF BTV 6626 F 8.6531 MMCF

#100   OKLA NAT GAS 80 TRINDLE #S1 PERF BTV 6588-614 USED FOR GAS STORAGE

#010   UNION 66 COLLETT #1 CWWO PERF M 6776-896 P 12/22/24

#102   ANDERSON-PRITCHARD 50 SMITH #2 PERF BTV 6696-712 F 127/-/24 GOR 1800-1

#103   ANDERSON-PRITCHARD 65 DICHERSON #1 PERF BTV 6714-765 OH F 152/-/24 GOR 1910-1 CWWO OKLA NAT GAS 65 PERF M 6852-6998 FC W/15M BBL WATR S 172/0/24

#104   BLALOCK 59 STATE B2 CWPB PERF PR 6560-86 F 975 MCF

#105   CWWO GLEASON & SANDERS 61 REHERMAN #1A PERF PR 6550-58 F 500 MCF

#106   CWWO GENERAL DRILL 61 ABOLL #1 COULDN'T CLEAN OUT HOLE

#107   ASNLAND 49 MAIDMENT A1 PERF BTV 6854 OH F 52/-/14 + 5.5 MMCF

#108   STANOLIND 45 HENSNICKER #2 PERF H 7033 OH P 97/140/24 GOR 734:1

#109   MARK RESOURCES 78 WILSON #1 PERF BTV 6842-73 P 10/2/24

#110   CONTINENTAL OIL 45 MURPHY #1A PERF H 6667-901 ACID F 175/5 1" + 2MMCF

#111   STANOLIND 47 YOUNG B1 26-14N-4W SE SW SE PERF BTV 6533-87 F 57/-/24 GOR 800:1

#112   DENVER 47 MCKEE #3 26-14N-4W SE SW SW PERF BTV 6411-47 F 30/-/24

#113   DENVER WHISTLER #1 27-14N-4W SE SE SE PERF BTV 6530-70 F 60/-24.5

#114   SOHIO 44 PATTON #1 27-14N-4W NW SW PERF H 6710-OH PROD AMT UKN.

#115 DENVER 47 MCKEE #1 26-14N-4W SE SE SW PERF BTV 2694-OH F 62/-/24

#116   DENVER PER 47 HOLMES 2A 35-14N-4W NE SE NW PERF H 6644 F 100/-/24

#117   THOMAS ENG 84 LEIGH #1 10-T13N-R4W SW SE SW PERF OSW 6520-030 DRY P CK 5870-80 F 48/54/24 + 288 MCF

#118   YALE OIL 65 NINA #1 8-T15N-R4W NE NE SE PERF M NTR

#119   HEARTLAND 66 VAN GRISSO #1 22-T15N-R4W NE SW NW PERF M NTR

VITA

Lonnie G. Kennedy

Candidate for the Degree of

Master of Science

Thesis: CONFINING LAYER STUDY IN THE WEST EDMOND OIL FIELD AREA USING SUBSURFACE, REMOTE SENSING, AND GEOCHEMICAL METHODS

Major Field: Geology

Biographical:

Personal Data: Born in Wynnewood, Oklahoma, September 19, 1955, the son of George M. and Jean Ann Kennedy.

Education: Graduated from Davis High School, Davis Oklahoma in June, 1974; received Bachelor of Science Degree in Geology from University of Oklahoma in March, 1986; completed requirements for the Master of Science degree at Oklahoma State University in May, 1990.

Professional Experience: Assistant Coal Geologist for Oklahoma Geological Survey from September, 1976 to June, 1977; Petroleum Geologist for Pathfinder Petroleum, Inc. from March, 1979 to March, 1982; Petroleum Geologist for Savant Energy, Ltd. from March, 1982 to August, 1987; Researcher under U.S. Environmental Protection Agency grant from August, 1987 to June, 1988; Environmental Hydrogeologist for Engineering Enterprises, Inc. from June, 1988 to September, 1989; Environmental Hydrogeologist for Coastal Biotechnology, Inc. from September, 1989 to current (January, 1990).

R5W

R4W

T15N

T14N

T13N

T12N
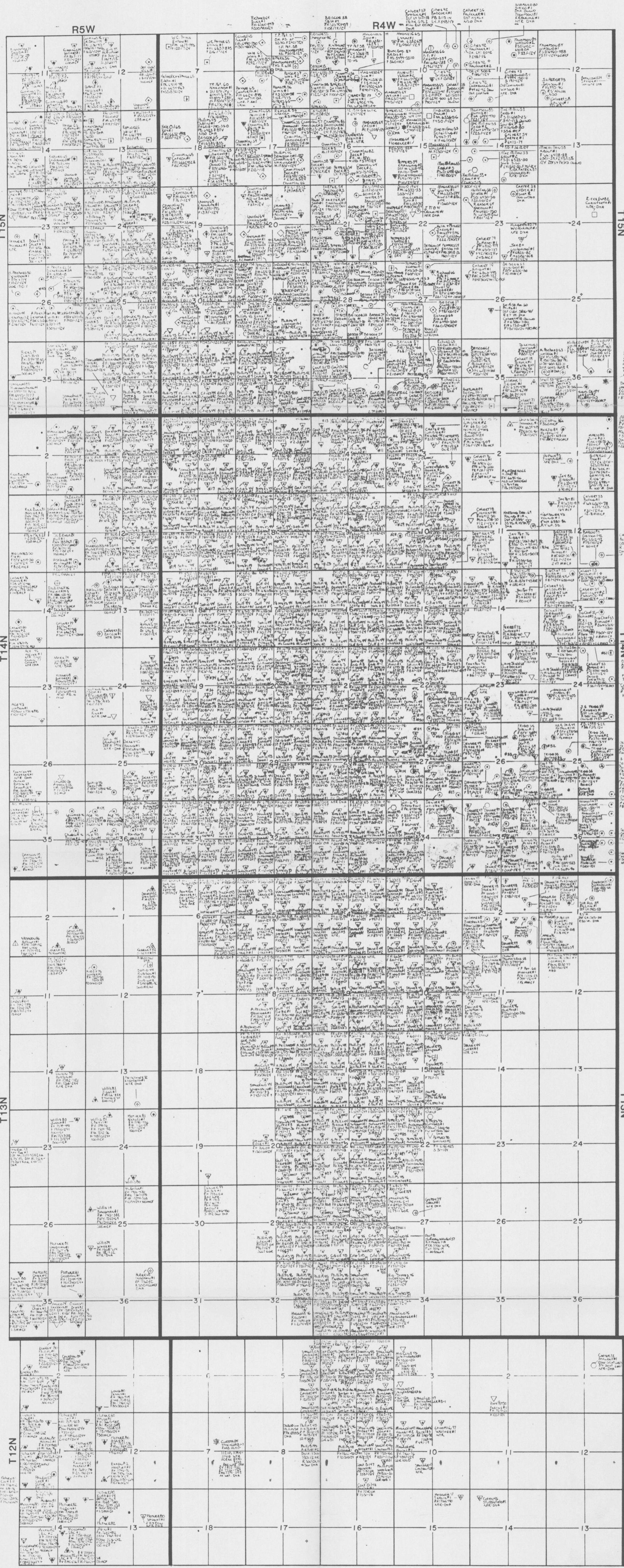
LEGEND

MAX. ZONE COLOR IF PENE'RATED	PRODUCTIVE FORMATION	CODE
	Hogshooter	Hg
	Layton	Ly
	Checkerboard	Ck
	Cleveland	Clv
	Oswego	Os
	Prue	Pr
	Skinner	Sk
	"Bartlesville"	Btv
	Mississippi	Ms
	Misener	Ma
	Woodford	Wd
	Hunton	H
	Sylvan	S
	Viola	V
	Dolomite	Dol
	Wilcox	Wx
	Arbuckle	Arb

Scale:
0   .5   0   1/4   1/2   1 Mile

N.
M.N.

PRODUCTION DATA CODE EXAMPLE

Operator Name ——— Phillips 48 ——— Year Drilled
Well Acres #1 ——— Well Name
Perforated Formation —— P. H. 7,200-20 —— Perforated Interval
Flow or Pump —— F. 279/24 —— Duration of Test In Hours
I.P. Oil In Barrels ——— GOR 1018 ——— Water If Known
Gas to Oil Ratio

PLATE 1

WEST EDMOND FIELD
OKLAHOMA COUNTY, OK.

PRODUCTION DATA MAP

LONNIE G. KENNEDY   SEPT. 1988

R5W   R4W

T15N

T14N

T13N

T12N

N.
M.N.

Scale:
0   .5   0   1/4 1/2   1 Mile
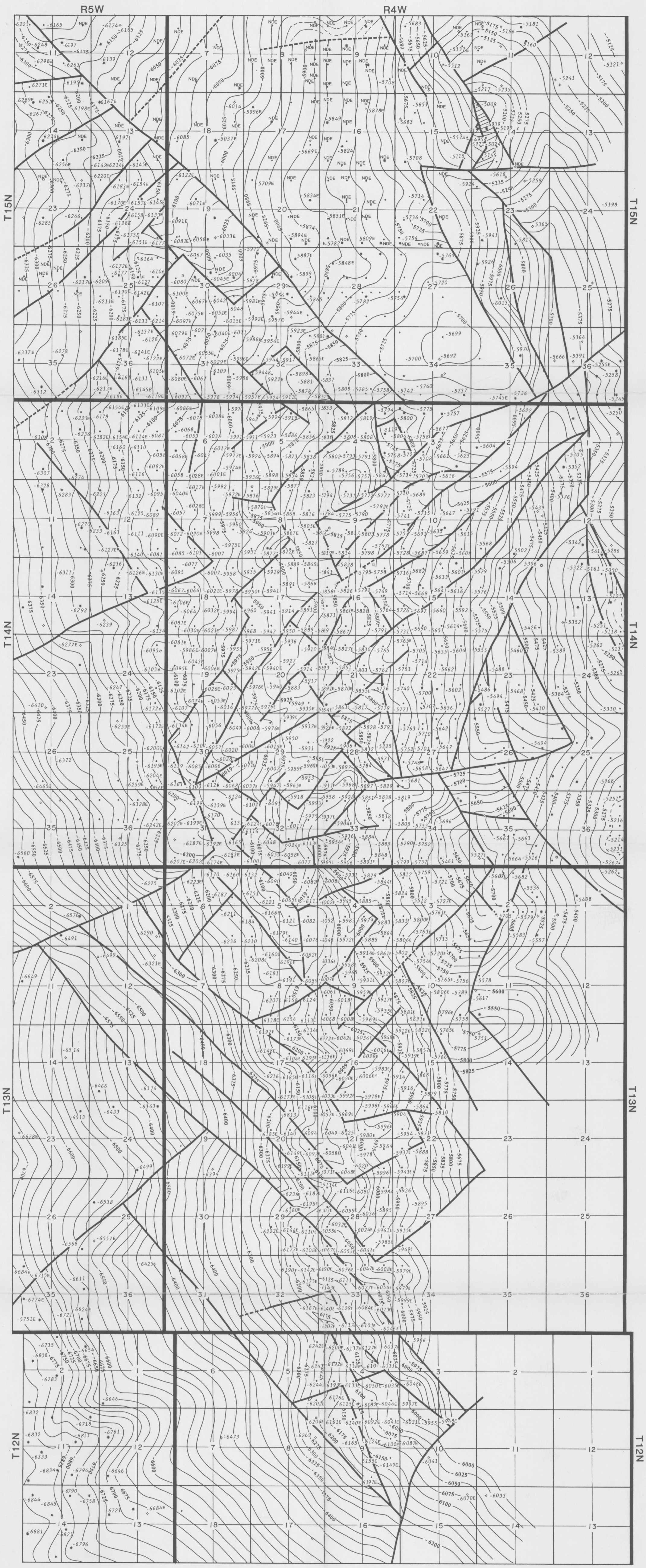
PLATE 2

WEST EDMOND FIELD
OKLAHOMA COUNTY, OK.

STRUCTURE BASE OF HUNTON
TOP OF SYLVAN

LONNIE G. KENNEDY APRIL 1988

R5W   R4W

T15N   T15N

T14N   T14N

T13N   T13N

T12N   T12N

Subcrop Limit Bois d'Arc-Frisco

Subcrop Limit Bois d'Arc-Frisco

N.
M.N.

Scale
0   .5   0   1/4 1/2   1 Mile
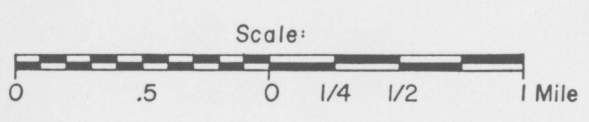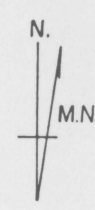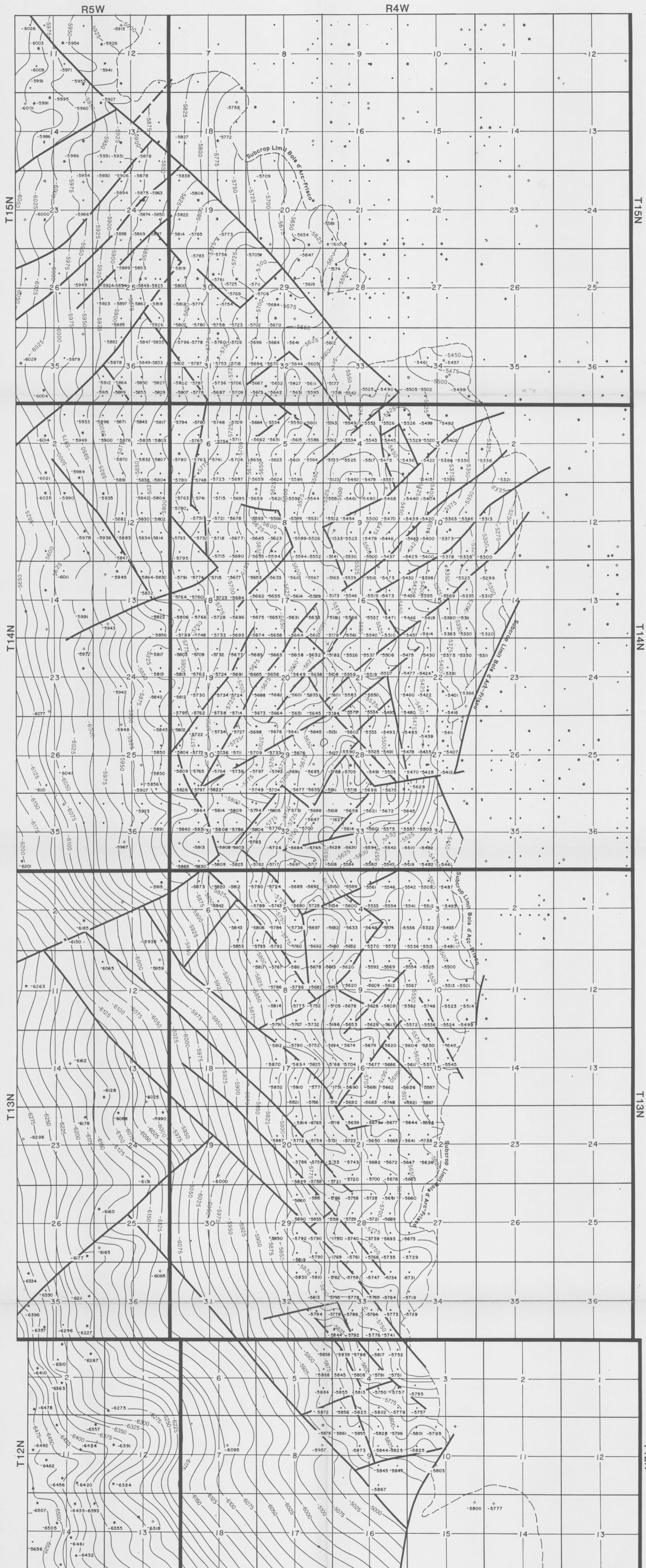
PLATE 3

WEST EDMOND FIELD
OKLAHOMA COUNTY, OK.

STRUCTURE TOP
BOIS D'ARC-FRISCO

LONNIE G. KENNEDY APRIL 1988

PLATE 4

WEST EDMOND FIELD
OKLAHOMA COUNTY, OK.

24 HOUR INITIAL
OIL PRODUCTION MAP

LONNIE G. KENNEDY APRIL 1986
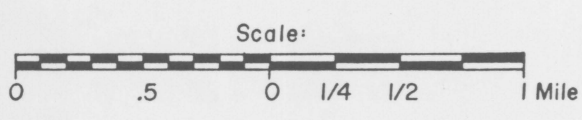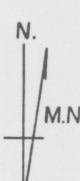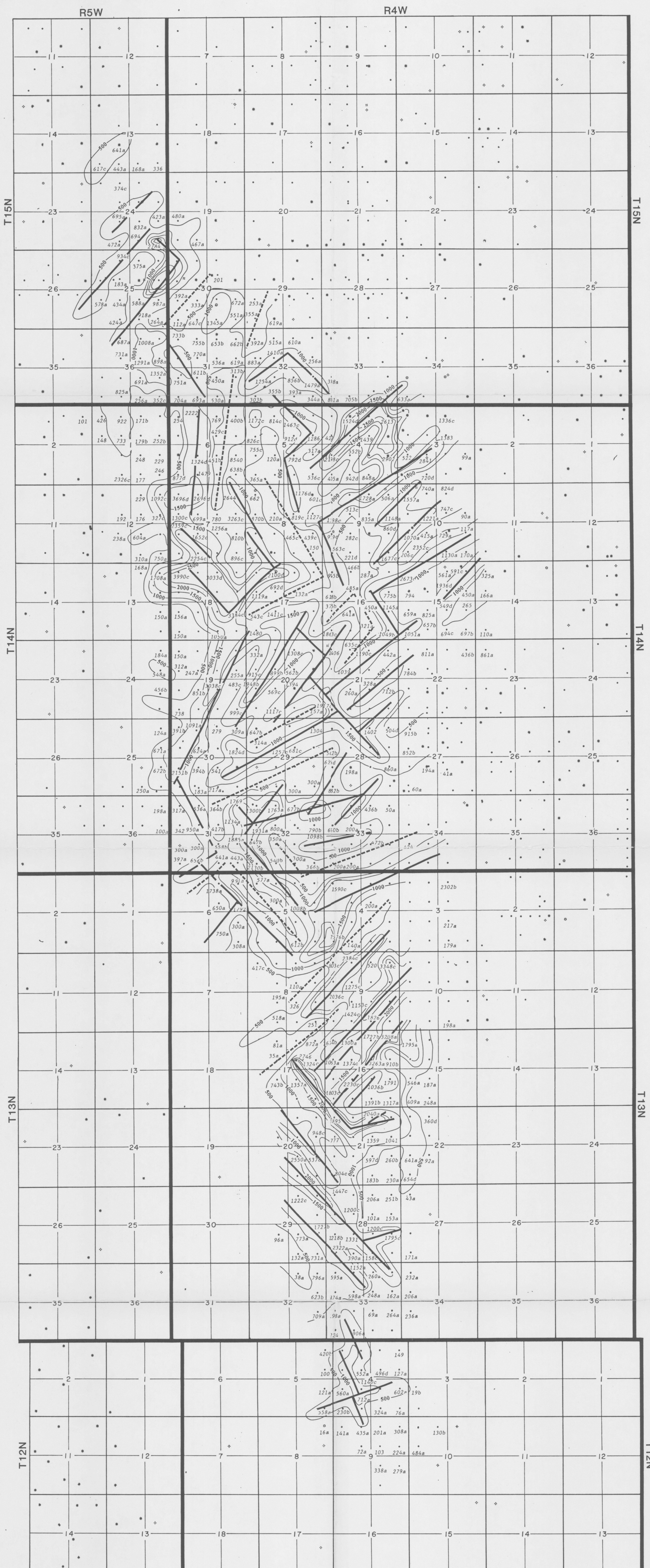
LEGEND
—— High Production Trend
---- Low Production Trend

N.
M.N.

Scale
0   .5   0 1/4 1/2   1 Mile
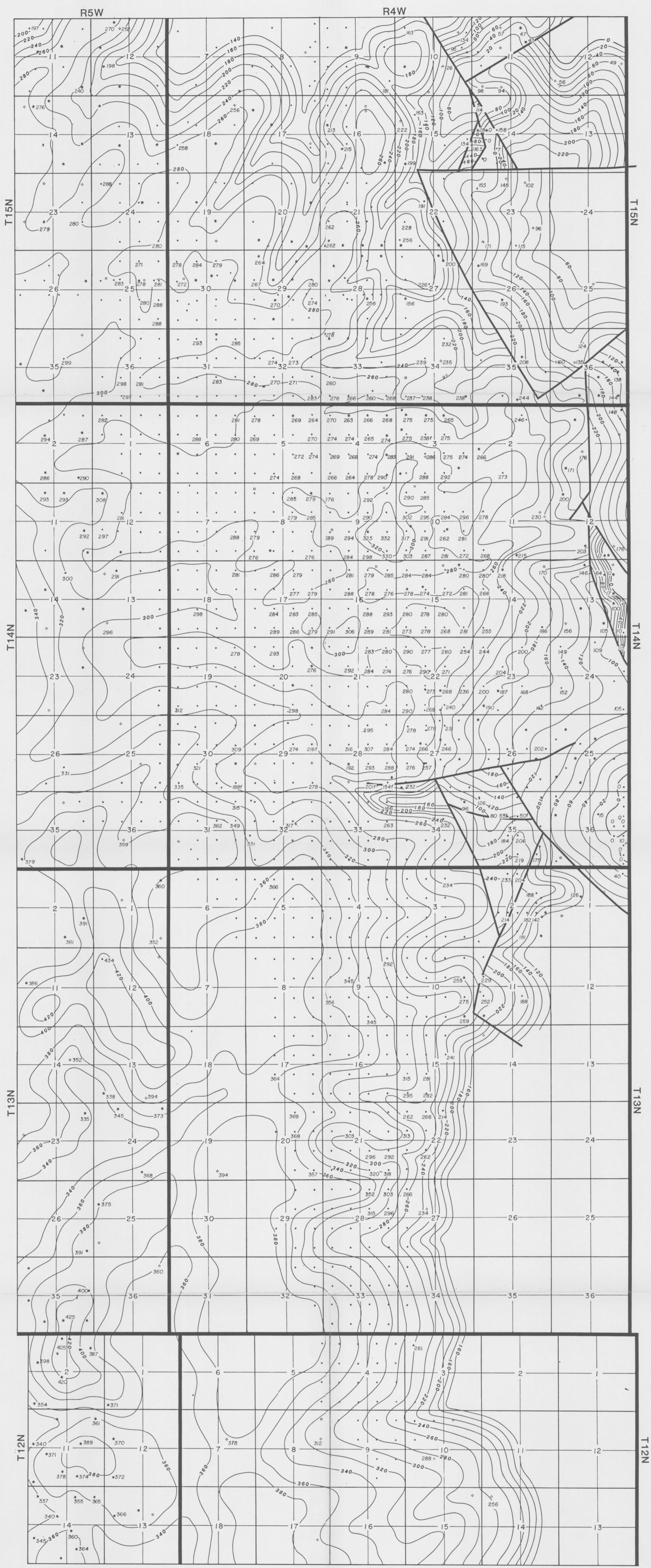
PLATE 5

WEST EDMOND FIELD
OKLAHOMA COUNTY, OK.

HUNTON LIME ISOPACH

Lonnie G. Kennedy   May 1988

N.
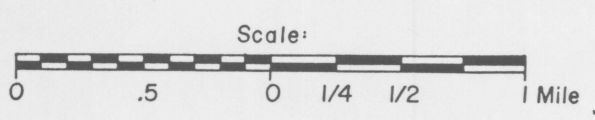M.N.

Scale:
0   .5   0   1/4 1/2   1 Mile
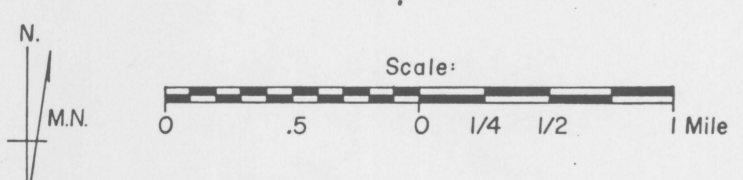
C.I.:20 feet
f.: fault removed section

R5W   R4W
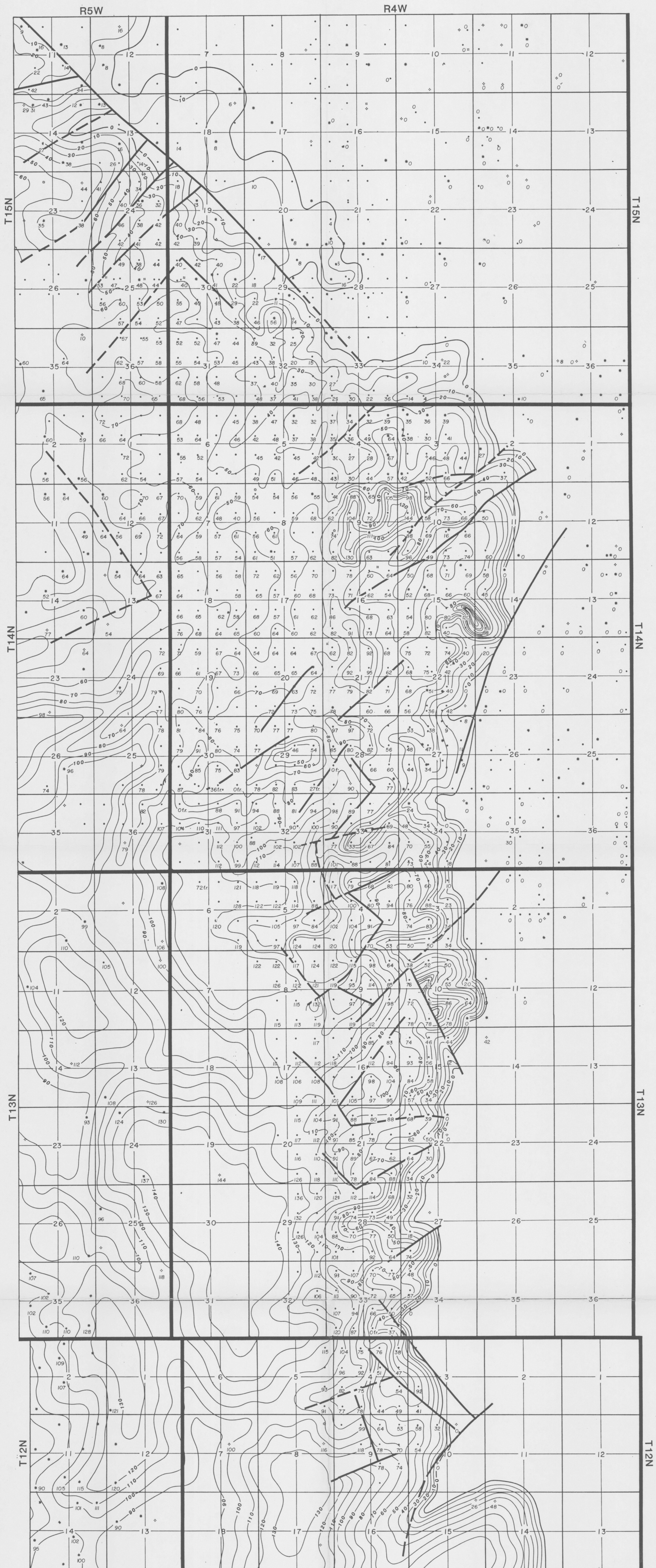
PLATE 6

WEST EDMOND FIELD
OKLAHOMA COUNTY, OK.

BOIS D'ARC-FRISCO
ISOPACH MAP

Lonnie G. Kennedy April 1988

LEGEND

— Fault
-- Fault Trace

Scale
0   .5   0 1/4 1/2   1 Mile
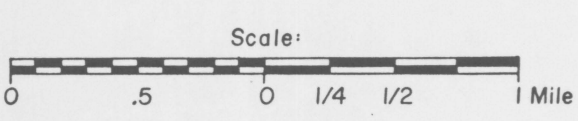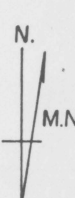
C.I.: 10 feet
f.r.: Fault Reduced Section

N.
M.N.
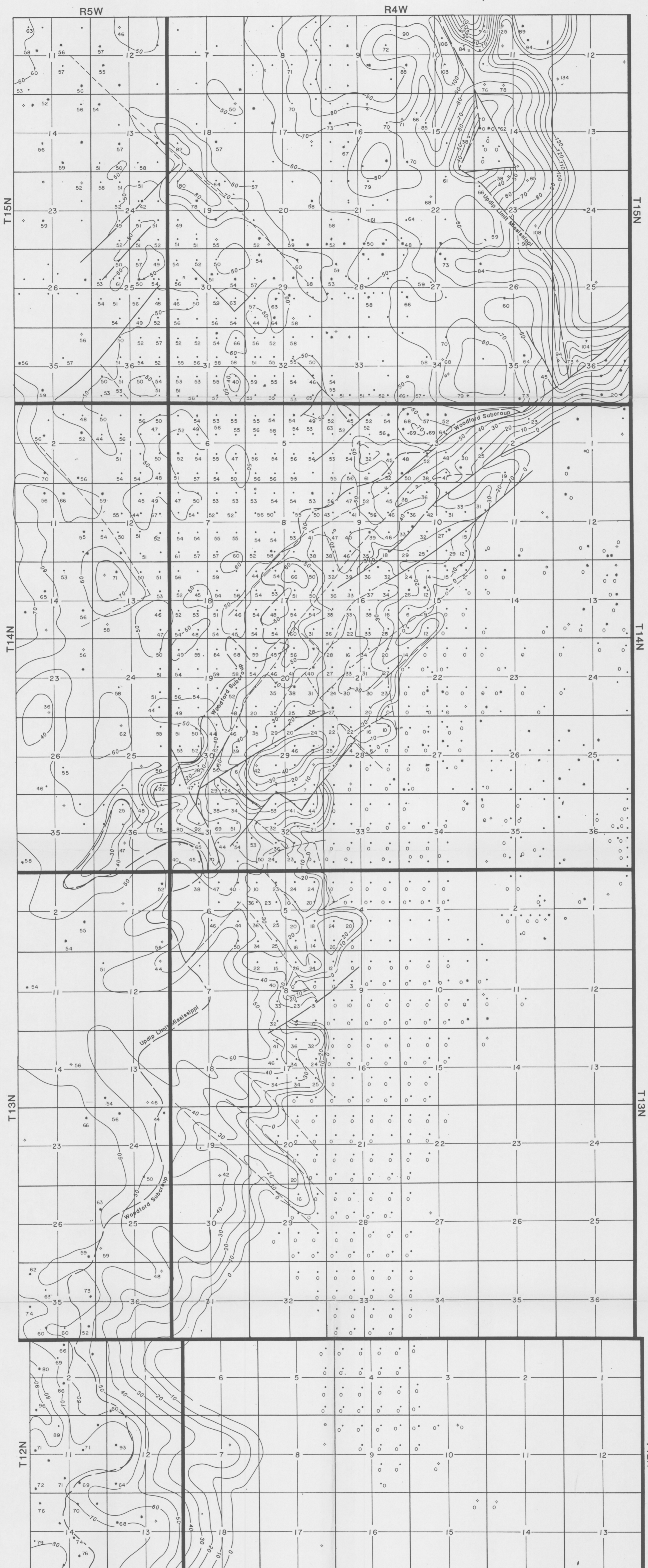
PLATE 7

WEST EDMOND FIELD
OKLAHOMA COUNTY, OK.

WOODFORD ISOPACH MAP

LONNIE G. KENNEDY   OCT. 88
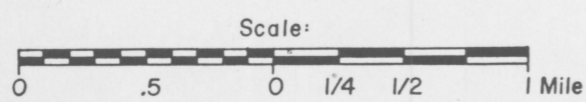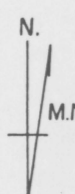
LEGEND
Fault _____
Fault Trace - - - - -
Woodford Subcrop - - -
C.I.=10 feet

Scale
0   .5   0 1/4 1/2   1 Mile

N.
M.N.
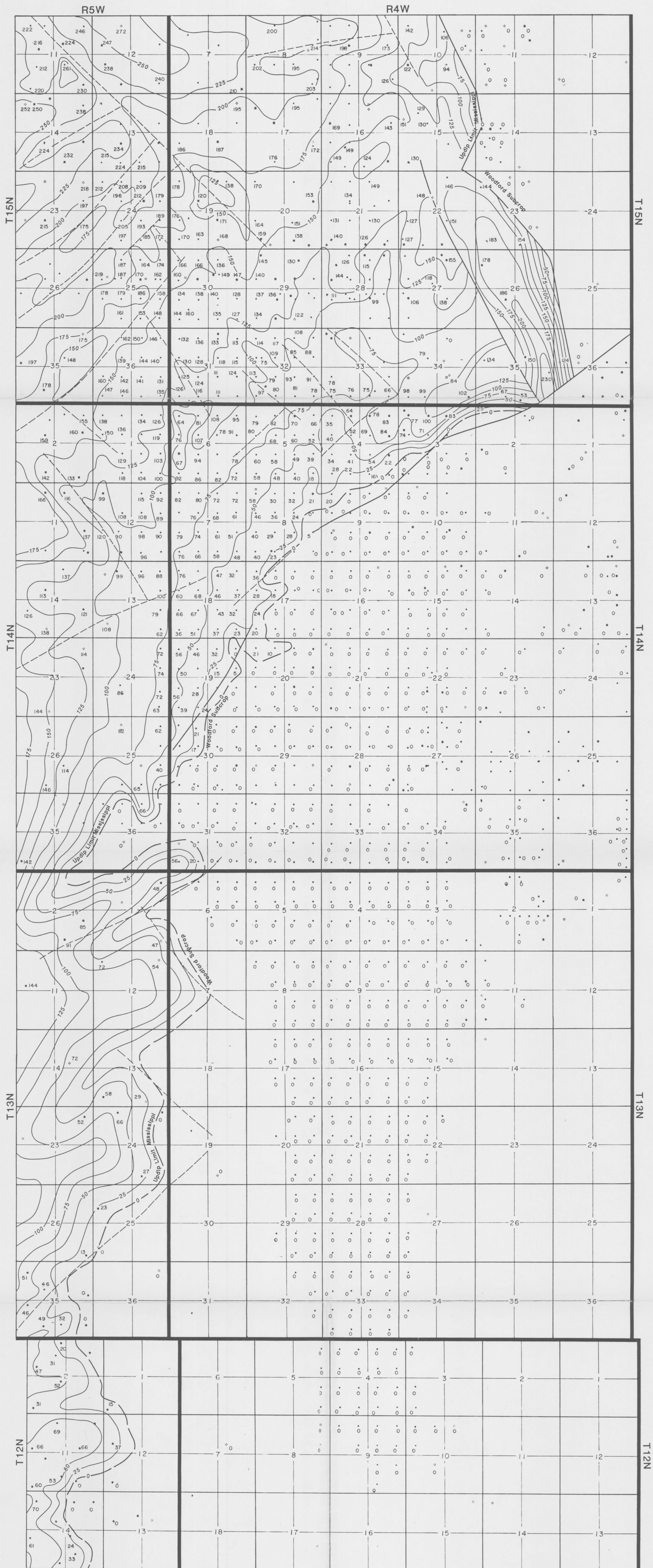
WEST EDMOND FIELD
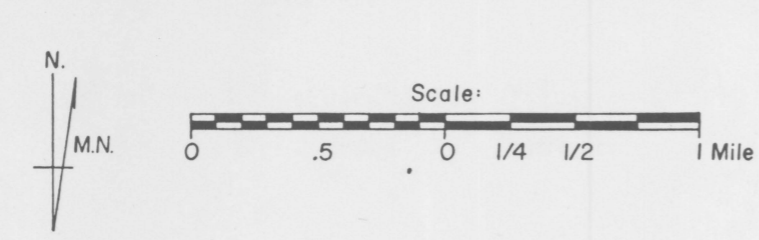OKLAHOMA COUNTY, OK.

MISSISSIPPI LIME ISOPACH

PLATE 8

LONNIE G. KENNEDY OCT. 1988

LEGEND

Fault ⎯⎯⎯
Fault Trace ⎯ ⎯ ⎯
Updip Limit of Mississippi ⎯ ⎯ ⎯
C.I.=25 feet

Scale:
0   .5   0   1/4   1/2   1 Mile

N
M.N.

R5W   R4W

LEGEND

—— Lineament Corresponding
to Subsurface Fault

········ Lineament Not Corresponding
to Subsurface Fault

Note: Original scale 1:60,000
enlarged to 1:2,400.

N.
M.N.

Scale:
0   .5   0   1/4   1/2   1 Mile

PLATE 11

WEST EDMOND FIELD
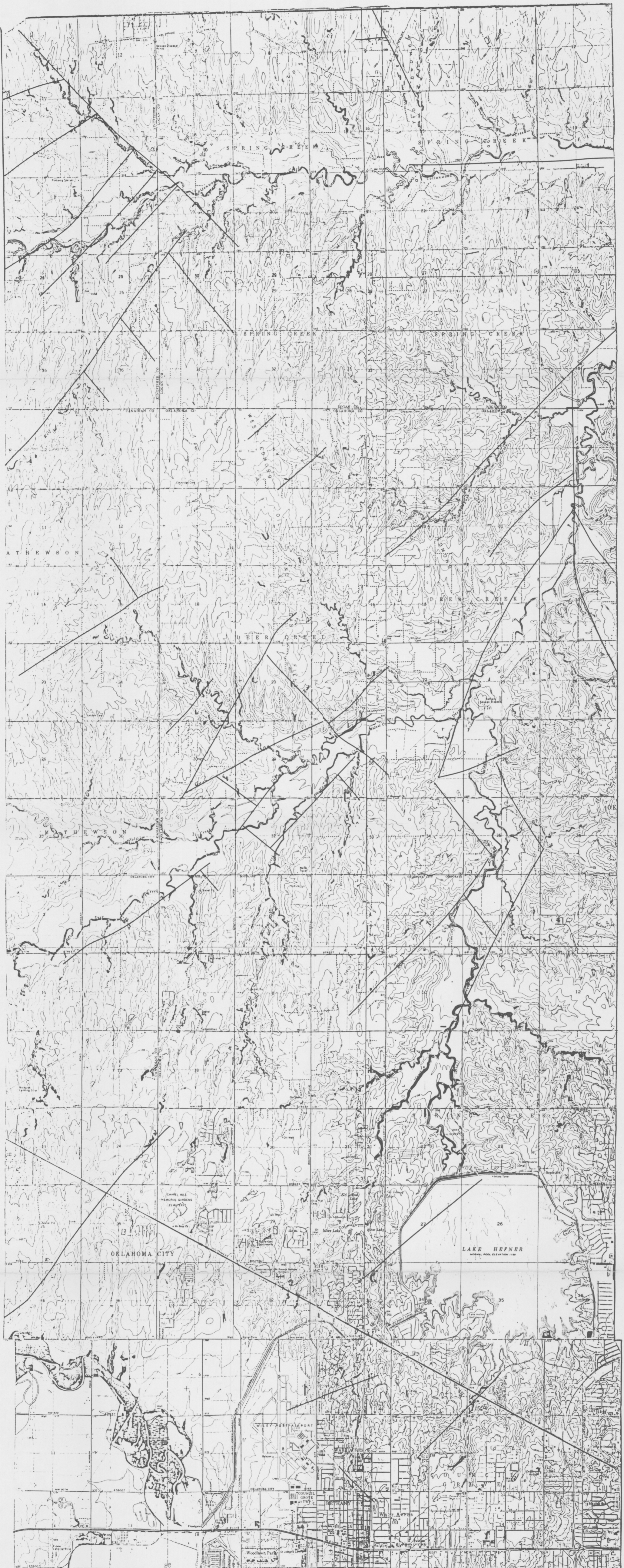OKLAHOMA COUNTY, OK.

COLOR INFRARED
LINEAMENT MAP

LONNIE G. KENNEDY   APRIL 1988
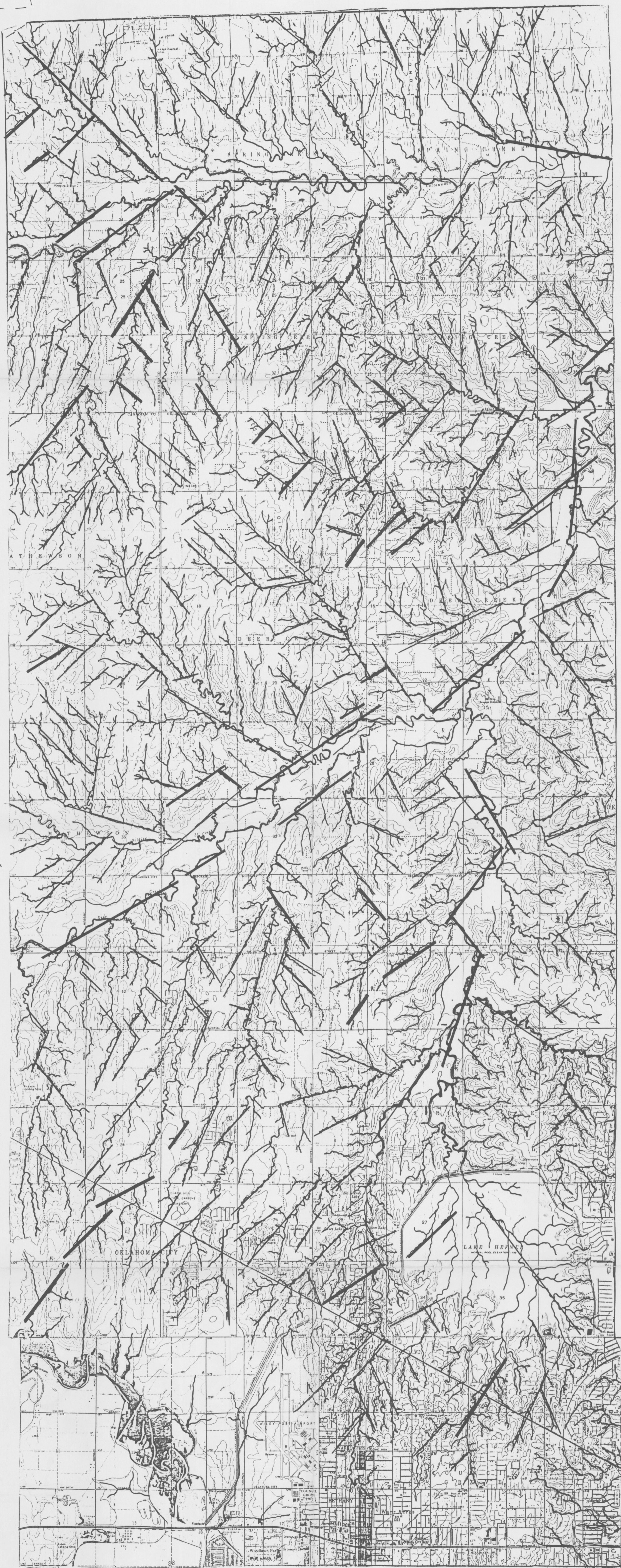
PLATE 12
TOPOGRAPHIC EXPRESSION
OF SUBSURFACE FAULTS

LEGEND

▬▬▬ Stream Corresponding
     to Subsurface Fault
─── Stream Not Corresponding
     to Subsurface Fault

PLATE 13
STREAM ORIENTATION MAP